TRANSPORTATION RESEARCH RECORD 659

Bituminous Concrete Materials, Mixtures, and Additives

TRANSPORTATION RESEARCH BOARD

COMMISSION ON SOCIOTECHNICAL SYSTEMS
NATIONAL RESEARCH COUNCIL

NATIONAL ACADEMY OF SCIENCES
WASHINGTON, D.C. 1977

Transportation Research Record 659
Price $4.00
Edited for TRB by Anne Ricker

subject areas
26 pavement performance
31 bituminous materials and mixes
33 construction

Transportation Research Board publications are available by ordering directly from the board. They may also be obtained on a regular basis through organizational or individual supporting membership in the board; members or library subscribers are eligible for substantial discounts. For further information, write to the Transportation Research Board, National Academy of Sciences, 2101 Constitution Avenue, N.W., Washington, D.C. 20418.

Library of Congress Cataloging in Publication Data
National Research Council. Transportation Research Board.
Bituminous concrete materials, mixtures, and additives.

(Transportation research record; 659)
1. Pavements, Asphalt concrete—Congresses. 2. Bituminous materials—Congresses. I. Title. II. Series.
TE7.H5 no. 659 [TE270] 380.5'08s [625.8'5] 78-26746
ISBN 0-309-02688-1

Sponsorship of the Papers in This Transportation Research Record

GROUP 2—DESIGN AND CONSTRUCTION OF TRANSPORTATION FACILITIES
Eldon J. Yoder, Purdue University, chairman

Bituminous Section
Moreland Herrin, University of Illinois at Urbana-Champaign, chairman

Committee on Characteristics of Bituminous Materials
J. Claine Petersen, U.S. Bureau of Mines, chairman
E. Keith Ensley, U.S. Bureau of Mines, Laramie, secretary
Chester J. Andres, L. W. Corbett, James R. Couper, Robert L. Dunning, Jack N. Dybalski, Felix C. Gzemski, Woodrow J. Halstead, Prithvi S. Kandhal, Willis C. Keith, L. C. Krchma, Robert P. Lottman, James J. Murphy, C. A. Pagen, Rowan J. Peters, Charles F. Potts, Vytautas P. Puzinauskas, F. S. Rostler, Donald Saylak, Charles G. Schmitz, Herbert E. Schweyer, J. York Welborn, Frank M. Williams, Leonard E. Wood

Committee on Characteristics of Bituminous-Aggregate Combinations to Meet Surface Requirements
Kamran Majidzadeh, Ohio State University, chairman
Sabir H. Dahir, Richard L. Davis, Miller C. Ford, Jr., Rudolf A. Jimenez, Bernard F. Kallas, Prithvi S. Kandhal, Larry L. Kole, G. W. Maupin, Jr., C. A. Pagen, James A. Scherocman, Russell H. Snow, Stewart R. Spelman, Leonard J. Stern, E. A. Whitehurst, John B. Wilee, Frank M. Williams

Committee on Characteristics of Bituminous Paving Mixtures to Meet Structural Requirements
Donald R. Schwartz, Illinois Department of Transportation, chairman
Grant J. Allen, Charles W. Beagle, Oliver E. Briscoe, H. W. Busching, J. T. Corkill, Jon A. Epps, Charles R. Foster, Erling Henrikson, R. G. Hicks, Rudolf A. Jimenez, Ignat V. Kalcheff, Bernard F. Kallas, Thomas W. Kennedy, Charles V. Owen, Charles F. Parker, David W. Rand, R. M. Ripple, Jack E. Stephens, Ronald L. Terrel, David G. Tunnicliff, James D. Zubiena

Construction Section
David S. Gedney, Federal Highway Administration, chairman

Committee on Flexible Pavement Construction
W. E. Latham, North Carolina Department of Transportation, chairman
Verdi Adam, Charles W. Beagle, R. W. Beaty, James A. Cechetini, Darrell S. Downey, Charles R. Foster, George F. Kemper, Duncan A. McCrae, James J. Murphy, Orrin Riley, W. L. Salmon, Jr., W. H. Shaw, Harrison S. Smith, R. R. Stander, Gerald S. Triplett, David G. Tunnicliff, Val Worona

Bob H. Welch, Transportation Research Board staff

Sponsorship is indicated by a footnote at the end of each report. The organizational units and officers and members are as of December 31, 1976.

Contents

Low Temperature Rheology of Asphalt Cements: Stiffness and Viscosity

H. E. Schweyer and A. M. Burns, Jr., Department of Chemical Engineering, University of Florida, Gainesville

Stiffness, as a material characteristic of asphalt cements, is attracting more attention in asphalt technology. This paper shows the quantitative relations between viscosity and stiffness and explains how the shear modulus and viscosity found by a constant stress rheometer can be used to evaluate stiffness. Experimental data from creep curve studies are given for a number of asphalt cements. The shear modulus is shown as the limiting asymptote that intersects the viscosity term asymptote at a stiffness limit time. These two asymptotes delineate the complete stiffness curve. Characteristic stiffness is shown to be a material property, but knowledge of the geometry of the system is prerequisite to its use in design, if the absolute deformation is to be considered. Variations in stiffness with shear rate (stress), temperature, and time are illustrated by data on absolute measurements for eight different types of asphalts at temperatures from 25 down to -5°C (77 to 23°F). The addition of viscosity and stiffness data at 5°C (41°F) to the usual viscosity data at 25 and 60°C (77 and 140°F) provides a better rheological profile for asphalt cements at low ambient temperatures than has previously been reported.

Although the concept of stiffness as a rheological property has been used in studies of asphalt bitumen and mixes, many authors do not explain what real rheological meaning it has. This has caused a proliferation of testing techniques and data reporting procedures. The purpose of this paper is (a) to clarify the meaning and significance of stiffness, (b) to suggest a format for data reporting, (c) to demonstrate by experiment a proposed model and the relations between stiffness and other rheological properties, and (d) to illustrate the variations in stiffness for certain selected asphalt bitumens at temperatures below 25°C (77°F) by using a constant stress shear mode apparatus.

In asphalt rheology the use of stiffness or resistance to stress as a function of time dates from Nijboer and van der Poel's 1953 description (1), although Nutting (2, 3, 4) proposed a generalized stress-strain-time concept in 1921.

The subject of stiffness was updated in 1958 by Saal and Labout (5), whose rather interesting results gave stiffness values for several types of asphalt bitumens and mixes over a range of temperatures from -50 to 50°C (-58 to 122°F) and at different stress levels. They also discussed the relation of dynamic to static creep for the combined Maxwell-Kelvin (Burgers) model and considered that all the behavior was related to the free volume concept and that the asphaltene content was related to gel-sol concepts. Their generalizations were made as approximations and were based somewhat on conjecture. They also commented on pressure effects and bulk modulus. The statement that Young's modulus of elasticity (E) has a value of about 2500 to 3000 MPa (362 592 to 435 111 lbf/in^2), which holds for all asphalts, is probably a fair approximation, but to consider it applicable to all asphalts at unspecified low temperatures is probably erroneous. However, Saal and Labout's review was an excellent summary of early work. Some of the data are reported in Table 1.

In 1954 van der Poel (6) also provided a summary of earlier work on viscoelasticity and data on mix stiffness. Much of this material presumably summarized his own previous work.

More recently, in 1969, Reiner (7) treated rheology theoretically and discussed asphalt deformations. Stiffness, as defined here, is the stress divided by the cumulative strain after a specified time and is therefore a function of temperature, time, and loading procedure. At times approaching zero (or instantaneous deformation), the stiffness is the same as the modulus of elasticity (E) in traction or the modulus of rigidity (G) in shear. However, at extended elapsed times, if the material is not a pure elastic solid and shows a permanent flow with time, the stiffness is almost directly proportional to the viscosity per unit time when the elastic strain is only a small proportion of the total strain. Accordingly, all factors that affect the elasticity and viscosity also affect the stiffness.

It is obvious, then, that factors such as shear susceptibility (variations in viscosity with shear rate), chronal susceptibility (history effects), temperature, compressibility, and mode of testing (traction or shear) all affect stiffness.

Because of the shear susceptibility of many asphalts, the standard rheological model of a spring and dashpot in parallel (Kelvin) combined in series with spring and dashpot (Maxwell) does not define the flow regime.

In their first paper on this subject, Schweyer, Baxley, and Burns (8) proposed a model that accommodates the shear susceptibility by a simple feedback mechanism as shown in Figure 1. This new model, the B-S model, will be discussed later in the paper but is essentially a modified version of the Burgers model for asphalt mentioned previously by Saal and Labout (5). It is for such a modified model that the mathematical relations referred to elsewhere (8) were confirmed experimentally for asphalt cements.

In the past, the problem of the shear susceptibility of the material (asphalt cement) has been conveniently neglected by assuming the bitumen to be a Newtonian material. In addition, because viscosity data were difficult to obtain at low temperatures (where stiffness becomes a very important descriptive property), many investigators relied on empirical tests for low temperature data.

Among such tests were the Fraas breaking test and the penetration index as a measure of temperature susceptibility. Fortunately, such obsolete tests are being replaced by direct measurements with more sophisticated creep and dynamic equipment.

It is important to remember, when comparing the data given in Table 1 with what is reported in this paper, that there are variations among the many test conditions. For example, the van der Poel data (9) are for both traction (creep) and dynamic test modes and assume that the asphalt bitumens used with his nomograph display "a purely Newtonian behavior," are incompressible, and "approach asymptotically to a limit of about 3000 MPa (435 111 lbf/in^2) for stiffness at low temperatures. Van der Poel assumes that the asphalts tested were Newtonian because the slope dS/dt at extended times approaches -1. But this is true for all fluids that fit the

Table 1. Comparative experimental viscoelastic data.

Source	Year	Asphalt Grading: Penetration (P25)	Asphalt Grading: Viscosity[a] (Pa·s)	Asphalt Grading: Temp. (°C)	Viscoelastic Data: Stress (kPa)	Viscoelastic Data: Time (s)	Viscoelastic Data: Stiffness (MPa)	Viscoelastic Data: G (MPa)	Viscoelastic Data: E (MPa)	Comments
Van der Poel (9)	1954									Data approximated from graphs dynamic viscosity and creep
Pitch type		–	–	5	–	1×10^{-3}	3000	–	3000	
		–	–	5	–	1×10^{2}	350	–	–	
		–	–	25	–	1×10^{-3}	1500	–	1500	
		–	–	25	–	1×10^{2}	170	–	–	
Air blown		–	–	0	–	1×10^{-3}	400	–	400	
		–	–	0	–	1×10^{2}	30	–	–	
		–	–	20	–	1×10^{-3}	120	–	120	
		–	–	20	–	1×10^{2}	6	–	–	
Brown, Sparks, and Smith (19)	1957	50	–	15.6	4 to 40	–	–	–	6.2	Tensile 100 by 25-mm cylinder
Brown and Sparks (20)	1958	59	–	2.5	2 to 20	–	–	–	125.0	Tensile 100 by 25-mm cylinder
Dormon and Jarman (21)	1958	40/50	–	-10	–	1×10^{-6}	690	–	690	Sliding plate (shear mode) converted to traction by factor of three (approximated from graph)
		40/50	–	-10	–	1×10^{2}	5.9	–	–	
		40/50	–	40	–	1×10^{-6}	200	–	200	
		40/50		40	–	1×10^{2}	0.0018	–	–	
Gaw (18)	1976	157	22.7	-10	–	1.8×10^{3}	8	–	–	Sliding plate
		157	22.7	0	–	1.8×10^{3}	0.68	–	–	
		157	22.7	10	–	1.8×10^{3}	0.046	–	–	
		170	59.0	-10	–	1.8×10^{3}	1.3	–	–	
		170	59.0	0	–	1.8×10^{3}	0.67	–	–	
		170	59.0	10	–	1.8×10^{3}	0.033	–	–	
Duthie (14)	1972	100		25	1 to 30	1×10^{-6}	40 to 300	40 to 300	–	Dynamic elastometer
		100		60	1 to 30	1×10^{-6}	3 to 158	3 to 158	–	
Dickinson and Witt (16)	1974	80/100		25	–	3×10^{-1}	15	–	–	Dynamic-coaxial
		80/100		15.4	–	3×10^{-1}	60	–	–	
		80/100		3.7	–	3×10^{-1}	150	–	–	
Fenijn and Krooshof (24)	1970									Sliding plate
Bitumen		96	–	-10	36	1	180	–	–	
		96	–	10	2.1	1	3.6	–	–	
		96	–	25	0.61	1	0.18	–	–	
		36	–	18	–	1	3.8	–	–	
Coal tar		4	–	40	0.55	1	1	–	–	
		4	–	25	5.6	1	130	–	–	
Gaw (18)	1976									Sliding plate, stress not known
AC-6		184	79.5	10	–	1	1.5	–	–	
		184	79.5	-5	–	1	180	–	–	
		184	79.5	-40	–	1	1600	–	–	
Propane asphalt		33	79.5	20	–	1	6.5	–	–	
		33	79.5	-5	–	1	140	–	–	
		33	79.5	-20	–	1	1300	–	–	

Note: $t\,°C = (t\,°F - 32)/1.8$; 1 Pa = 0.000 145 lbf/in²; 1 kPa = 0.145 lbf/in²; 1 MPa = 145 lbf/in²; and 1 mm = 0.039 in.

[a] Refers to viscosity at 60°C.

Ostwald-de Waele power law model (7) and will be shown later when the viscosity is not time dependent.

Another assumption is that the bitumens are incompressible when one converts moduli data from a shear to a traction basis. This appears to be reasonable, based on the Saal and Labout (5) discussion using data of Nederbrogt (10) and confirmed by Ronk's (11) bulk compression modulus K of the order of 2500 MPa (462 592 lbf/in²) at 0°C, which is about 10 times the elastic modulus for asphalt cements at that temperature.

However, another major consideration and source of some misunderstanding is the variation of stiffness with temperature. When stiffness is measured at any time longer than zero, there must be flow; otherwise the material is a solid. Even van der Poel's data (9) show a temperature effect, although his nomograph for mixes implies that stiffness at a finite time is independent of temperature.

Evaluating stiffness is further complicated by whether the evaluation is made in traction (compression or tension) or in shear. This will be discussed later.

APPARATUS AND B-S MODEL ANALYSIS

The experiments reported here were run in the constant stress rheometer reported in 1976 by Schweyer, Smith, and Fish (12). The plug flow tube and the optional capillary flow arrangements appear in Figure 2, and a picture of the apparatus is shown in Figure 3. The operation consists of applying a constant known shear stress to one end of the tube and measuring the velocity of movement down the tube. For soft asphalts the viscosity data are obtained by using a capillary in the sample tube.

The B-S model previously proposed (8) may be considered a modified classical Burgers rheological model for a non-Newtonian material as shown in Figure 1. The lower Newtonian dashpot has been modified in the B-S

Figure 1. Burns-Schweyer model for elastic power law fluid.

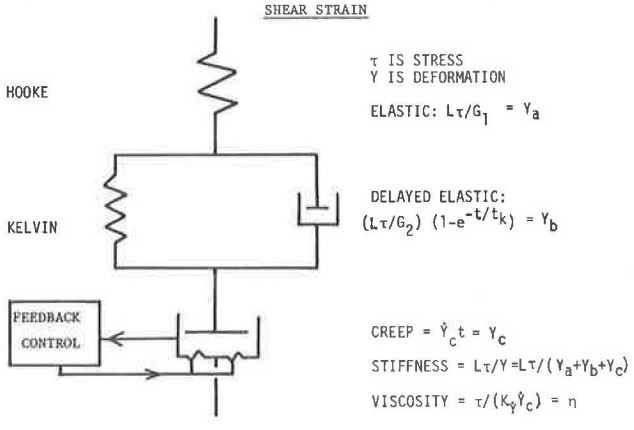

model to accommodate the generalized Newtonian material, of which asphalt bitumen is an example. (A generalized Newtonian material is one for which an analytical expression relating the viscosity, stress, and shear rate can be written, whether or not the material is Newtonian.)

The B-S model incorporates a feedback mechanism that adjusts the lower dashpot clearances to accommodate for the type of non-Newtonian flow involved (usually a power law flow for the stress-shear rate relation).

Other investigators have verified the power law relation for asphalts by measuring shear rate in the constant shear stress apparatus previously described (8). Figure 4 shows a typical set of experimental curves obtained in the apparatus at several force levels measured by movement (or creep) down the tube. This movement, convertible to shear deformation, consists of three phases. The first phase, almost instantaneous and shown as the top spring (Hooke) of Figure 1, is the elastic deformation (Y_a); the second phase is a curve that connects the first and third phases; and the third phase is the terminal permanent deformation, shown by the lower dashpot in Figure 1 and the constant rate ($\dot{Y}_o$) in Figure 4.

The connecting second phase of each line in Figure 4 is the delayed elastic plus the viscous flow of the Kelvin body as diagramed in Figure 1. It also includes the initial viscous flow of the lower dashpot at short times. In general, this curved section is only a minor portion of the total deformation movement. The slopes of the straight part of the creep curves vary with stress in Figure 4. If this variation is not directly proportional to stress, the material is non-Newtonian and will necessitate the use of the feedback control mechanism on the lower dashpot of Figure 1.

Force is converted to shear stress and movement rate to shear rate in order to provide the data for the shear rheogram in Figure 5, which is based on the Ostwald-de Waele power law concept (7) for the relation

$$\log \tau_i = \log \tau_1 + C \log \dot{\gamma}_i \quad (1)$$

in pascals, where shear stress (τ_1) at any shear rate ($\dot{\gamma}_1$) is a constant multiplied by $\dot{Y}_o$; τ_1 is the value of τ_1 at $\dot{\gamma}_1$ equals 1 s^{-1}; and C is the rheogram slope that describes shear susceptibility.

Figure 2. Schematic diagram of constant stress rheometer.

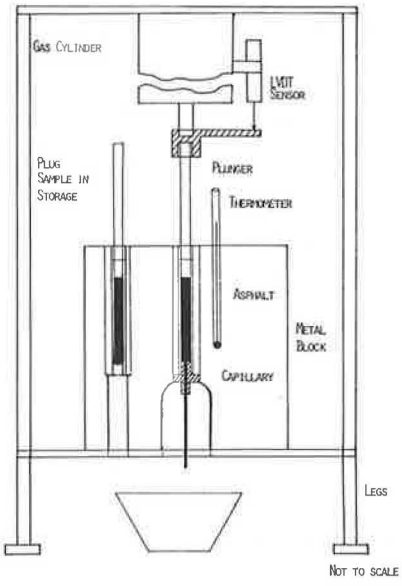

Thus

$$\tau_i = \tau_1 \dot{\gamma}_i^C \quad (2)$$

and the validity of Equation 2 is confirmed by the plot in Figure 5. The apparent viscosity (η_a) is defined as

$$\eta_a = \tau_i / \dot{\gamma}_i \quad (3)$$

in pascals per second, so the apparent viscosity at any shear rate ($\dot{\gamma}_1$) may be written for a power law fluid as

$$\eta_i = \eta_1 \dot{\gamma}_i^{C-1} \quad (4)$$

where η_1 is a characteristic reference viscosity at $\dot{\gamma}$ equals 1 s^{-1}, as has been discussed in detail previously (8).

Equation 4, therefore, permits the calculation of viscosity at any shear rate, when C is known and the material follows the power law relation of Equation 2. The magnitude of C is obtained from the slope of Figure 5 and controls the signal to the feedback control of Figure 1. This depends on the particular shear rate that develops under the applied stress rate, which in turn depends on the characteristic viscosity (η_1) of the material. If the material is a Newtonian fluid, C equals 1, and the apparent viscosity is constant at any rate of shear (or shear stress). For materials that are shear thinning, the value of C is less than 1.

The preceding discussion provides the information needed to understand the stiffness evaluation diagram in Figures 6 and 7 at the extended time levels. This confirms the need for the B-S model. In the log plot of Figure 5, the straight line demonstrates the applicability of Equation 1 and is the basis for the concept in Figure 1 of a dashpot with variable clearance that accommodates the response of shear rate to stress for non-Newtonian materials. (A Newtonian material would have a slope of 1 in Figure 5.)

Figure 3. Third generation design of rheometer.

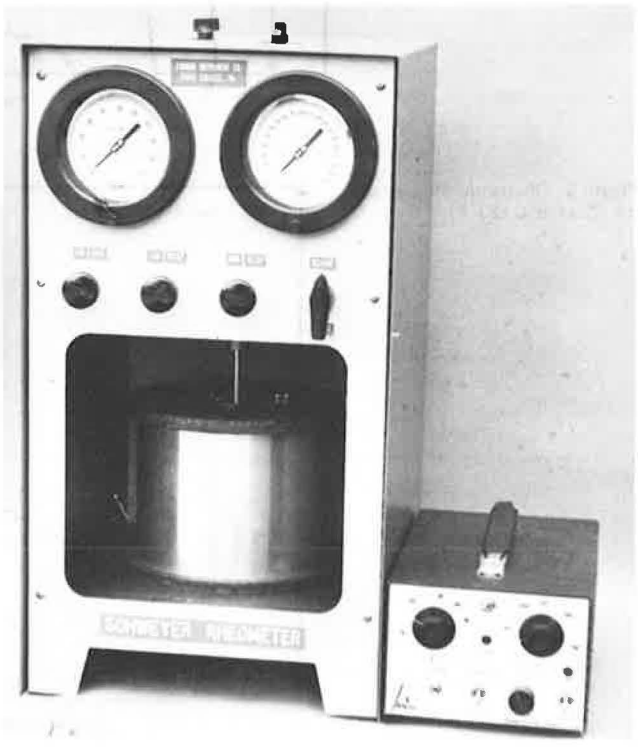

VISCOELASTIC STIFFNESS

As discussed, the stiffness (S) property is defined quite simply as the stress divided by the cumulative normalized deformation (strain) at any given time. Thus, when computing total cumulative strain, all deformations for a chart such as in Figure 4 must be corrected for the sample length.

The system stiffness as evaluated in a particular apparatus with sample length (L) may be defined as a function of time (t), shear rate ($\dot{\gamma}$), and temperature (T) as follows:

$$S'_{t,\dot{\gamma},T} = \text{stress}/[(Y_a/L) + (Y_b/L) + (Y_c/L)] = \tau \Big/ \int_0^t \frac{\dot{Y}\,dt}{L}$$

$$= \frac{L\tau}{\text{total deformation}}\Bigg|_{t,\dot{\gamma},T} \qquad (5)$$

in pascals, where the three strains—elastic (Y_a/L), delayed (Y_b/L), and viscous (Y_c/L)—correspond to the three parts of each curve in Figure 4. [The total deformation per unit of stress, when normalized for the sample geometry, is the compliance (J) in reciprocal pascals and therefore is the reciprocal of the stiffness.]

The total normalized deformation for the model in Figure 1 is defined mathematically from the classic model discussed earlier in detail (8) at a given stress (τ) as

$$Y/L = \tau/G_1 + (\tau/G_2)(1 - e^{-t/t_K}) + \dot{Y}_c\, t/L \qquad (6)$$

where

G_1 = shear modulus of elasticity;
G_2 = shear delayed modulus of elasticity;

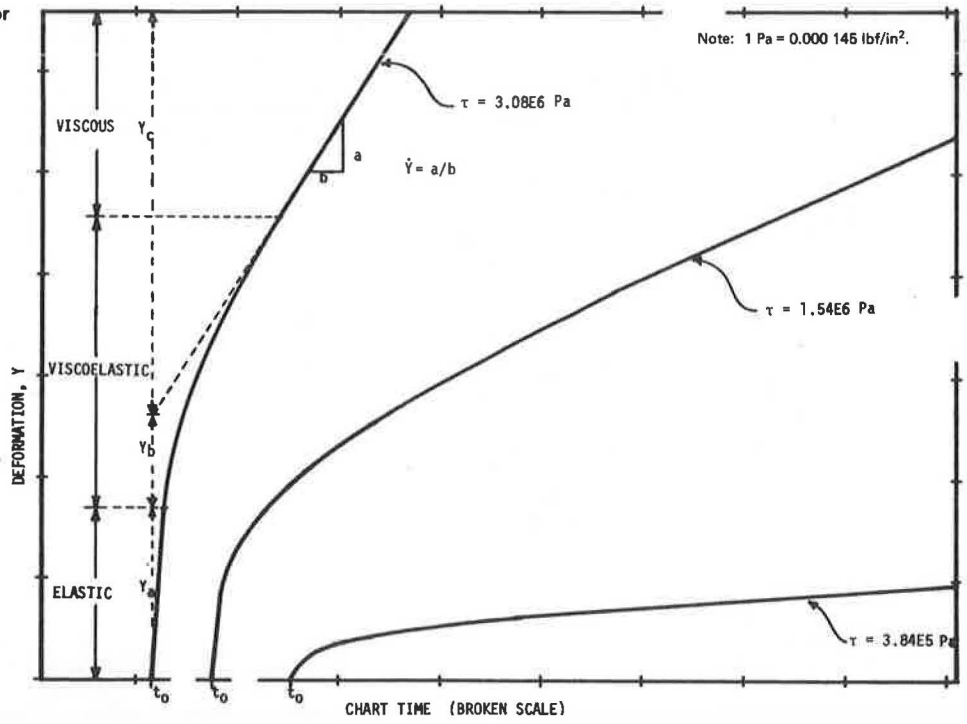

Figure 4. Shear creep curves for asphalt no. 22 at -5°C (23°F).

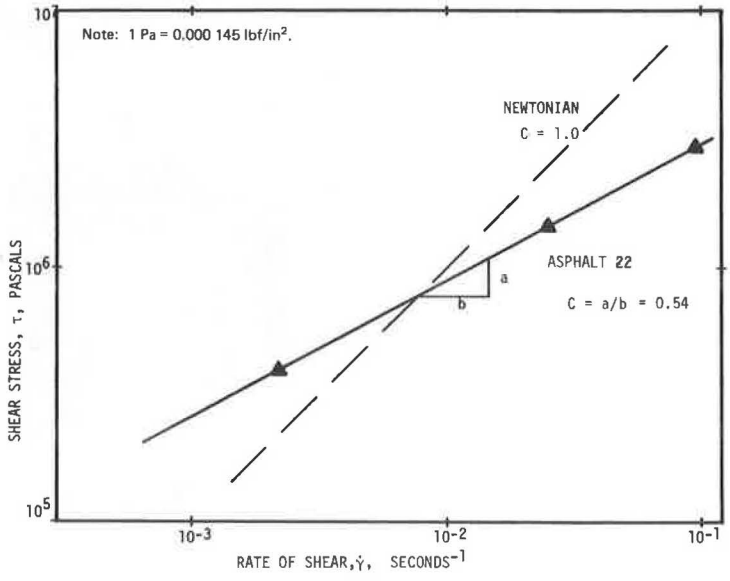

Figure 5. Rheogram for asphalt no. 22 at -5°C (23°F).

t = time (with t_k as a time constant equal to η_2/G_2 where η_2 is the Newtonian viscosity of the Kelvin body);
$\dot{Y}_o$ = constant creep deformation rate (dY_o/dt); and
L = the original sample length.

Although the experimental confirmation of this equation has been shown for bitumen (8), the last term of Equation 6 involves a shear rate $\dot{Y}_c$, which is a function of the geometry of the sample.

An isothermal, isostress working equation is

$$S'_{t,\dot{\gamma},T} = \left.\frac{L\tau}{Y_a + Y_b + Y_c}\right|_t \qquad (7)$$

Thus the observed stiffness (S′) is readily computed from the observed total deformations. All strains, having been normalized by the sample length (L), are dimensionless.

The deformation (Y_a) is the elastic deformation that, theoretically, occurs instantaneously. However, because of machine lags, the experimental line has a less

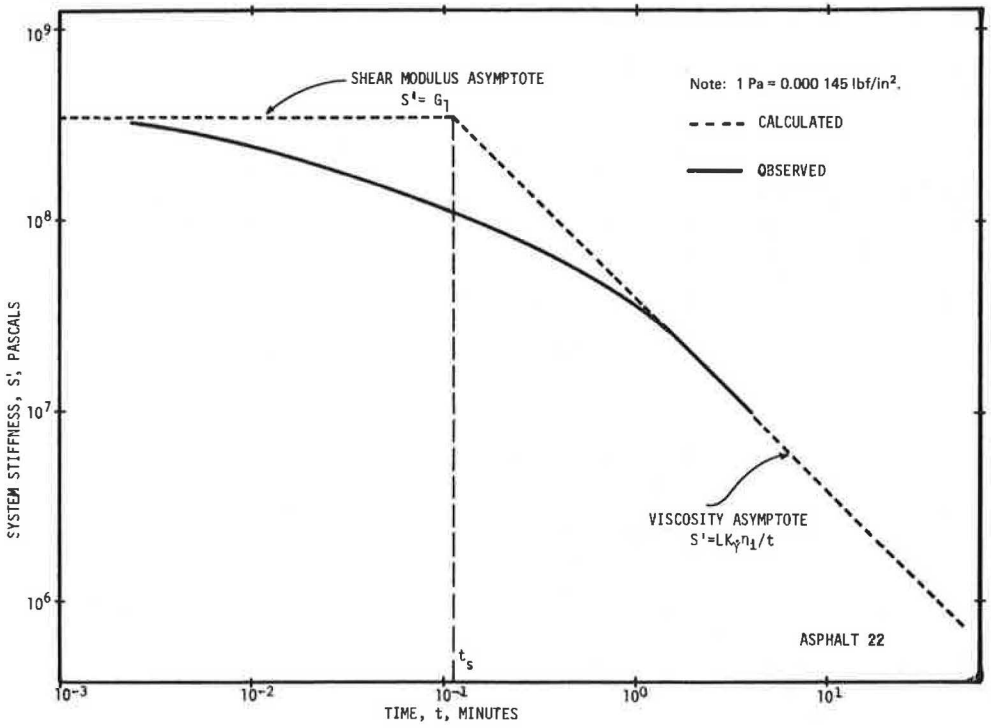

Figure 6. System stiffness at $\dot{\gamma}$ = 0.025 s^{-1} and -5°C (23° F).

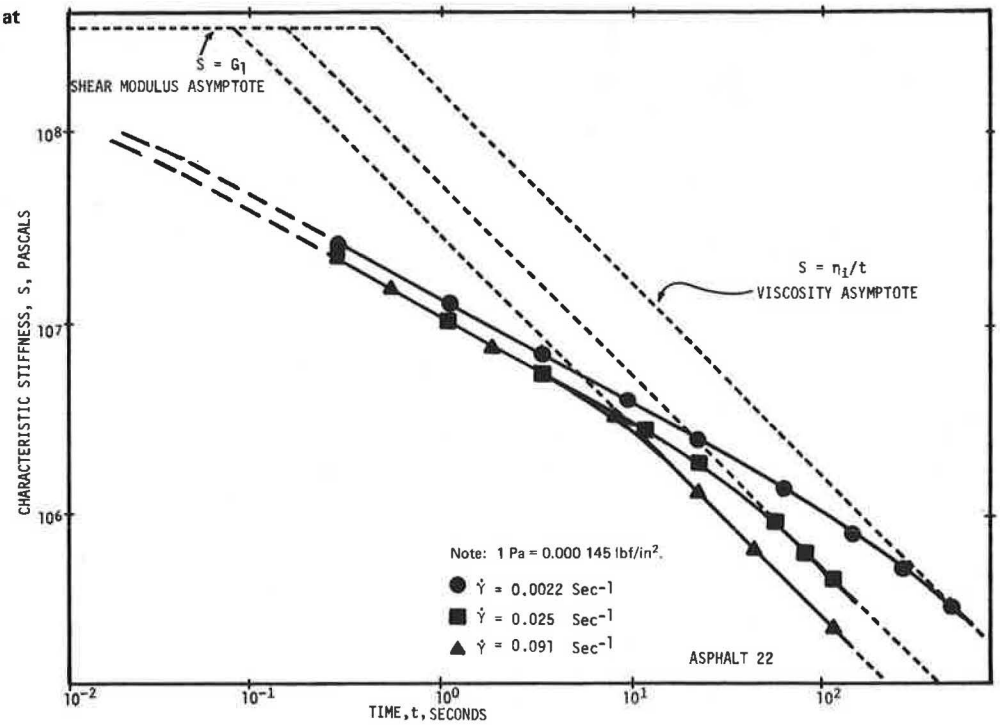

Figure 7. Characteristic stiffness at -5°C (23°F).

than infinite slope. A straightedge is placed on the initial experimental lines of Figure 4, and the initial point of curvature is marked to define Y_a. The shear elastic modulus (G_1) may then be computed in pascals from

$$G_1 = L\tau/Y_a \tag{8}$$

This is shown in Figure 6 as the horizontal asymptote for all stresses.

In general, the delayed elastic deformation (Y_b) contributes little to the total viscoelastic evaluation (Figure 4). Y_b represents a decreasing proportion of total deformation with increasing time (Figure 6) as stiffness approaches the viscosity asymptote.

The viscous deformation (Y_o) of Equation 7 is a very important element in stiffness studies. As shown in Figures 1 and 4, as elapsed time lengthens greatly above zero, permanent deformation (creep) becomes the only changing component of total deformation. In Figure 6 the system stiffness (S′) at extended times approaches a limiting slope of -1. This has been observed by others and is a result of the total viscous deformation in terms of Equation 6 being $Y_o = \dot{Y}_o t$. Since the apparent viscosity controls the deformation rate ($\dot{Y}_o$), it is possible to equate stiffness with viscosity at times much greater than zero, or, from Equations 4 and 6,

$$S'_{t>>0} \approx L\tau/Y_c = L\tau/Y_c t = L\tau_i K_{\dot{\gamma}}/\dot{\gamma}_i t = LK_{\dot{\gamma}}\eta_i/t \tag{9}$$

where η_i is the apparent viscosity at a shear rate of $\dot{\gamma}_i$ equals $K_{\dot{\gamma}}\dot{Y}_o$ when $K_{\dot{\gamma}}$ is a shear rate conversion factor and $\dot{Y}_o$ is a system deformation rate.

The viscosity relation of Equation 9 was shown by van der Poel (1) for Newtonian materials, but the implications for a model with shear susceptibility, as in the B-S model of Figure 1, have not been shown in the literature as far as we know.

The system stiffness (S′) of Equation 9 includes the constants L and $K_{\dot{\gamma}}$, which describe the geometry of the system and determine the quantitative amount of deformation that will vary from system to system. However, the material property of stiffness should be described as independent of the system, if one wants to tabulate its value for use in any geometric arrangement. Accordingly, we suggest that the term "characteristic stiffness" be used to describe this material property.

The characteristic stiffness (S), distinguished from the system value by lacking a prime sign, is obtained by correcting the system stiffness (S′) for the machine geometry factor ($LK_{\dot{\gamma}}$). This produces a change in value, but it makes the stiffness for $t >> 0$ a direct approximate function of the viscosity as shown in Equation 10 and in Figure 6 for the viscosity asymptote, as Y_a and Y_b of Equations 5 and 7 become less significant in the total deformation, and

$$S_{t,\dot{\gamma},T\ t>>0} \approx S'_{t,\dot{\gamma},T}/(LK_{\dot{\gamma}}) = \eta_i/t \tag{10}$$

Thus, it will be observed that stiffness at a given temperature is a cumulative function based on cumulative deformation, whereas shear viscosity is based on a deformation rate (in shear). But the two are related through time.

The obvious simplicity of Equation 10 permits computation of the characteristic stiffness directly from the time of interest and the viscosity. If the material is Newtonian (C = 1), the shear rate is immaterial; otherwise the correct viscosity (η_i) at a selected shear rate must be used in Equation 10. These variations can be incorporated directly into Equation 10 by using Equation 4 and shear susceptibility (C). Thus

$$S_{t,\dot{\gamma},T\ t>>0} \approx \eta_i \dot{\gamma}_i^{C-1}/t \tag{11}$$

becomes a working equation. If this characteristic stiffness is to be employed for design purposes or for correlations with deformations required in specific units, the appropriate factors for converting the characteristic stiffness to the system behavior must be incorporated into a modified Equation 11. The characteristic stiffness of Equation 11 is shown in Figure 7 and is reported in Table 2 for the properties of the asphalts in this paper.

Starting with Equation 11 and plotting as in Figure 7 for the long time isothermal characteristic stiffness at any rate of shear ($\dot{\gamma}_i$) or its associated stress (τ_i),

$$\text{Log } S_{t\ t>>0} = -\log t + \log(\eta_i \dot{\gamma}_i^{C-1}) \tag{12}$$

which is the equation that each of the viscosity asymptotes of Figure 7 fits. Because the particular stiffness plot desired must be defined by the rate of shear ($\dot{\gamma}_i = \tau_i/\eta_i$, $1\ s^{-1}$), one should compare the stiffness of different materials at a common rate of shear (such as $\dot{\gamma}_i = 0.05\ s^{-1}$ or $1\ s^{-1}$). The former is usually in the practical testing rate range, so we suggest it be a suitable datum value.

It will be observed from Figure 7 that any particular asymptote in the viscous region for a given shear rate intercepts the horizontal G_1 asymptote at a specific time. This intersection, called stiffness "limit time," is of special interest for tabulation. Its value varies with the material, temperature, and shear rate; for discussion purposes it is shown as a dotted line for a shear rate of $\dot{\gamma}_{05}$ equals $0.05\ s^{-1}$.

The time (t_s) of intersection can be obtained algebraically by equating the initial stiffness (or shear modulus) (G_1 of Equation 8) to the stiffness at long times at a given shear rate (Equation 10). Thus

$$t_s = \eta_i/G_1 \tag{13}$$

in seconds. This particular time could be a specification parameter for the material when the shear rate $\dot{\gamma}_i$ is selected.

The values of t'_s (as for S′) are affected by the geometry of the system. Therefore, in order to obtain an observed t'_s in a specific system, the t_s of Equation 13 must be corrected in minutes for that geometry, or

$$t'_s = LK_{\dot{\gamma}} t_s \tag{14}$$

These terms, as used in this paper, may be summarized as in the following table, where we chose minutes as time units in $K_{\dot{\gamma}}$ to simplify converting the measured deformation rate.

Term	System Value	Characteristic Value
Stiffness for $t >> 0$ in seconds	$S' = LK_{\dot{\gamma}}\eta_i/t$	$S = \eta_i/t$
Equation number	9	10
Measurement unit	Pascals	Pascals
Stiffness limit time	$t'_s = LK_{\dot{\gamma}}\eta_i/G_1$	$t_s = \eta_i/G_1$
Equation number	14	13
Measurement unit	Minutes	Seconds
Viscosity at any $\dot{\gamma}$	$\eta_i = \eta_1 \dot{\gamma}_i^{C-1}$	$\eta_i = \eta_1 \dot{\gamma}_i^{C-1}$
Equation number	4	4
Measurement unit	Pascal-seconds	Pascal-seconds
Shear modulus for $t \to 0$	$G_1 = L\tau/Y_a$	$G_1 = L\tau/Y_a$
Equation number	8	8
Measurement unit	Pascals	Pascals
Stiffness for $t \to 0$	$S' = G_1$	$S = G_1$

As we pointed out in the beginning of this section, the system stiffness must be used whenever one wants to

Table 2. Rheological profiles of selected asphalts.

Asphalt Sample No.	Type	Temperature (°C)	Shear Susceptibility	Shear Modulus (MPa)	Viscosity (MPa)	Characteristic Stiffness[a] (MPa)	Stiffness Limit Time (t_s)
9	Canadian (P77/V103.4)[b]	-5	0.76	709	125	256	0.361
		0	0.74	515	79.6	173	0.336
		5	0.66	283	5.16	14.3	0.051
		15	0.90	–	1.25	1.69	–
		25	0.92	–	0.079	0.1	–
12	Air blown (P68/V396)	-5	0.52	179	11.1	46.8	0.261
		0	–	–	–	–	–
		5	0.56	116	1.34	5.02	0.043
		15	–	–	–	–	–
		25	0.65	–	0.065	0.187	–
17	High viscosity (P29/V304)	-5	0.73	350	1670	3860	11
		0	0.76	326	565	1160	3.56
		5	0.64	290	72.9	217	0.748
		15	0.61	241	4.9	15.6	0.065
		25	0.66	–	0.654	1.84	–
22	Midcontinent (P93/V208)	-5	0.54	346	10	39.6	0.115
		0	0.55	218	3.77	14.1	0.065
		5	0.56	135	2.1	7.1	0.053
		15	–	–	–	–	–
		25	0.67	–	0.077	0.206	–
39	Propane (P99/V99.3)	-5	0.82	437	78.7	135	0.309
		0	0.70	308	30.3	74.5	0.242
		5	0.77	207	4.06	8.09	0.039
		15	–	–	–	–	–
		25	1.00	–	0.006	0.059	–
42	Heavy Arabian (P84/V218)	-5	0.75	586	72.7	154	0.363
		0	0.67	438	13.5	36.3	0.083
		5	0.69	334	4.75	12	0.036
		15	–	212	–	–	–
		25	0.93	–	0.12	0.152	–
47	Californian (P83/V102)	-5	0.81	677	194	343	0.507
		0	0.79	525	46.3	92.2	0.176
		5	0.80	359	8.71	15.9	0.044
		15	1.00	–	2.4	2.4	–
		25	1.01	–	0.075	0.075	–
62	High viscosity (P62/V981)	-5	0.70	531	600	1470	2.77
		0	0.60	395	87.7	288	0.729
		5	0.63	279	32.7	98.8	0.354
		15	0.65	151	4.79	13.7	0.091
		25	0.53	–	0.569	2.37	–

Note: 1 Pa = 0.000 145 lbf/in^2; t°C = (t°F - 32)/1.8; 1 MPa = 145 lbf/in^2.

[a] Characteristic stiffness ($S_{t,05}$) in pascals, at 1 s and a shear rate of 0.05 s^{-1}, and 1.0 s, numerically equals viscosity (η_{05}) in pascal-seconds. [b] Refers to viscosity at 60°C.

obtain absolute deformation values in different geometries. Also, it should be noted that, if the material is considered incompressible, the concept of viscous traction as proposed by Trouton (13) and explained in detail by Reiner (7) can be used to relate all three shear deformations of Equations 5 and 7 to their corresponding axial values in tension or compression by multiplying by 3 (provided the material acts as a Newtonian material). Thus

$$S_{t,\dot{\gamma},T}\Big|_{axial} = 3S_{t,\dot{\gamma},T}\Big|_{shear} \quad (15)$$

However, the real material requires consideration of compressibility and non-Newtonian flow. For the present, we assume the general relation is valid for tensile stress and strain and shear viscosity of a Newtonian incompressible fluid. Based on Reiner (7) for a Poisson ratio ν equals 0.5, the shear viscosity can be expressed as η equals $\tau/\dot{\gamma}$, or shear stress divided by shear rate; the axial viscous traction, then, is λ equals $\sigma/\dot{\epsilon}$, or axial stress divided by strain rate. Thus

$$\eta = \lambda/[2(1 + \nu)] = \lambda/3 \quad (16)$$

The remainder of this paper will deal with the experimental results summarized in Table 2.

EXPERIMENTAL RESULTS

In a previous paper (8), the validity of Equation 6 was demonstrated with experimental data (Figure 8). The superimposed points were calculated from the parameters drawn from raw data. The last term of Equation 6 differentiates between the B-S and the standard Burgers model, where $\dot{Y}_o$ is a function of stress and shear susceptibility for a given asphalt and temperature, as shown in Equations 1 and 2 and confirmed in Figure 5 for a power law fluid at the stress ranges reported.

As an example of analytical procedures, possible methods of data reporting, and fit of the experimental data to the model, a complete rheological study of one sample (no. 22 asphalt) is shown in Figures 4, 5, 6, 7, 9, 10, and 11.

The isothermal shear creep response of the midcontinent sample is shown in Figure 4 at three different stress levels. The steady-state response ($\dot{Y}_o$) at several different stresses obtained from Figure 4 is then converted to shear rate ($\dot{\gamma}_t$) and is used in the standard rheogram of Figure 5.

If the plot of log shear stress versus log shear rate is linear, then the material fits the Ostwald-de Waele power law model (7). Further, if the slope of the linear plot is not equal to 1, then the material is non-Newtonian. Thus the slope gives the shear susceptibility (C). As can be seen in Table 2, the value of the shear susceptibility of the asphalts tested ranged from a low of 0.52 for the air-blown asphalt to a high of 1.0+ for the Californian asphalt.

The stiffness is approximated by dividing viscosity by time at extended times, so the effect of shear susceptibility on both viscosity and stiffness is also demonstrated. This extreme variation in viscosity and stiffness with shear rate confirms the necessity of the B-S modification to the Burgers model (Figure 1).

Figure 8. Shear creep curves at different stresses.

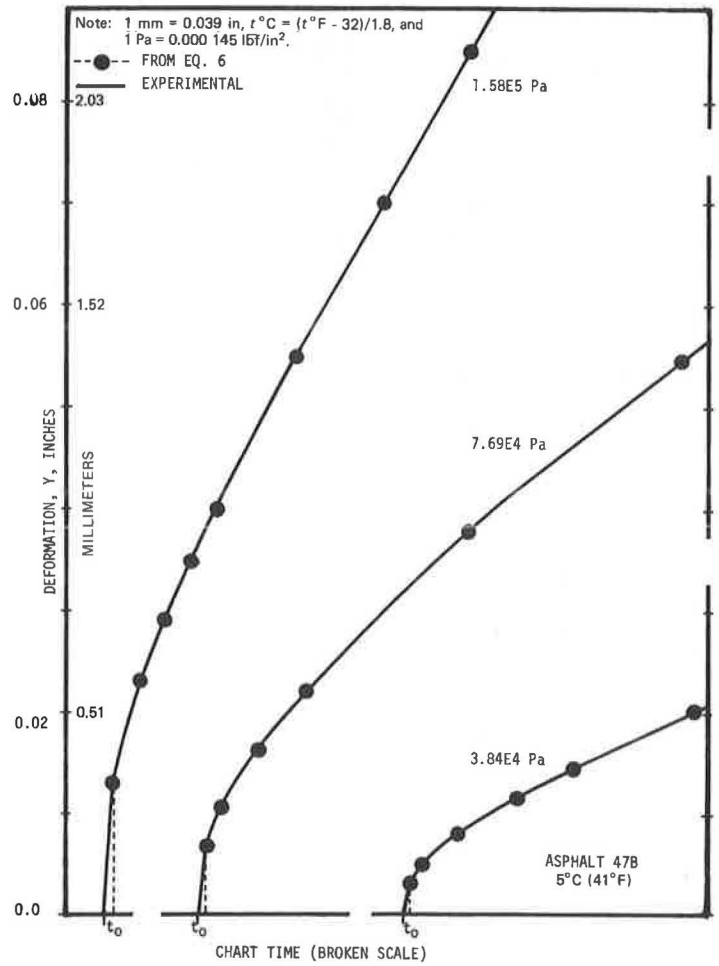

Figure 9. Viscosity for temperature susceptibility at $\dot{\gamma} = 1\ s^{-1}$.

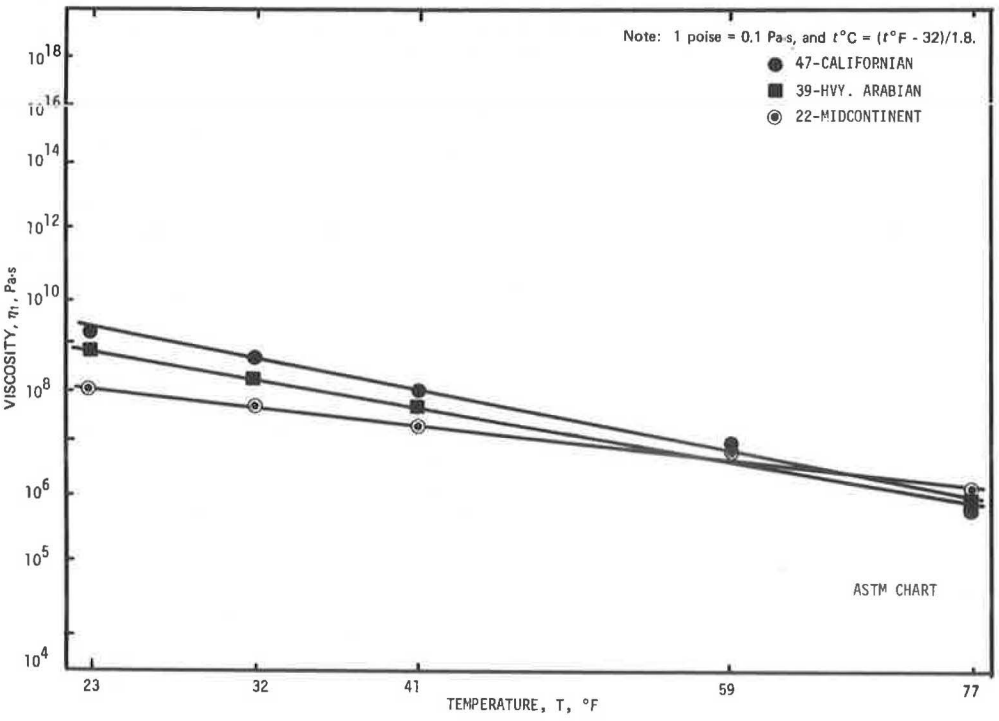

In 1972 Duthie (14), in proposing specifications for low temperature stiffness based on dynamic measurements and an empirical shear susceptibility, indicated that a "shear modulus, G," is a function of the shear rate at a finite time. However, this is somewhat misleading, because the basic concept of a characterizing modulus is one that uses only instantaneous deformation.

Figure 6 demonstrates the system stiffness (S′) for no. 22 asphalt at one rate of shear. The observed values obtained from Figure 4 and Equation 5 approach the asymptotic values predicted by Equations 8 and 9. It must be noted that Equation 9, which describes the viscosity asymptote, contains geometric constants that are not characteristics of the sample. These constants are introduced when deformation rate is converted to shear rate for the particular geometry of the system that normalizes the data.

The characteristic stiffness shown in Figure 7 for the same shear rate differs from the system stiffness of Figure 6 only in that the geometric constants have been divided out, leaving the sample-related responses G_1 (shear modulus) and η_1 (apparent viscosity). Thus, the stiffness for one geometry can be compared with that of any other geometry. Figure 7 also shows the shear susceptibility of the characteristic stiffness calculated from Equations 8 and 11 and observed from the creep response of Figure 4. The observed data approach the viscosity asymptote, but the machine capabilities we used only provide approximate measurements below 0.5 s, and the elasticity asymptote is not reached.

The standard reference viscosity (η_1, or viscosity at a shear rate of 1 s^{-1}) has been plotted in Figure 9 for three asphalts, including no. 22, on a standard ASTM viscosity-temperature chart. Characteristic and system stiffness at 1 s and long times approximates the viscosity at a given shear rate, so the plots also show the stiffness variation with temperature. It must be noted that, although there is little difference in viscosity between these asphalts at 25°C (77°F), their temperature susceptibilities may differ and yield quite different responses at lower temperatures.

Table 2 gives data on other asphalts, and it is interesting to note that these can be separated into two groups according to the raw ratio of their viscosity at 25°C to that at 60°C (140°F). This is an empirical temperature susceptibility, as shown in Table 3. There is quite an appreciable difference between the two groups in their shear stiffness values at -5°C (23°F) and also in their shear susceptibilities (C). It would appear that the low C values indicate low stiffness and vice-versa.

This C will also be directly related to the β of Jongepier and Kuilman (15), who used an isoviscosity temperature to generalize dynamic data on bitumens, and to the β of Dickinson and Witt (16), who used an empirical approach to generalize dynamic data based on a hyperbolic model. Dobson (17) employed the ratio of log (V25/V60) (the log of the ratio shown in Table 3) to estimate a "b" parameter for generalizing the temperature-viscosity data and the dynamic shear modulus, which may also be related to the C in Table 3.

A generalized temperature susceptibility plot of the characteristic stiffness for no. 22 asphalt is shown in Figure 10 for a shear rate standardized at 0.05 s^{-1}. This rate was selected to fall in the range in which experimental results are usually obtained. Gaw (18) reported stiffness data based on sliding plate measurements from -20 to 10°C (-4 to 50°F) on selected soft asphalts at 0.5-h intervals.

Table 3. An analysis of stiffness at -5°C (23°F).

Asphalt No.	Type	Viscosity Ratio* (Pa·s)	Shear Modulus (MPa)	Shear Susceptibility (-5 to 25°C)	Stiffness (MPa)
9	Canada	1198	709	0.66/0.92	256
22	Midcontinent	48	346	0.54/0.67	39.6
39	Propane	792	437	0.77/1.0	135
42	Heavy Arabian	333	586	0.67/0.93	154
47	Californian	735	677	0.79/1.0+	343
48	Air blown	28	179	0.52/0.65	46.8

Note: 1 Pa·s = 0.67 lbf·s/ft²; 1 MPa = 145 lbf/in²; and t °C = (t °F - 32)/1.8.
*V25/V60, or viscosity at 25°C at $\dot{\gamma}$ = 1 s^{-1} and 60°C.

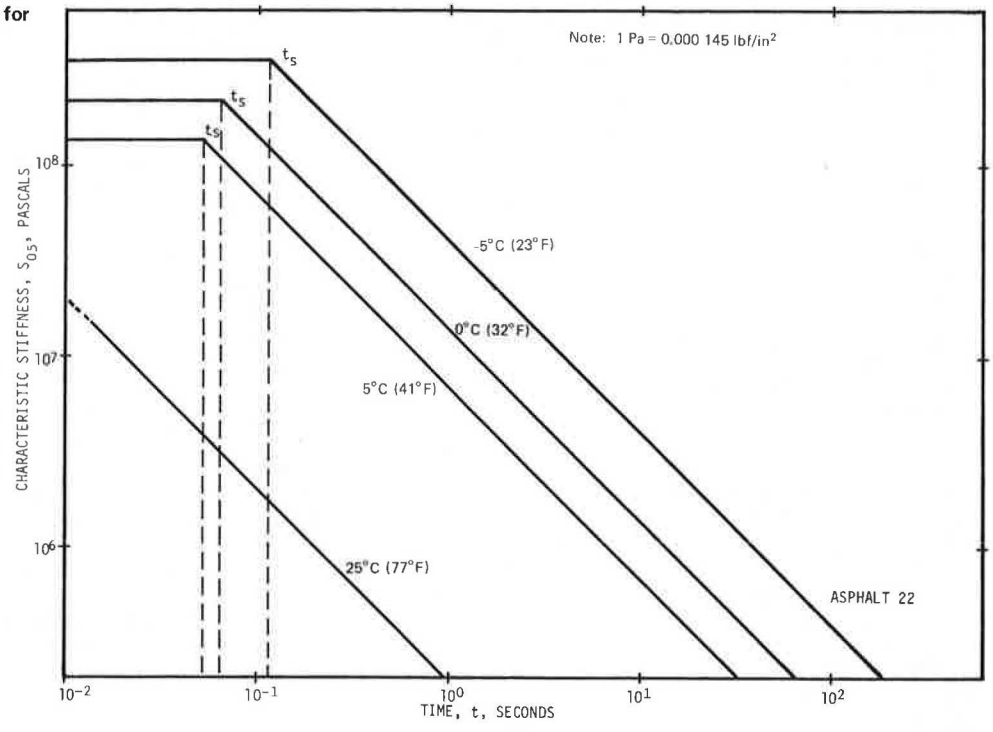

Figure 10. Characteristic stiffness for temperature susceptibility at $\dot{\gamma}$ = 0.05 s^{-1}.

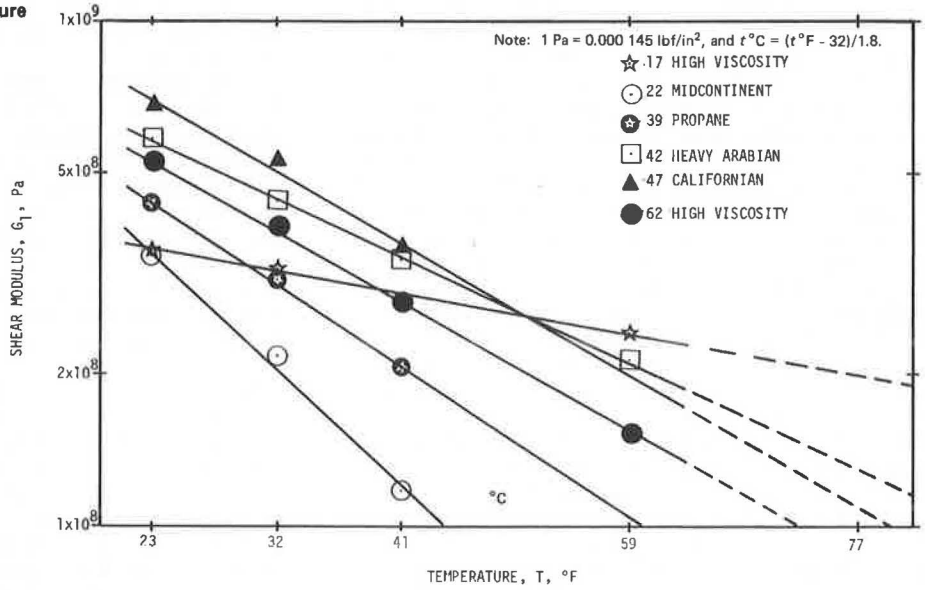

Figure 11. Shear modulus for temperature susceptibility.

In Figure 11, the temperature susceptibility of the shear modulus is illustrated as a power law relation of the absolute temperature T in degrees Rankine

$$\log G_1 = \log G_1^\dagger + M_G \log T \qquad (17)$$

where $G_1^\dagger$ is a reference point (at T = 1) and M_G is the slope of the plot. Thus

$$G_1 = G_1^\dagger T^{M_G} \qquad (18)$$

in pascals. There appear to be quite large differences in the temperature susceptibility of the shear modulus among the six asphalts shown in Figure 11. This is a measure of the short time stiffness response, but this susceptibility is small compared with the temperature susceptibility of the viscosity (or the long time stiffness response) (Table 2). The Rankine scale was selected in Figure 11 to agree with the ASTM viscosity chart.

A modified least squares fit to the data shown in Figure 11 was used to obtain the parameters for Equation 18 shown below, where $G_1^\dagger$ (1 MPa = 145 lbf/in^2) is a mathematical parameter that delineates the line in Figure 11 by stating the value of G_1 at 0.5 K (1°R).

Asphalt Sample No.	Type	log $G_1^\dagger$ (MPa)	M_G
9	Canadian	70.2	-25.1
12	Air blown	34.1	-11.9
17	High viscosity	16.8	-5.3
22	Midcontinent	71.6	-25.7
39	Propane	57.4	-20.4
42	Heavy Arabian	40.6	-14.1
47	Californian	49.3	-17.3
62	High viscosity	50.0	-17.6

The slope (M_G) of the plot is a direct measure of the temperature susceptibility of the shear modulus. The midcontinent asphalt no. 22 is approximately five times more susceptible than the high viscosity asphalt no. 17.

If all asphalts are considered to have the same temperature susceptibility, then the material with a higher viscosity at 60°C (140°F) would be expected to have the higher stiffness at the lower temperatures. That this is not the case is shown for asphalts 22 and 39 in the preceding tabulation (see also Table 2 and Figure 11, where the shear modulus is the same as stiffness at short times).

Gaw gives evidence substantiating the difference in temperature susceptibility of viscosity and stiffness among different asphalts. Gaw also studied the effect of asphalt aging on stiffness and compared some experimental data with the predictions of van der Poel's nomograph.

Van der Poel (7) suggests that Young's modulus (E) for traction approaches asymptotically to a limit of about 3000 MPa. This might be true in a region below the glass transition temperature, but all evidence shows that, on asphalts tested above their glass transition temperatures, the relation shown in Equation 18 is applicable over a large temperature range.

The value of $G_1^\dagger$ of Equation 18 (as the standard reference viscosity, η_1) is a fictitious value of the shear modulus unless it falls in the range where Equation 18 is valid. Its primary purpose is to provide a correlation capable of predicting the shear modulus in the range of testing temperatures.

Saal and Labout (5) showed that the stiffness of a 50-penetration asphalt at a loading time of 0.0008 s varies with reciprocal temperature in a manner similar to that predicted by Equation 17 over a range of 0 to 100°C (32 to 212°F). At this short loading time, the value of stiffness corresponds to the elastic modulus. Saal and Labout gave a stiffness value at these short times that ranged from 600 MPa at -50°C to 0.012 MPa at 100°C. The asphalts tested in Table 2 show stiffness values at short times (shear modulus) that ranged from 116 MPa at 5°C to 709 MPa at -5°C. This range of values for the modulus appears to be consistent with that previously reported by van der Poel (7), Brown, Sparks, and Smith (19), Gaw (18, 20), and Dorman and Jarman (21).

Haas (22) compared the various methods available for indirectly estimating the stiffness of bitumen and included the van der Poel nomograph with Pfeiffer and Van Doormaal and "corrected" penetration index, the Heukelom and Klomp (23) modified nomograph with both penetration indices, and McLeod's method. Gaw found for an asphalt of 192 penetration at 25°C (77°F) that the value for stiffness at 10 000 s and -20°C (-4°F) varied from 0.0396 to 9.9 MPa and showed some discrepancies among these methods (18).

The use of a simple, generalized chart for stiffness of asphalt cements based on sound rheological experi-

mental data at low ambient temperatures would be a useful tool for asphalt technologists. The concept of a confluence point of the shear modulus asymptote (G_1) and the viscosity asymptote as given by Equation 13 and shown in Figure 10 is suggested as a potential correlating parameter. Such a correlation is being studied (24) with t_s in a generalized time-temperature-source relation based on Equations 4, 8, 13, and 18.

CONCLUSIONS

From these studies we conclude that

1. Viscoelasticity can be evaluated by tube flow geometries for shear strain elastic moduli and shear viscosities to obtain shear characteristic stiffness;
2. In the constant stress rheometer at nominal stress ranges for asphalt cements, the flow follows the power law relation for shear susceptibility at low ambient temperatures as evidenced by experimental data;
3. Based on the preceding conclusion, the suggested B-S model of Figure 1 with feedback control appears to be a valid phenomenological model; and
4. For the asphalts reported herein, the relation between the stiffness (shear elastic modulus) and the Kelvin (absolute Rankine) temperatures approximates the following form over the range of 268 to 298 K (483 to 537°R or 23 to 77°F)

$$G_1 = G_1^{\dagger} T^{M_G} \qquad (18)$$

Because of the great importance of shear susceptibility and temperature susceptibility at low ambient temperatures, we hope that future studies on stiffness will use direct measurements over these temperature ranges. Future work in this area should aim toward establishing the significance of the bitumen stiffness in specifications insofar as it affects mix design and service characteristics.

ACKNOWLEDGMENT

We acknowledge the financial assistance of the Florida Department of Transportation in supporting, in part, the research presented in this paper.

REFERENCES

1. L. W. Nijboer and C. van der Poel. A Study of Vibration Phenomena in Asphaltic Road Constructions. Proc., AAPT, No. 197, 1953, p. 22.
2. P. G. Nutting. A New General View of Deformation. Journal of the Franklin Institute, Vol. 191, 1921, p. 679.
3. P. G. Nutting. A Study of Elastic Viscous Deformation. Proc., ASTM, Vol. 21, 1921, p. 1162.
4. P. G. Nutting. A General Stress-Strain-Time Formula. Journal of the Franklin Institute, Vol. 235, 1943, p. 513.
5. R. N. J. Saal and J. W. A. Labout. Rheology. F. R. Eirich, ed., Academic Press, New York, Vol. 2, 1958.
6. C. van der Poel. Building Materials. M. Reiner and A. G. Ward, eds., Interscience Publishers, New York, 1954.
7. M. Reiner. Deformation, Strain and Flow. H. K. Lewis Co., London, 3rd Ed., 1969.
8. H. E. Schweyer, R. L. Baxley, and A. M. Burns, Jr. Low Temperature Rheology of Asphalt Cements: I. ASTM, STP Vol. 628, No. 1, 1976.
9. C. van der Poel. A General System Describing the Visco-Elastic Properties of Bitumens and Its Relation to Routine Test Data. Journal of Applied Chemistry, Vol. 4, 1954, p. 221.
10. G. W. Nederbrogt. The Properties of Asphaltic Bitumen With Special Reference to Its Technical Application. J. P. Pfeiffer, ed., Elsevier, Houston, 1950.
11. D. Ronk. Compressibility and Expansivity of Asphalts. Univ. of Florida, master's thesis, 1968.
12. H. E. Schweyer, L. L. Smith,and G. W. Fish. A Constant Stress Rheometer for Asphalt Cements. Proc., AAPT, Vol. 45, 1976, p. 53.
13. F. T. Trouton. On the Coefficient of Viscous Traction and Its Relation to That of Viscosity. Proc. Royal Society, Vol. A77, 1906, p. 426.
14. J. L. Duthie. Proposed Bitumen Specifications Derived From Fundamental Parameters. Proc., AAPT, Vol. 39, 1972, p. 70.
15. R. Jongepier and B. Kuilman. Characteristics of Rheology of Bitumens. Proc., AAPT, Vol. 38, 1969, p. 98.
16. E. J. Dickinson and H. P. Witt. The Dynamic Shear Modulus of Paving Asphalt as a Function of Frequency. Trans., Society of Rheologists, Vol. 18, 1974, p. 591.
17. G. R. Dobson. The Viscoelastic Properties of Asphaltic Mixes. Institute of Petroleum Rept. No. IP76-004, 1976.
18. W. J. Gaw. Measurement and Prediction of Asphalt Stiffness and Their Use in Developing Specifications to Control Low Temperature Pavement Transverse Cracking. ASTM, STP, Vol. 628, 1976, p. 57.
19. A. B. Brown, J. W. Sparks, and F. M. Smith. Viscoelastic Properties of a High-Consistency Asphalt. Journal of Colloid Science, Vol. 12, 1957, p. 283.
20. A. B. Brown and J. W. Sparks. Viscoelastic Properties of a Penetration Grade Paving Asphalt at Winter Temperature. Proc., AAPT, Vol. 27, 1958, p. 35.
21. G. M. Dorman and A. W. Jarman. Some Factors Influencing the Behavior of Bitumen Road Surfaces. Journal of Applied Chemistry, Vol. 8, 1958, p. 832.
22. R. C. G. Haas. Asphalt Institute Research Rept. No. 73-1, 1973.
23. W. Heukelom and A. J. G. Klomp. Road Design and Dynamic Loading. Proc., AAPT, Vol. 33, 1964, p. 92.
24. A. M. Burns. Stiffness of Asphalt Cements. Univ. of Florida, master's thesis, 1977.

Publication of this paper sponsored by Committee on Characteristics of Bituminous Materials.

Engineering Evaluation of Sulphur-Asphalt Mixtures

Thomas W. Kennedy, Council for Advanced Transportation Studies, Department of Civil Engineering, University of Texas at Austin
Ralph Haas, Department of Civil Engineering, University of Waterloo, Ontario
Phil Smith, Staff Engineer, ARE, Inc., Austin, Texas
G. A. Kennepohl and E. T. Hignell, Research and Development Department, Gulf Oil Canada Limited, Toronto

A comprehensive laboratory testing program was conducted as a part of an engineering evaluation of sulphur-asphalt paving mixtures. The purpose was to see (a) if sulphur-asphalt mixtures have better engineering properties than similar conventional asphalt mixtures and (b) what effects various sulphur-asphalt mixture variables and testing variables produce. Static and repeated load indirect tensile tests were used to evaluate these engineering properties: fatigue life, resilient modulus of elasticity, and tensile strength. The major factors evaluated were asphalt consistency in terms of penetration, type of asphalt in terms of temperature susceptibility, binder content, sulphur-asphalt ratio, stress level, and test temperature. The results indicated that sulphur-asphalt mixtures exhibit significantly better engineering properties, in terms of the above three, than comparable asphalt mixtures. All these engineering properties were significantly improved by the use of up to 50 percent sulphur. In addition, using sulphur-asphalt binders can improve the stiffness and fatigue characteristics of softer asphalts. Additional field and laboratory work to verify potential economic and structural benefits of using sulphur-asphalt mixtures is recommended.

The benefits of using sulphur in conventional paving mixtures have been successfully demonstrated in field trials during the past few years (1,2). A sulphur-asphalt binder must be produced by high shear rate mixing of liquid sulphur with liquid asphalt and no additives, using a patented process (2). This binder, in which a part of the asphalt normally used has actually been replaced by sulphur, is then used in a conventional manner with conventional equipment for mix production, transport to the job site, placing, and compaction. Because of the potential economy of replacing part of the asphalt with sulphur, which will be abundant for some years to come, the process has attracted attention from both user agencies and industry.

Field trials have demonstrated the full-scale construction capability of the process, but continued laboratory experiments and periodic in-service performance measurements remain to be done. Therefore, we conducted a comprehensive laboratory testing program to answer these two basic questions: Do sulphur-asphalt mixtures have better, equal, or inferior engineering properties than similar mixtures with asphalt alone? What are the effects of various sulphur-asphalt mixture and testing variables?

Sulphur-asphalt mixtures and comparable mixtures with asphalt alone were evaluated for their engineering properties: (a) tensile strength, (b) resilient modulus of elasticity, and (c) fatigue life.

The purpose of this paper is to report the results of the laboratory experiments and the potential implications of these results.

TEST METHOD

The basic test method was the static and repeated load indirect tensile test, in which a cylindrical specimen is loaded with a single or repeated compressive load that acts parallel to and along the vertical diametral plane. This loading configuration develops a relatively uniform tensile stress perpendicular to the direction of the applied load and along the vertical diametral plane. This stress ultimately causes the specimen to fail by splitting along the vertical diameter. Loads were transmitted to the specimen through a 19-mm (0.75-in) wide, curved loading strip.

In the repeated load tests, the specimens were subjected to a 1.0 Hz load pulse applied for 0.1 s and followed by a 0.9-s rest period (Figure 1). During testing, the resulting horizontal deformations were recorded on a light-beam oscillograph. The equipment used for the repeated load tests is shown in Figure 2.

First we established tensile strength and then used this information to generate fatigue life versus stress relations, under dynamic loading. Stress was chosen as a percentage of the strength. Resilient modulus of elasticity was measured as a part of the dynamic testing for fatigue life.

Because of the unique nature of the sulphur-asphalt binder, the foregoing sequence was applied to a num-

Figure 1. Load pulse and associated deformation data for repeated load indirect tensile test.

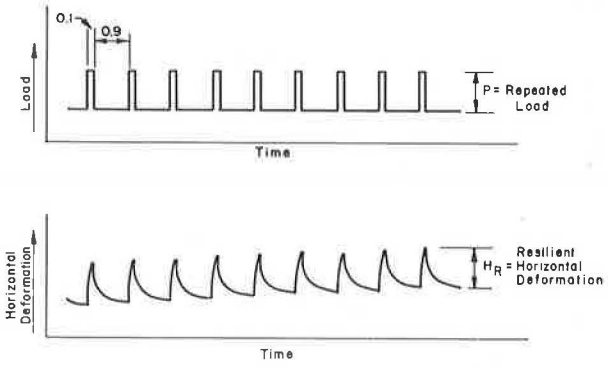

Figure 2. Laboratory equipment used in repeated load tests.

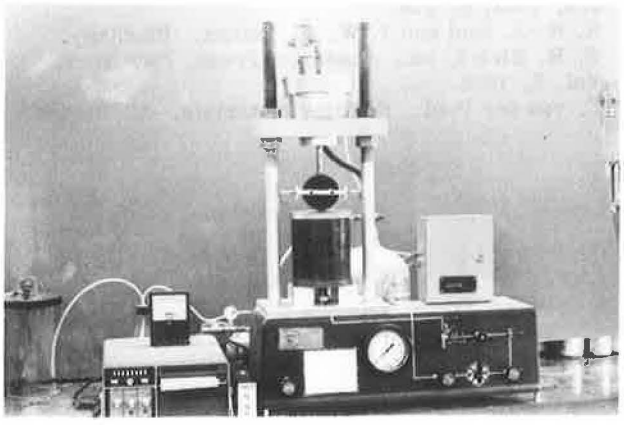

ber of possible combinations of variables in order to define as clearly as possible the binder's use limitations.

Tensile Strength

The tensile strength (S_T) is the horizontal tensile stress (σ_T) produced by the maximum load, or the load at failure, and can be calculated by using Hardy, Hudson, and Kennedy's equation (3):

$$S_T = (2P/\pi ah)(\sin 2\alpha - a/2R) \quad (1)$$

where

S_T = indirect tensile stress in megapascals,
P = total vertical load applied to the specimen in newtons,
a = width of the loading strip in millimeters,
h = height of the specimen at the beginning of the test in millimeters,
2α = angle at the center of the specimen subtended by the width of the loading strip in radians, and
R = radius of the specimen in millimeters.

The primary purpose of conducting tensile strength tests was to establish stress levels for subsequent fatigue testing.

Resilient Modulus of Elasticity

The resilient modulus of elasticity (E_R) is related to the recoverable, or resilient, deformation (H_R) (Figure 1) and can be calculated from the following equation (4) by assuming a value for Poisson's ratio.

$$E_R = (P/H_R h)(\nu + 0.27) \quad (2)$$

where

E_R = resilient modulus of elasticity in megapascals,
P = repeated load in newtons,
H_R = recoverable horizontal deformation in millimeters,
h = height of specimen in millimeters, and
ν = Poisson's ratio.

Values of Poisson's ratio can theoretically range from 0 to 0.50 and can vary with temperature, stiffness, and stress level. A review of past studies suggested that we could reasonably assume that Poisson's ratio varied from 0.18 to 0.50 for the testing temperature range of 10 to 52°C (50 to 125°F).

Fatigue Life

Fatigue life is the number of load applications required for the specimen to completely fail. Because fatigue life is obviously a function of the magnitude of the applied stress, the results are often expressed in terms of the logarithmic relation between stress and fatigue life, which for asphalt mixtures is generally linear. Although it is possible that this linearity does not exist for sulphur-asphalt mixtures, we considered it acceptable for the purposes of our investigation. This relation for the indirect tensile test can be expressed as

$$N_f = K_2(1/\sigma_T)^{n2} = K_2'(1/\Delta\sigma)^{n2} \simeq K_2'(1/4\sigma_T)^{n2} \quad (3)$$

where

N_f = fatigue life in cycles to failure,
σ_T = repeated tensile stress,
$\Delta\sigma$ = stress difference or deviator stress,
n_2 = slope of the logarithmic relation,
K_2 = antilog of the intercept of the logarithmic relation between N_f and σ_T, and
K_2' = antilog of the intercept of the logarithmic relation between N_f and $\Delta\sigma$.

The form, based on stress difference, partially accounts for the biaxial state of stress present in the indirect tensile test. The value $4\sigma_T$ approximates the stress difference, or deviator stress, that acts on the center element.

EXPERIMENT DESIGN

The major factors incorporated into the design were

1. Asphalt consistency at two levels: 40/50 and 85/100 penetration grades. These two grades represent a medium and a hard asphalt cement, respectively, and should provide an estimate of the importance of consistency.
2. Temperature susceptibility at two levels: low and high viscosity. Asphalts from two different crude sources in Alberta and Saskatchewan were obtained. The characteristics of the asphalts are summarized elsewhere (6).
3. Binder content at four levels: 6.0, 6.5, 7.0, and 8.0 percent by weight. The range included the optimum binder content obtained by the Marshall method, which allowed nonlinear behavior to be evaluated.
4. Sulphur-asphalt ratio at three levels: 0/100, 20/80, and 50/50. This allowed nonlinear behavior to be evaluated. We could also determine whether the addition of sulphur improved the engineering properties of the final mixtures.
5. Test temperature at four levels: 10, 24, 38, and 52°C (50, 75, 100, and 125°F). The majority of the tests were conducted at 10, 24, and 38°C; a limited number were conducted at 52°C and provided an estimate of behavior at high temperatures.
6. Tensile stress at two levels: low and high. In order to characterize the fatigue behavior (stress-fatigue relations), it was necessary to test at least two stress levels and to assume a linear logarithmic relation. Because of the wide temperature range, it was impossible to use the same two stress levels for all four temperatures. Therefore, two stress levels were used but were defined as high and low stress-to-strength ratios. The high ratio was selected as 35 percent and the low ratio as 24 percent.

These factors are described in more detail and the combinations shown elsewhere (6).

MATERIALS AND SPECIMENS

The specimens, 102 mm (4 in) in diameter and 51 mm (2 in) thick, were produced by the Research and Development Department of Gulf Oil Canada Limited. We tested 180 specimens statically for strength and 198 under repeated loads for resilient modulus of elasticity and fatigue life.

These specimens were prepared according to ASTM D-1559 and mechanically compacted at 60 blows per face [(6) contains data on aggregate gradation and Marshall test results].

The optimum binder contents as determined by the Marshall methods were 6.0 percent by weight for the conventional asphalt mixtures, 6.5 percent for the 20/80 sulphur-asphalt mixtures, and 8.0 percent for the 50/50 sulphur-asphalt mixtures.

DISCUSSION OF RESULTS

Fatigue Life

Fatigue lives were difficult to analyze in their "raw" form, because the various combinations of variables produced specimens with different tensile strengths. We therefore applied a different absolute stress level of each test or combination of variables, which normalized the actual fatigue lives. Fatigue behavior was expressed as a linear relation between the logarithm of fatigue life and the logarithm of stress (Equation 3). These relations were generally parallel and had similar n_2 values.

By extrapolating or interpolating these relations, it was possible to obtain an estimated fatigue life for a high tensile stress of 490 kPa (71 lbf/in^2 and for a low tensile stress of 331 kPa (48 lbf/in^2), which were the average of the high and low stresses used at 24°C (75°F).

Values of n_2 and K_2' (6) can be used to predict fatigue cracking in actual pavement structures by applying certain computerized design and analysis systems (the U.S. Federal Highway Administration's VESYS IIM system). They can also be used to estimate the fatigue life of a given pavement structure, under given conditions, using elastic layer analysis to calculate stresses.

An analysis of variance conducted on the estimated fatigue lives at 331 and 490 kPa indicated that, in addition to the effect of stress, fatigue life was significantly affected by sulphur-asphalt ratio, penetration of the asphalt cement, and temperature.

Effect of Sulphur-Asphalt Ratio

The addition of sulphur increased the fatigue life of the mixtures, but the nature of the increase is uncertain.

As shown in Figure 3, the fatigue lives for the mixtures containing 50 percent sulphur at a stress of 331 kPa were generally greater than for the conventional mixtures. In some cases the effect of adding 20 percent sulphur was inconsistent, in that the fatigue lives were actually somewhat lower than for 0 percent sulphur. However, all of these lower fatigue lives are well within the limits of experimental error, and it is quite possible that, under field conditions, mixtures with 0 and 20 percent sulphur would have similar fatigue lives. The estimated fatigue relations at 490 kPa were essentially the same (6).

Figure 4 shows the effect of temperature on fatigue life. As might be expected, temperature is a very dominant factor. However, the major point of interest of Figures 3 and 4 is that the use of 50 percent sulphur has an effect similar to that achieved by decreasing the penetration from 85/100 to 40/50.

Effects of Temperature and Penetration

Penetration is also shown in Figure 4 to be a major factor, especially at the lower temperatures. The 40/50 penetration asphalt exhibits a significantly longer fatigue life. Thus, for controlled stress tests similar to those conducted in this study or for thick pavement sections, fatigue life would be expected to increase significantly with decreased temperature and decreased penetration.

Effect of Binder Content

In this study, binder content was not significant. However, the range was not large and the effects of binder content were very erratic. Nevertheless, we can conclude that there was an optimum for maximum fatigue

Figure 3. Relation between estimated fatigue life and sulphur content for mixtures subjected to low tensile stress.

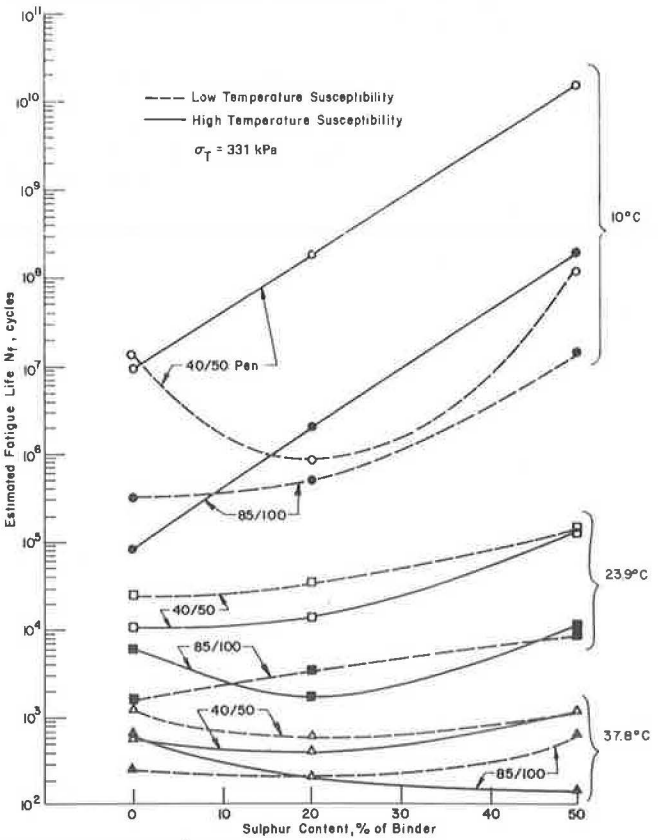

Note: 1 kPa = 0.145 lbf/in^2 and $t°C = (t°F - 32)/1.8$.

Figure 4. Relation between fatigue life and temperature for sulphur-asphalt mixtures subjected to low stress.

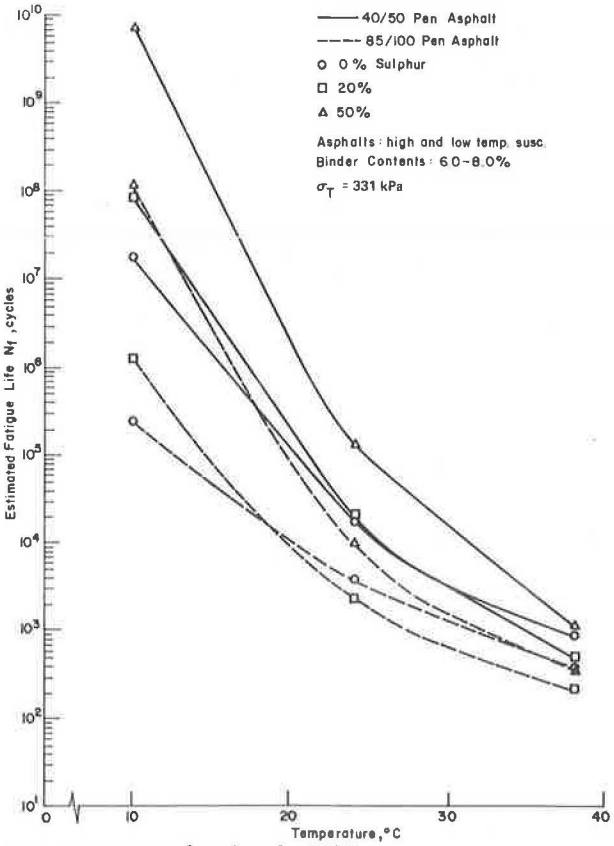

Note: 1 kPa = 0.145 lbf/in^2 and $t°C = (t°F - 32)/1.8$.

life and that this optimum was larger than the optimum for maximum strength. This finding would be consistent with the normal mix design approach of using sufficient binder for durability.

Summary of Fatigue Life Results

The addition of more than 20 percent sulphur produced a significant increase in fatigue life, whereas the increase produced by adding 50 percent sulphur was approximately equal to that by using a 40/50 rather than an 85/100 penetration asphalt.

There is an optimum binder content for maximum fatigue life, and it is somewhat greater than the optimum for maximum strength or resilient modulus of elasticity.

Resilient Modulus of Elasticity

The sulphur-asphalt mixtures exhibited higher stiffnesses, in terms of resilient moduli of elasticity, than the conventional asphalt mixtures. In general, moduli values ranged from 145 000 to 19 500 000 kPa (21 000 to 2 830 000 lbf/in^2); the actual values depended on sulphur-asphalt ratio, penetration of the asphalt cement, and temperature, each of which produced highly significant effects.

Binder content had a relatively small effect for the range considered, and stress level and temperature susceptibility had no effect. A number of interaction effects involving two or more factors were also found to be statistically significant but to have no practical engineering importance.

Effect of Sulphur-Asphalt Ratio

The addition of sulphur produced a substantial increase in stiffness in terms of resilient modulus of elasticity (Figure 5). Twenty percent sulphur did not significantly increase the modulus of the sulphur-asphalt mixtures containing the 85/100 penetration asphalt, but the addition of 50 percent sulphur produced a substantial increase. For the 40/50 penetration asphalt, at 10 and 24°C (50 and 75°F), the addition of 20 percent sulphur produced a substantial increase. This would suggest an interaction effect involving sulphur content, penetration of the asphalt, and temperature.

Effects of Temperature and Penetration

Temperature was again a dominant factor, as might be expected, and produced approximately 75 percent of the total observed variation. As shown in Figure 6, most of the increase occurred between 10 and 24°C.

Mixtures with the 40/50 penetration asphalt, again as might be expected, were much stiffer than those with the 85/100 penetration asphalt (Figures 5 and 6). The absolute magnitude of the difference was much larger at the lower testing temperatures, although the relative magnitude of the difference was much larger at the higher temperatures.

Effect of Binder Content

For maximum resilient modulus of elasticity, there seemed to be an optimum binder content of less than 6 percent in many cases, which is similar to the optimum for maximum strength. In addition, the modulus did not appear to be sensitive to small changes in binder content within the range of values investigated.

Summary of Modulus Results

The addition of sulphur produced a significant increase in stiffness in terms of resilient modulus of elasticity. Generally, this increase required the addition of 50 percent sulphur, although in a few cases 20 percent sulphur produced a substantial increase.

The optimum binder content for maximum resilient modulus of elasticity was not well defined but appeared to be 6 percent or less. However, higher binder contents, which are more consistent with mix durability considerations, only resulted in a marginal decrease in modulus.

Figure 5. Relation between resilient modulus of elasticity and content.

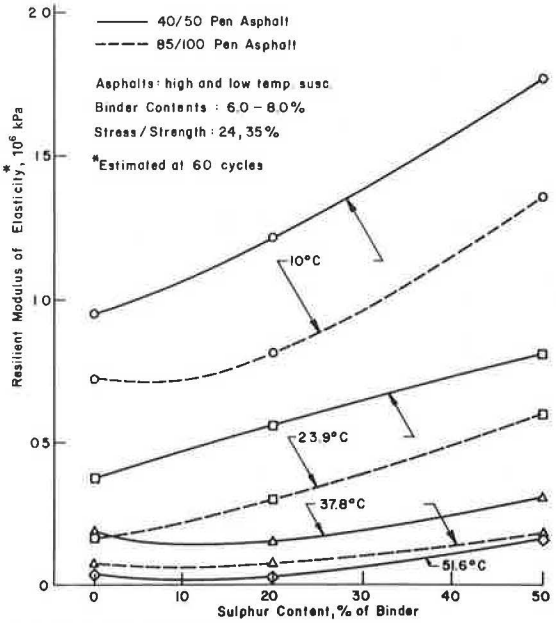

Note: 1 kPa = 0.145 lbf/in^2 and $t°C = (t°F - 32)/1.8$.

Figure 6. Relation between resilient modulus of elasticity and temperature.

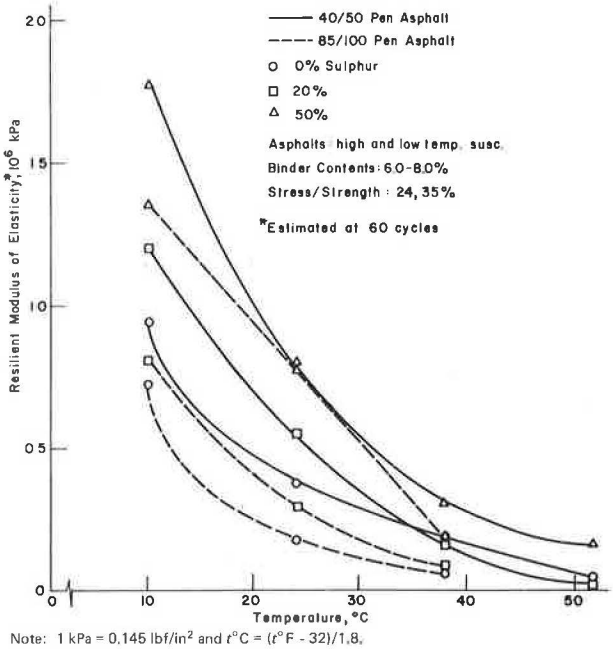

Note: 1 kPa = 0.145 lbf/in^2 and $t°C = (t°F - 32)/1.8$.

Tensile Strength

The strengths of the sulphur-asphalt mixtures were higher than the strengths of the conventional mixtures. Strength values ranged from 103 to 4650 kPa (15 to 674 lbf/in^2) and were found by analysis of variance to be significantly affected by sulphur-asphalt ratio, penetration of the asphalt cement, and temperature. The binder content was also found to influence strength, but only slightly.

Strengths did not depend on the type of asphalt, as identified by temperature susceptibility. In addition, there were numerous interaction effects, many of which involved temperature. However, in a practical sense, there was no real engineering significance.

Effect of Sulphur-Asphalt Ratio

As shown in Figures 7 and 8, there was little, if any, increase in strength produced by adding 20 percent sulphur. However, the addition of 50 percent sulphur resulted in a significant increase in strength and had the same effect as decreasing the penetration from 85/100 to 40/50 penetration (Figure 7).

Thus, the addition of sulphur is beneficial in terms of strength. Furthermore, although the addition of 20 percent sulphur did not improve the strength of the mixtures, the asphalt content and thus the potential cost were lowered without a loss of strength. The addition of 50 percent brought cost savings and significantly increased strength.

Effects of Temperature and Penetration

Temperature, as expected, had the greatest effect on the strength values (Figure 7) and accounted for approximately 88 percent of the strength differences. This increase in strength should continue with decreasing temperature until the strength of the aggregate becomes the determining influence.

Only about 5 percent of the total variation was caused by the change in penetration. The 40/50 pentration asphalt cements produced signficantly stronger mixtures than the 85/100 penetration asphalts.

Effect of Binder Content

Strength was not sensitive to binder content within the range tested, except possibly at lower temperatures. The results suggest an optimum binder content that appears to have been less than 6 percent in many cases. Strength, however, is not the controlling factor. In addition, low total binder content can adversely affect factors such as durability.

Relation Between Tensile Strength and Marshall Stability

There was no strong relation between Marshall stability and tensile strength, although there did appear to be some general trends for a given temperature and asphalt penetration. These differences, in terms of penetration, tended to diminish as the test temperature increased and approached the temperature used with the Marshall test [-60°C (-140°F)]. At best, it can only be said that mixtures with high Marshall stabilities tended to have higher tensile strengths.

Summary of Strength Test Results

The addition of 20 percent sulphur did not increase the strength, but the addition of more than 20 percent increased strength significantly. The increase produced by adding 50 percent sulphur was approximately

Figure 7. Relation between tensile strength and temperature.

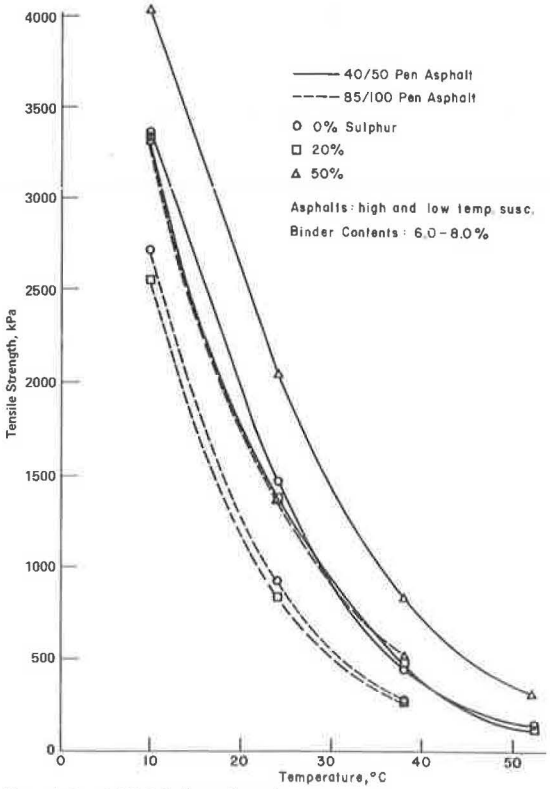

Note: 1 kPa = 0.145 lbf/in^2 and $t°C = (t°F - 32)/1.8$.

Figure 8. Relation between tensile strength and sulphur content.

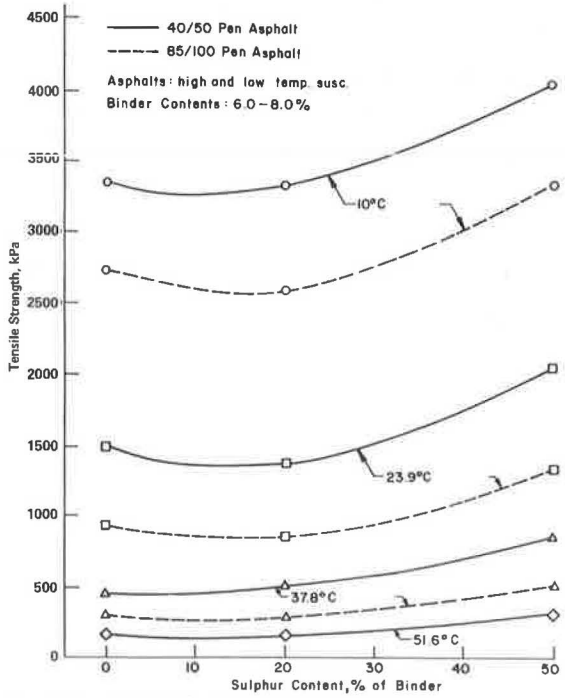

Note: 1 kPa = 0.145 lbf/in^2 and $t°C = (t°F - 32)/1.8$.

equal to that achieved with a 40/50 rather than an 85/100 penetration asphalt cement.

An optimum binder content for maximum strength exists but, again, is not well defined, and a change in binder content for the range evaluated had little, if any, effect on strength.

There was no significant relation between indirect tensile strength and Marshall stability.

POTENTIAL BENEFITS OF SULPHUR-ASPHALT MIXTURES

The use of sulphur-asphalt binders in paving mixtures has potential benefits in terms of economy, resource conservation, and improved pavement performance.

The economic benefits can result from replacing a portion of more expensive material, asphalt, with a less expensive and more plentiful material, sulphur. In some areas of North America, sulphur is substantially less expensive than asphalt. In other areas, however, shipping costs may make sulphur nearly as expensive as asphalt. Nevertheless, the long-term benefits of sulphur use are based on stable costs because of relative abundance. In addition, increased use of low-grade, high sulphur content coal for electric power generation and the removal of substantial quantities of sulphur from the Alaskan crude oils could add significantly to projected North American sulphur supplies.

Asphalt can be conserved as a resource by partially replacing it with sulphur. In view of dwindling petroleum reserves, it is possible that at some future time the demand for asphalt may exceed both raw supply and the capacity of refineries to produce it.

Pavement performance can be improved in terms of increased fatigue life for thick sections, as indicated by the stress-controlled fatigue testing of this investigation. Of course, this must be verified by field observations. For thinner sections, some caution may be required, especially where very stiff sulphur-asphalt mixtures are used on a weak foundation, which could result in a thin, stiff slab effect.

Fortunately, the pavement designer has considerable flexibility in tailoring a sulphur-asphalt mixture to the particular design situation. Both sulphur-asphalt ratio and grade of asphalt can be varied to modify the temperature susceptibility of the mix, thereby adapting it to a very wide range of in-service temperature, load, and foundation conditions (5).

CONCLUSIONS

The results of this experimental program indicate that sulphur-asphalt mixtures exhibit significantly better engineering properties than conventional mixtures. Fatigue life in a stress-controlled testing, resilient modulus of elasticity, and tensile strength were significantly improved by the addition of up to 50 percent sulphur. The effects produced by various mixture and test variables have been summarized and illustrated.

Further work with sulphur-asphalt mixtures seems well justified in terms of both engineering properties and potential cost effectiveness. This work should identify the combinations of pavement layer materials, thicknesses, and subgrade conditions where sulphur-asphalt mixtures can be demonstrated to have clear economic and performance advantages.

ACKNOWLEDGMENTS

The project on which this paper was based was supported by Gulf Oil Canada Limited. This support and general cooperation are gratefully acknowledged. The efforts of Mr. Laverne Miller of Gulf Oil in producing specimens are also appreciated.

The Transportation Research Board does not endorse products or manufacturers. Trade names appear in this report because they are considered essential to its object.

REFERENCES

1. G. J. A. Kennepohl, A. Logan, and D. C. Bean. "Conventional" Paving Mixes With Sulphur-Asphalt Binders. Proc., AAPT, 1975.
2. B. J. A. Kennepohl. The Gulf Canada Sulphur-Asphalt Process for Pavements. Proc., Symposium on New Uses of Sulphur and Pyrites, Madrid, 1976.
3. W. O. Hadley, W. R. Hudson, and T. W. Kennedy. A Method of Estimating Tensile Properties of Materials Tested in Indirect Tension. Center for Highway Research, Univ. of Texas at Austin, Research Rept. 98-7, July 1970.
4. G. Gonzalez, T. W. Kennedy, and J. N. Anagnos. Evaluation of the Resilient Elastic Characteristics of Asphalt Mixtures Using the Indirect Tensile Test. Center for Highway Research, Univ. of Texas at Austin, Research Rept. 183-6, Dec. 1975.
5. F. R. P. Meyer, E. T. Hignell, G. J. A. Kennepohl, and R. Haas. Temperature Susceptibility Evaluation of Sulphur-Asphalt Mixtures. Paper presented to AAPT, San Antonio, Feb. 1977.
6. T. W. Kennedy, P. Smith, and R. Haas. An Engineering Evaluation of Sulphur-Asphalt Mixtures. Austin Research Engineers, Contract Rept. GC-1, June 1976.

Publication of this paper sponsored by Committee on Characteristics of Bituminous Paving Mixtures to Meet Structural Requirements.

Design, Construction, and Performance of Asphalt Friction Courses

Prithvi S. Kandhal, Raymond J. Brunner, and Thomas H. Nichols,
Bureau of Materials, Testing, and Research, Pennsylvania
Department of Transportation

During 1969 to 1971, eight test pavements of open-graded asphalt friction courses were constructed in Pennsylvania. Details of design, construction, and performance of these pavements are discussed. Four test pavements incorporating two aggregate types and control sections of dense-graded bituminous surface were constructed in 1974 near Philadelphia. The asphalt friction courses were designed according to the Federal Highway Administration procedure modified in terms of asphalt mixing viscosities. The performance of the 1974 test pavements is evaluated every 6 months by obtaining skid test data at three speeds, by measuring air permeability, and by determining the average surface texture depths. Interim data obtained so far suggest that a minimum air void content of 25 percent is necessary to maintain the desired permeability that is lost in most pavements from traffic action and clogging by debris. A highly skid-resistant gravel aggregate was used for this project in the asphalt friction course and the dense-graded surface course. After 1½ years' service, the skid-speed gradient of both pavements is almost equal and approaches 0.45. In the case of dolomite aggregate (medium skid resistance), the asphalt friction course has a substantially lower speed gradient compared to the dense-graded surface course. These tests are being continued to study long-range performance and durability.

High-speed rubber-tired vehicles operating on wet pavements can experience a hazardous phenomenon known as hydroplaning. A layer of water on the pavement causes the tire to lose contact with the pavement surface. The result is the vehicle's loss of maneuverability and braking capability.

Obviously, we must devise some method to remove the water from the pavement surface. Open-graded asphalt friction courses (also called open-graded plant-mix seal coat and porous friction course, among others), which are high-void bituminous mixtures placed on existing pavement surfaces in thin layers [nominally 19 mm (¾ in)], have been used to drain surface water through their porous structures. In addition to reducing the risk of hydroplaning, asphalt friction courses are believed to have several other advantages (1), such as improved skid resistance at higher speeds during wet weather, minimized wheel path rutting, minimized splash and spray during wet weather, lowered highway noise levels, improved visibility of painted traffic markings, and retarded ice formation on the surface.

A survey of the literature (2,3,4,5,6,7,8,9) reveals that several agencies have used this type of asphalt surfacing, but with different mix compositions and mix design methods (Table 1). Evidently, this resulted in both success and failure in the construction and performance of the open-graded mixes, but the experience gained has helped develop suitable interim specifications and design methods for such applications. It is with this intent that the experience of the Pennsylvania Department of Transportation (PennDOT) with the design, construction, and performance of asphalt friction courses is being reported in this paper.

TEST PAVEMENTS, 1969 TO 1971

Eight separate projects (Table 2) were constructed in Pennsylvania between September 1969 and September 1971. In September 1969, 22.4 km (14 miles) of two-lane pavement were constructed and an additional 6.2 km (3.9 miles) in June 1970 in the north central region, and, in September 1971, 7.2 km (4.5 miles) were constructed in the same region and 2.4 km (1.5 miles) in south central Pennsylvania. This provided a total of 38.2 km (23.9 miles) for evaluation.

Design and Materials

The open-graded mixes first used in the four western states of Colorado, Wyoming, Utah, and New Mexico were also used in Pennsylvania (Table 1). Both limestone and gravel aggregates were used for comparison on projects 3 and 5; AC-20 asphalt cement was used on all projects. Initially, the asphalt content was established by calculating the percentage of asphalt as 1.5 Kc (surface capacity) plus 3.5.

The value of Kc was obtained by the CKE test using the coarse aggregate fraction and SAE 10 lubricating oil (1). Trial mixes with different percentages of asphalt were made and stored overnight at 140°F (60°C) in pans. We selected the mixes that met the following criteria.

Table 1. Comparison of mix gradations.

State	Gradation (% passing)					
	12.5 mm	9.5 mm	4.75 mm	2.36 mm	75 μm	Asphalt Content (%)
North Carolina	100	90 to 100	25 to 45	4 to 17[a]	0 to 2	6 to 10
Colorado, Wyoming, Utah, New Mexico	100	95 to 100	30 to 50	10 to 25	0 to 5	6 to 7
California, Arizona, Nevada, Hawaii	100	90 to 100	30 to 50	15 to 32	0 to 3	5 to 7
Louisiana	100	95 to 100	30 to 55	5 to 26[a]	0 to 6	4 to 10
Texas	100	90 to 100	40 to 60	9 to 20[a]	0 to 5	5 to 7.5
Virginia (1973)	100	84 to 100	10 to 40	0 to 10	0 to 2	6 to 12
FHWA recommendation (1974)	—	100	30 to 50	5 to 15	2 to 5	—

Note: 1 mm = 0.039 in and 1 μm = 0.0039 in.
[a]Sieve size converted from 2 mm (no. 10) to 2.36 mm (no. 8) for comparison.

Table 2. Test pavements, 1969 to 1971.

Project	County	Date Placed	ADT	Depth (mm)	Substrate Condition	Present Status
1	Centre	9/69	2 600	12.5	Fair, minimum cracking and rutting, slippery	Poor, 40% surface material lost from traffic wear; failure due to thin application; scheduled for resurfacing
2	Centre	9/69	9 400	12.5	Fair, slight wheel track rutting, slippery	Poor, 50% surface material lost from traffic wear; failure due to thin application; scheduled for resurfacing
3	Clearfield	9/69	6 000	12.5	Poor, heaved and sunken areas, wide transverse cracks	Resurfaced in 1973; failure due to poor pavement structure and thin application
4	McKean	9/69	2 650	12.5	Extremely poor, extensive cracking and rutting	Resurfaced in 1972; failure due to poor pavement structure and thin application
5	Centre	6/70	26 000	16.0	Good, slippery[a]	Good; in-service; original open surface texture kneaded and tightened by traffic
6	McKean	8/71	3 500	12.5	Fair, transverse and longitudinal cracks, raveling	Good; in-service; some reflective cracks present; slightly kneaded surface texture; 5% surface lost from raveling
7	Franklin	9/71	3 200	16.0	Good, slippery	Good; in-service; slightly kneaded surface texture
8	Mifflin	10/71	14 600	16.0	Good, slippery, some scattered cracks and rutting	Good; in-service; surface worn through to original surface in scattered areas; very tightly kneaded mat

Note: 1 mm = 0.039 in.
[a]Skid number 29.

1. A small but not excessive amount should drain to the bottom of the pan;
2. The mix should appear glossy rather than dull; and,
3. If a freshly prepared mix is molded into [102 by 102 by 16-mm (4 by 4 by 5/8-in)] pats on the glass plate, the mix should exhibit a complete seal on the glass plate and open texture on the surface.

The composition of the mixes based on laboratory extractions is given elsewhere (10). The average percentage passing the 6.35-mm (no. 3) sieve was 18.

Construction Data and Procedure

The condition of the roadways prior to the application of the friction course was documented (10). A brief description is given in Table 2. In most cases RS-1 emulsified asphalt was applied at 0.23 L/m^2 (0.05 gal/yd^2) as a tack coat, which was often damaged by construction traffic. Mix temperatures ranged from 127 to 135°C (260 to 275°F). Although the mix design method allows some extra binder for flow-down during and immediately after placement to form a complete seal, such flow was not observed.

No serious problems were encountered during transport, placement, or compaction of these mixes. Compaction was accomplished with two to three passes of a 9-Mg (10-ton) steel-wheeled roller. Traffic permitted on the friction courses immediately after completion of rolling caused no damage.

Performance and Skid Data

The present status of the projects is described briefly in Table 2. The first four projects are of dubious experimental value, because the friction course was placed at a thickness of 13 mm (½ in) or less. This caused premature loss of aggregate and, consequently, early failure of the test sections. Failure resulted from the structurally unsound pavements underneath these applications. The raveling of the open-graded mix usually began near structural or reflective cracks.

It has been observed that debris and traffic action have closed up the voids in open-graded friction courses and that for all practical purposes these surfaces are impermeable. Although the friction courses in areas of low average daily traffic (ADT) volume have maintained good surface texture, those in areas of high traffic volume (12 000 to 24 000 ADT) have developed a tight, coarse texture similar to that of a dense-graded mix. The average percentage passing the 2.36-mm (no. 8) sieve in these mixes was 18, which should obviously be lowered if permeability is to be maintained as traffic becomes heavier.

The skid test data from these projects (Figure 1), with the exception of one carbonate aggregate source (project 8), show generally good to excellent results. Those projects using coarse gravel aggregate are consistently higher in skid resistance. The averages (total of eight projects) show gravel surfaces to be about 20 skid numbers higher than carbonate surfaces. For individual projects, where both aggregate types were used on the same site, the gravel surfaces are about 10 to 15 skid numbers higher.

It is evident from Figure 1 that initially these test pavement skid resistances were lower because of the presence of a thick asphalt film surrounding the aggregates at the surface. Skid resistance increased when aggregate microtexture was exposed by traffic wear.

All skid test data were obtained at 64 km/h (40 mph) on a one-wheel towed trailer as per ASTM test designation E-274.

TEST PAVEMENTS, 1974

Judging from experience gained from the 1969 to 1971 test pavements, we felt it was necessary to consider the following factors.

1. Gradation. We observed, as mentioned earlier, that the gradation should be made coarser to maintain permeability of the open-graded mixes. The amount of material passing the 2.36-mm (no. 8) sieve should be decreased.
2. Asphalt content. The percentage of asphalt had previously been selected by conducting a series of asphalt "drainage" tests on several trial mixtures made with various asphalt percentages. It was still possible that the mix could contain either too little asphalt, which could cause raveling, or too much, which could result in flushing. A more reliable method was needed.
3. Mix temperature. Mix temperatures were chosen arbitrarily. Logically, viscosity should be used in establishing mix temperatures.

The design procedure described by Smith, Rice, and Spelman (1) seemed to be reliable and logical. This method had been used successfully on several Federal Highway Aministration (FHWA) R&D demonstration projects. In the design procedure, the optimum content of fine aggregate is established by finding the void

Figure 1. Pavement skid data, 1969 to 1971.

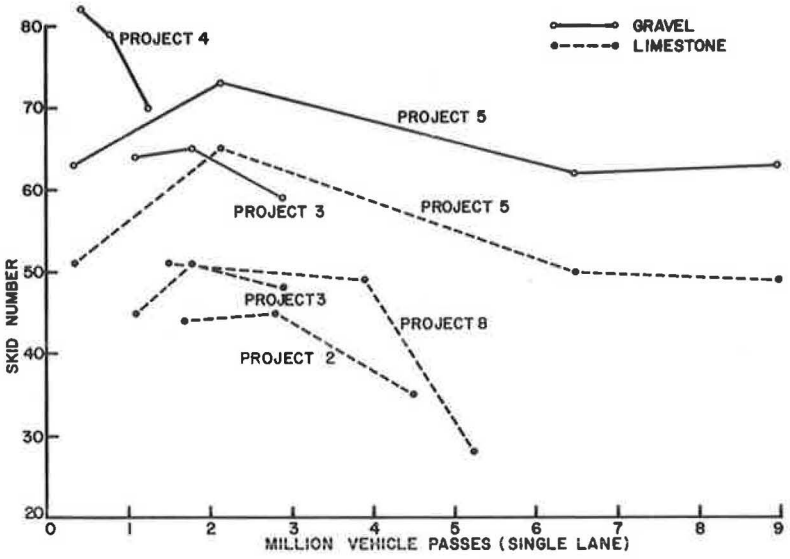

capacity of coarse aggregate and providing a minimum air void content of 15 percent. The asphalt content is determined from the surface capacity of the predominant aggregate size fraction. Optimum mixing temperature is based on asphalt viscosity.

Therefore 1974 test pavements of open-graded asphalt friction course were designed and placed according to the FHWA procedure. The project is located near Philadelphia on Route 252 (LR 144) in Delaware County (Figure 2). The roadway is 7.3 to 9.1 m (24 to 30 ft) wide and carries an ADT of 18 000. High traffic volume and heavy use of studded tires (35 percent during winter months) had badly worn the existing bituminous pavement, which was otherwise structurally sound with a minimum of cracking. Before paving, maintenance forces placed a thin leveling course in some areas of excessive rutting.

Design and Materials

The project included these four test sections (1 mm = 0.039 in) constructed in October 1974:

Section	Material	Aggregate	Thickness (mm)
Control	ID-2A wearing course	Gravel	38
Experimental	Asphalt friction course	Gravel	19
Control	ID-2A wearing course	Dolomite	38
Experimental	Asphalt friction course	Dolomite	19

Pennsylvania ID-2A is a dense-graded surface course mix that is widely used in the state and served here as a control for comparison purposes. Crushed gravel was used to provide a highly skid-resistant surface, and the dolomite aggregate was specified for medium skid resistance.

The mix designs for asphalt friction courses were prepared at PennDOT's Bureau of Materials, Testing, and Research (BMTR). The design data are given in the table below [1 mm = 0.039 in and 1°C = (1°F - 32)/1.8]. The mixes were designed to provide 15 percent air voids. The voids in mineral aggregate (VMA) ranged from 37.2 to 39.2 percent.

Test	Asphalt Friction Course Mix	
	Gravel	Dolomite
Coarse aggregate in blend, %	85	95
Fine aggregate in blend, %	15	5
Specific gravity of coarse aggregate	2.545	2.819
Specific gravity of fine aggregate	2.747	2.700
Specific gravity of 9.50 to 4.75 mm fraction	2.622	2.847
Unit weight (vibrated), PCF	96.5	110.3
Voids mineral aggregate, %	39.2	37.2
Optimum fine aggregate, %	16.4	13.4
Kc	1.60	1.40
AC = 2 Kc + 4.0	7.2	6.8
AC (corrected), aggregate basis, %	7.3	6.3
AC, mix basis, %	6.8	5.9
Optimum mix temperature, °C	110	112.8
Asphalt viscosity at the optimum mix temperature, CST	1700	1400

According to the FHWA procedure, the target mixing temperature lies in the range corresponding to asphalt cement viscosities of 7 to 9 m^2/S (700 to 900 centistokes). However, while designing these mixes we observed that the 7- to 9-m^2/S range resulted in too much drainage. The optimum mix temperatures yielding satisfactory drainage corresponded to asphalt cement viscosities of 14 and 17 m^2/S (1400 and 1700 centistokes) for dolomite and gravel, respectively. Several other designs by BMTR have confirmed that a higher range of asphalt viscosity is required.

Figure 2. Pavement location map, 1974.

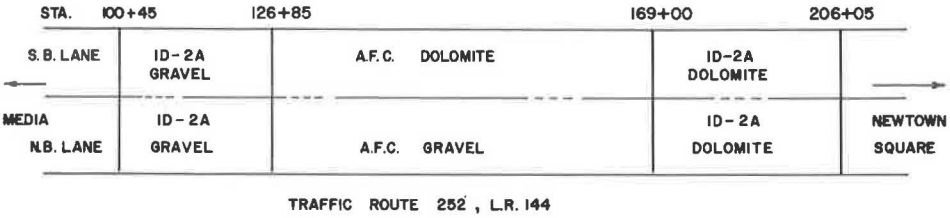

Construction Data and Procedure

Placement of the open-graded friction course mix went smoothly, and the mix that showed no signs of asphalt drainage or aggregate segregation had a somewhat rich appearance, as expected.

One or two passes of a steel-wheeled roller easily compacted the mix. Repeated rolling was of no value and even caused some degradation of the aggregate. The thickness of the compacted mat averaged 22 mm (⅞ in), slightly higher than the 19 mm (¾ in) specified.

Because of the delays between trucks arriving at the job site, the paver remained stationary for periods of time. As a result, the screed heaters, by lowering viscosity, caused the asphalt in the mat to drain, leaving dry-looking strips about 0.3 m (1 ft) wide across the lane. The condition did not seem to be detrimental, but it will be observed for any future effects.

The open-graded gravel mix appeared to be somewhat more open textured than the dolomite, as shown in Figure 3, which also shows the dense-graded ID-2A surface courses.

The mix designs and results of the plant and field test samples for the open-graded mixes are shown in Table 3. Samples of the open-graded gravel mix conformed well to the design. The plant sample of the open-graded dolomite mix was high on the 4.75-mm (no. 4) sieve, and the field sample was high on both that and the 2.36-mm (no. 8) sieve, as well as on asphalt content.

The mixes for the ID-2A wearing course also used the same gravel and dolomite aggregates. The material was designed to meet the requirements of PennDOT specifications.

Table 3. Mix design and test sample results for open-graded mixes.

Item	Percentage Passing						
		Gravel			Dolomite		
	Specification Limits	Design	Plant Sample	Job Sample	Design	Plant Sample	Job Sample
Sieve size							
9.5 mm	100	100	100	100	100	100	100
4.75 mm	30-50	31.3	42.4	41.8	34.9	53.9	51.9
2.36 mm	5-15	14.7	14.7	15.5	12.7	11.5	17.0
75 μm	2-5	1.9	3.5	2.8	3.6	3.2	4.6
Percentage of asphalt by weight of mix	6.0-8.0	6.8	6.8	6.8	5.9	5.9	6.4
Mixing temperature, °C	126.7 (max)	107.2-112.8	—	—	110-115.6	—	—

Note: 1 mm = 0.039 in; 1 μm = 0.0039 in; and $t°C = (t°F - 32)/1.8$.

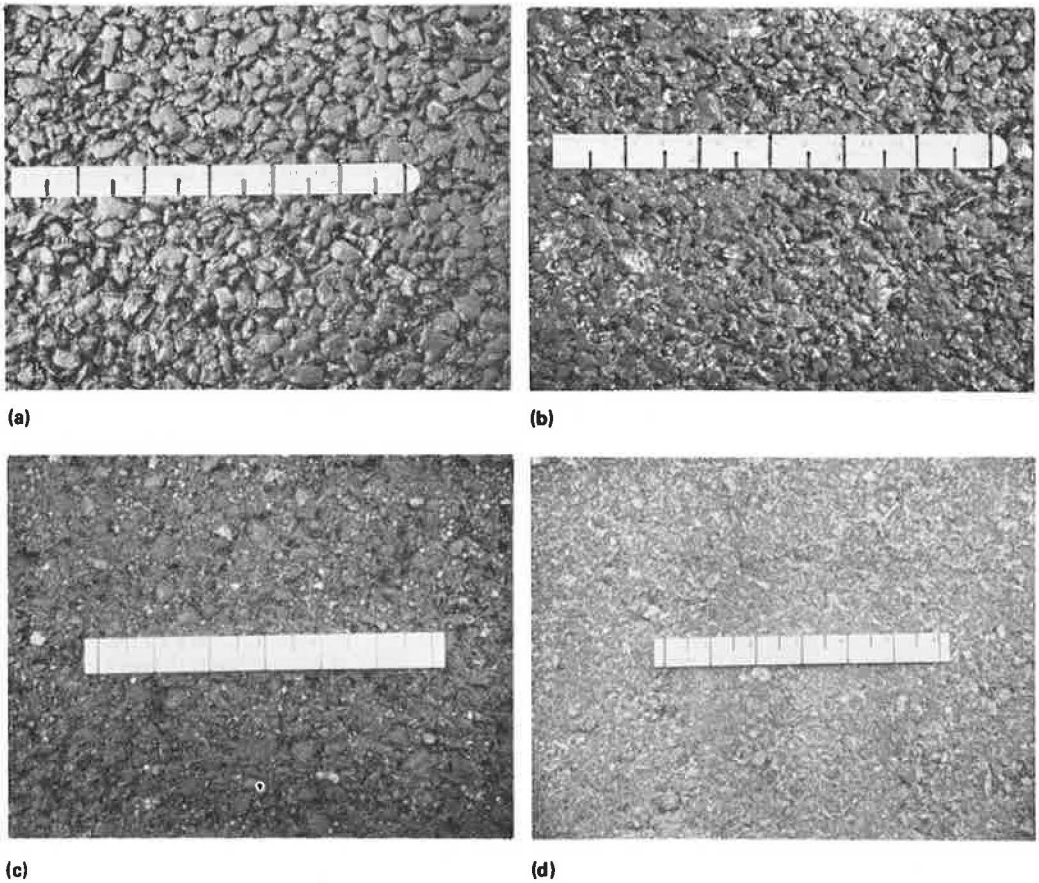

Figure 3. Comparison of mixes: (a) open-graded gravel, (b) open-graded dolomite, (c) ID-2A dense-graded gravel, and (d) ID-2A dense-graded dolomite.

Figure 4. Skid data on gravel mixes.

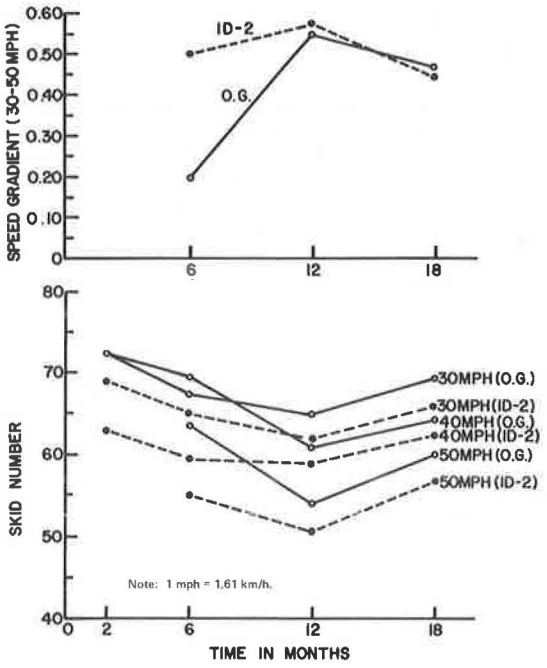

Figure 5. Skid data on dolomite mixes.

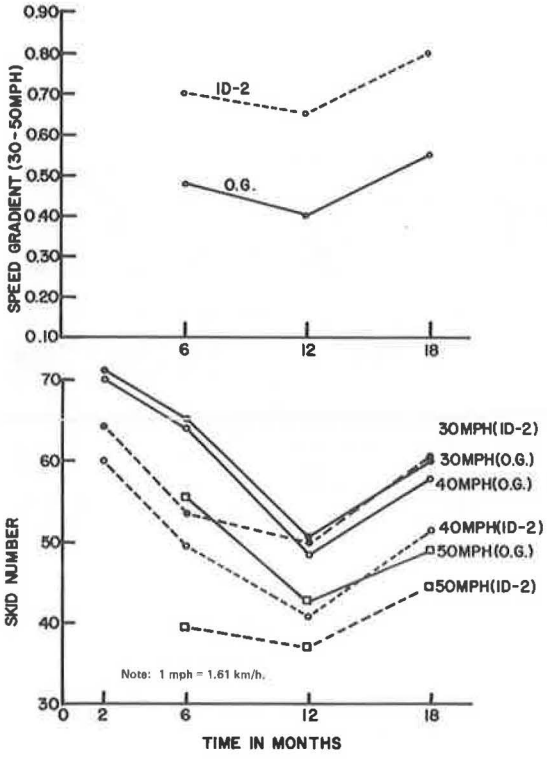

Performance Evaluation

The test pavements were constructed in October 1974 and have been evaluated at 6-month intervals since 2 months after placement. The evaluation includes judging visual appearance and measuring skid, permeability, and surface texture.

Table 4. Air permeability data.

Mix Type	Permeability (cm^3/min) At 20 Days	At 6 Months	At 12 Months	At 18 Months
Open-graded gravel				
W[a]	20 000+	1567	460	0
C[a]	20 000+	193	0	0
Open-graded dolomite				
W	8 600	57	560	78
C	6 100	740	1150	38
ID-2A gravel				
W	5	440	0	0
C	20	230	0	0
ID-2A dolomite				
W	114	13	0	0
C	269	4	0	0

Note: 1 cm^3 = 3.38 fluid oz.
[a]W = in the wheel track area and C = in the center of the lane.

Skid Testing

Tests were conducted at speeds of 48, 64, and 80 km/h (30, 40, and 50 mph) so that we could determine speed gradients. The skid level for each test section was taken as the average of 10 tests taken at two test sites. Skid test data for ID-2A gravel mix and open-graded gravel mix are shown in Figure 4. After 1½ years in service, the open-graded gravel mix is only two or three skid numbers higher than the ID-2A gravel mix. The speed gradient of both mixes is almost equal and approaches 0.45.

The open-graded mixes are generally thought to have lower speed gradients when compared with conventional dense-graded surface mixes. However, it is evident from this study that, if the aggregate possesses high skid resistance, this may not be generally true. If the aggregate—such as dolomite in this study—is not shown to be highly skid resistant, the open-graded mix has a substantially lower speed gradient (Figure 5). It seems that the microtexture predominates over the macrotexture when the mix contains highly skid-resistant aggregate, whereas macrotexture becomes a predominant factor when the mix contains relatively less skid-resistant aggregate. Continual evaluation of this project is necessary to drawing any firm conclusions.

Permeability

Permeability of the pavement surfaces has been measured periodically with the air permeability meter developed by the Pennsylvania State University (11). This device measures the rate of air flow in cubic centiliters per minute through the pavement at selected pressure differentials. Air pressure is applied to the surface of the pavement via a circular chamber sealed to the pavement with grease. Permeability readings are shown in Table 4.

Initially, the open-graded mixes had considerably higher permeability than the ID-2A dense-graded mixes. However, after 1½ years' service, the test pavements, compacted under traffic and clogged with debris, lost their permeability. Only the open-graded dolomite mix has so far retained some permeability, although it is insignificant and is approaching zero.

A minimum air void content of 15 percent was provided in the mix, according to the FHWA procedure, to ensure adequate subsurface water drainage, but apparently this minimum content will have to be increased to 25 percent, by reducing the fine aggregate content in the mix. This can have other implications.

A maximum amount of fine aggregate is desirable

because it imparts a "chocking" action to the coarse aggregate particles and because it prevents mixture raveling (1). A possible compromise is to limit the amount of aggregate passing the 4.75-mm (no. 8) sieve to a maximum of 10 percent.

Surface Texture

Measurements of the pavement surface texture are being made with the sand track device developed by the Pennsylvania State University and modified by PennDOT (11). This device works first by placing the tester on a level area of the pavement. Then the hopper is filled with a specific amount of sand and, driven along by a spring motor, deposits a strip of sand on the pavement surface. The length of the strip will vary according to the roughness of the surface. The readings are then converted to the average texture depths shown in the following table (1 mm = 0.039 in). After 18 months in service, there is no significant difference between the open-graded mix and the ID-2A surface mix.

	Surface Texture Depth (mm)			
Mix Type	At 20 Days	At 6 Months	At 12 Months	At 18 Months
Open-graded gravel	0.0036	0.0046	0.0042	0.0029
Open-graded dolomite	0.0033	0.0030	0.0030	0.0026
ID-2A gravel	0.0025	0.0044	0.0043	0.0029
ID-2A dolomite	0.0017	0.0033	0.0018	0.0023

CONCLUSIONS AND RECOMMENDATIONS

Test Pavements, 1969 to 1971

We have been evaluating these pavements for 5 to 6 years and have made the following observations.

1. Open-graded mixes should not be placed less than 19 mm (¾ in) thick.
2. Structurally unsound pavements cannot be corrected by applying an open-graded mix, which only results in premature failure of the application.
3. Debris and traffic action have closed up the voids in the open-graded mixes. In areas having an ADT over 12 000, the mixes developed a tight, coarse texture somewhat similar to that of a dense-graded mix. The average percentage of aggregate passing the 4.75-mm (no. 8) sieve in these mixes was 18, which is evidently excessive.
4. The open-graded pavement surfaces became impermeable, for all practical purposes, within 1 to 2 years.
5. Raveling usually began either where the mix was placed thinly over high spots or where there were edges or perimeters of cracks and joints in the pavement.
6. If properly laid, the average service life of an open-graded surface seems to be 5 to 6 years.

Test Pavements, 1974

Because the pavements have been evaluated for just 1½ years, this is only a progress report. We have made the following observations.

1. Optimum mix temperatures yielding satisfactory drainage corresponded to asphalt viscosities of 14 and 17 m^2/S (1400 and 1700 centistokes) respectively for dolomite and gravel aggregates. The range 7 to 8 m^2/S 700 to 900 centistokes recommended in the FHWA design procedure seems too low.
2. Open-graded mixes were designed, according to the FHWA design procedure, with 15 percent air voids to provide adequate permeability. However, after 1½ years' service the pavements lost their permeability from compacting under traffic and clogging of voids with debris. We estimate that a minimum air void content of 25 percent is necessary to maintaining permeability. The possible disadvantages of very high air void content (raveling, for instance) are not very clear.
3. After 1½ years in service, the open-graded gravel mix is only two to three skid numbers higher than the dense-graded ID-2A gravel mix. The speed gradient of 48 to 80 km/h (30 to 50 mph) for both mixes is almost equal and is approaching 0.45. This runs contrary to the general belief that the macrotexture of open-graded mixes gives them lower speed gradients than dense-graded mixes. It seems that microtexture predominates over macrotexture if a mix contains a highly skid-resistant aggregate, such as the gravel used in this project.
4. If the aggregate, such as the dolomite aggregate used in this project, is not highly skid resistant, the open-graded mix has a substantially lower speed gradient compared with the ID-2A dolomite mix after 1½ years in service. Macrotexture becomes a predominant factor if the mix contains relatively lower skid-resistant aggregate.

The evaluation of these test pavements will continue so that long-range performance and durability of the open-graded mixes can be compared with those of the dense-graded mixes.

REFERENCES

1. R. W. Smith, J. M. Rice, and S. R. Spelman. Design of Open-Graded Asphalt Friction Courses. Federal Highway Administration, Rept. FHWA-RD-74-2, Jan. 1974.
2. J. A. Mills. A Skid Resistance Study in Four Western States. HRB, Special Rept. 101, 1969.
3. J. W. Hewett. Open-Graded Plant-Mixed Seals. HRB, Highway Research Record 300, 1970, pp. 52-57.
4. B. A. Brakey. Design, Construction and Performance of Plant Mix Seals. Paper presented at the 58th Annual Meeting of AASHTO, Phoenix, 1972.
5. W. B. Betenson. Plant Mixed Seal Coats in Utah. Proc., AAPT, Vol. 41, 1972.
6. M. P. Jones. Friction Overlay Improves Runway Skid Resistance. Civil Engineering, Mar. 1973, pp. 45-48.
7. V. Adam and S. C. Shah. Evaluation of Open Graded Plant Mix Seal Surfaces for Correction of Slippery Pavements. Paper presented at the 53rd Annual Meeting, TRB, Jan. 1974.
8. B. M. Gallaway and J. A. Epps. Mixture Design Concepts, Laboratory Tests and Construction Guides for Open Graded Bituminous Overlays. Texas Transporation Institute Research Rept. 36-1 F, Oct. 1974.
9. G. W. Maupin, Jr. Virginia's Experience With Open Graded Surface Mix. Paper presented at the 55th Annual Meeting of the TRB, Jan. 1976.
10. P. Stewart and T. Nichols. Open Graded Plant Mixed Seal Coats. Pennsylvania Department of Transportation, Research Project No. 69-2 Repts., Oct. 1970 and Mar. 1972.
11. W. H. Gotolski, R. W. Smith, and J. M. Roberts. Permeability as a Mix Design Criteria for Asphaltic Concrete Pavements. Pennsylvania State Univ. Research Rept., June 1970.

Publication of this paper sponsored by Committee on Characteristics of Bituminous-Aggregate Combinations to Meet Surface Requirements.

Pavement Design Characteristics of In-Service Asphalt Mixtures

Thomas W. Kennedy, Council for Advanced Transportation Studies,
University of Texas at Austin

This paper summarizes the findings of a pavement design study on evaluating fatigue and resiliency characteristics and their variations in asphalt materials from in-service pavements in Texas. Cores from seven recently constructed highway pavements in Texas were tested with the repeated load indirect tensile test. Mean values of fatigue life, resilient modulus of elasticity, and resilient Poisson's ratio were determined, and their variations were estimated. In addition, stress-fatigue life relations were evaluated in terms of applied tensile stress and applied stress difference. The relations between repeated load fatigue properties and static properties were also evaluated. Fatigue lives were found to be essentially the same as those reported by other investigators. The mean resilient moduli of elasticity were fairly consistent for the various projects and ranged from 1520 to 4240 MPa (221 000 to 615 000 lbf/in^2). The majority of the Poisson's ratios were in the 0.10 to 0.22 range. The coefficient of variation for fatigue life, which was relatively large, ranged from 30 to 80 percent; the amount of variation was stress and project dependent. The coefficient for resilient modulus was relatively small, from 4 to 28 percent. No correlations for estimating purposes were found, although the relation between fatigue life and tensile strain looked promising.

Most current pavement design procedures are largely empirical and deterministic in nature. The state of the art, however, has advanced to the point at which attempts are being made both to apply elasticity concepts to design and to understand the fatigue behavior of various pavement layers and materials. Probabilistic concepts also need to be included. While theories are being developed and integrated into design and analysis systems, we still need to determine elastic and fatigue properties and their variations in pavement materials.

This paper summarizes the findings of a study on estimating these properties and variations in asphalt materials from actual pavements in Texas.

EXPERIMENTAL PROGRAM

The principal objectives of this investigation were to characterize in-service black-base materials in terms of fatigue life and of resilient elastic properties under repeated applications of low tensile stresses, to estimate the amount of expected variation in these properties, and to investigate possible correlations between behavior under a single load and that under repeated loading.

Therefore, field cores of black-base and asphalt surfacing materials from recently constructed highway pavements in Texas were tested with the static test and the repeated load indirect tensile test. The fatigue lives, elastic properties, and the variations among these properties were estimated by using the repeated load indirect tensile test; values of strength, modulus of elasticity, and Poisson's ratio were determined by using static loading.

Projects Tested and Core Sampling

Cores from seven projects in five locations in Texas were tested. General information on the projects is contained in Table 1.

Normally, black-base pavement layers are cored at equally spaced longitudinal intervals. Even though they were obtained in this systematic fashion, these cores can be considered to have been randomly sampled, because the sampling location function does not coincide with any variation distribution function known to exist in the pavement.

All cores were obtained with either a 102- or a 152-mm (4- or 6-in) inside diameter core barrel. The cores were sawed at the interface between lifts so that each specimen represented its respective lift. At least 10 specimens from each project were selected randomly and tested with the repeated load indirect tensile test; 3 to 5 specimens were tested under a single, slowly applied load to determine static strengths and static elastic properties of the black base and the asphalt concrete. Before testing, the specimen dimensions were carefully measured, and each specimen was weighed for density.

Test Method

In the indirect tensile test, a cylindrical specimen is loaded with either static or repeated compressive loads that act parallel to and along the vertical diametral plane. The load is distributed and the loading area maintained a constant by applying the compressive load through a 13-mm (0.5-in) wide steel loading strip curved at the interface to fit the specimen. This loading configuration develops a relatively uniform tensile stress, perpendicular to the plane of the applied load and along the vertical diametral plane, that ultimately causes the specimen to fail by splitting or rupturing along the vertical diameter.

By monitoring the applied load and the horizontal and vertical deformations of the specimen, one can estimate the specimen's tensile strength, Poisson's ratio, and modulus of elasticity. Under repeated loads, one can estimate the resilient modulus of elasticity and Poisson's ratio for any given application of load, the permanent deformation accumulated for any given number of load applications, and the fatigue life, by continuously or periodically monitoring load, horizontal deformation, and vertical deformation.

Static Testing

The indirect tensile test procedure for static loading was the same as that used by Marshall and Kennedy (1). The basic testing apparatus included a loading system and a means of monitoring the applied loads and the specimen's horizontal and the vertical deformations.

The loading system consisted of a loading apparatus, a load-aligning device, and loading strips. In this study, a closed-loop electrohydraulic system was used to apply the load and to control the deformation rate. A deformation rate of 51 mm/min (2 in/min) at approximately 24°C (75°F) was used. A special loading device ensured that the loading platens and strips remained parallel during the test.

The load was monitored with a load cell, and the horizontal deformation was measured with a device with two cantilevered arms having attached strain gauges. Vertical deformation was measured with a DC linear variable differential transformer (LVDT). The loads and deformations were monitored by two X-Y plotters,

Table 1. Black-base and asphalt concrete projects.

Project	Material	Number of Specimens		Asphalt		Aggregates	Specimen Diameter (mm)
		Fatigue	Static	Type	Percentage by Weight		
2	Black base	18	5	AC-20	6.2 to 6.5	Limestone	152
5	Black base	15	5	AC-10	6.9 to 7.2	Limestone	152
8B	Black base	15	5	AC-20	4.6 to 5.3	Caliche conglomerate gravel	152
8C	Black base	11	3	AC-20	5.6 to 5.9	Limestone	152
17B(1)	Black base (first lift)	15	100[a]	AC-10 and AC-20	4	River gravel	102
17B(2)	Black base (second lift)	15		AC-10 and AC-20	4	River gravel	102
25 to 97(1)	Black base (first lift)	12	3	AC-20	6	Sandstone	102
25 to 97(2)	Black base (second lift)	11	3	AC-20	6	Sandstone	102
25 to 97(3)	Black base (third lift)	12	3	AC-20	3.5	Gravel	102
25 to 97(S)	Asphalt concrete (surface course)	12	3	AC-20	5	Gravel	102
25 to 100 (1, 2)	Black base (first and second lifts)	12	4	AC-20	4.5	Gravel	102
25 to 100(3)	Black base (third lift)	10	2	AC-20	3.2	Gravel	102
25 to 100(S)	Asphalt concrete (surface course)	10	2	AC-20	4.7	Gravel	102

Note: 1 mm = 0.039 in.

[a] From Moore and Kennedy (1).

one recording load and horizontal deformation and one recording load and vertical deformation.

Points picked from the X-Y plots and other weight and volume information were used as input for computer program MODLAS 9, which calculates the tensile and elastic properties of the materials by using the indirect tensile test.

Repeated Load Testing

The basic test equipment used in the repeated load tests was the same as that used for the static loading tests, except for an additional horizontal deformation transducer consisting of two LVDT's that were used to monitor the horizontal deformation of the specimen for any particular load application.

Loads were applied at one cycle per second for 0.4 s followed by a rest period of 0.6 s (Figure 1). All tests were conducted at approximately 24°C (75°F).

Figure 1. Load time pulse for repeated load indirect tensile test.

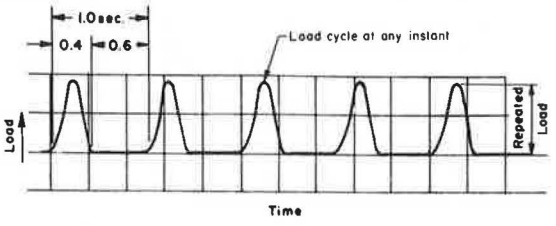

Figure 2. Typical load and deformation versus time relation for repeated load indirect tensile test.

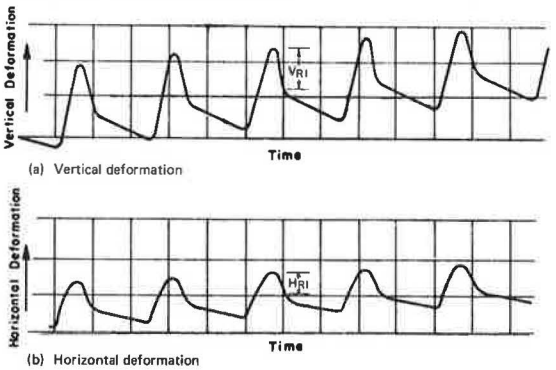

The loads and elastic deformations from a given load application were recorded on a two-channel strip chart recorder. The permanent deformations were recorded on a digital data logging system. The specimen's load, elastic deformations, and permanent deformations were measured continuously during the first 200 cycles and were then monitored at increments of approximately 100 cycles. Typical vertical and horizontal deformation-time relations for a given load impulse are shown in Figure 2, and typical relations between total and permanent deformation and the number of cycles are shown in Figure 3.

Figure 3. Typical relation between deformation and number of load applications for the repeated load indirect tensile test.

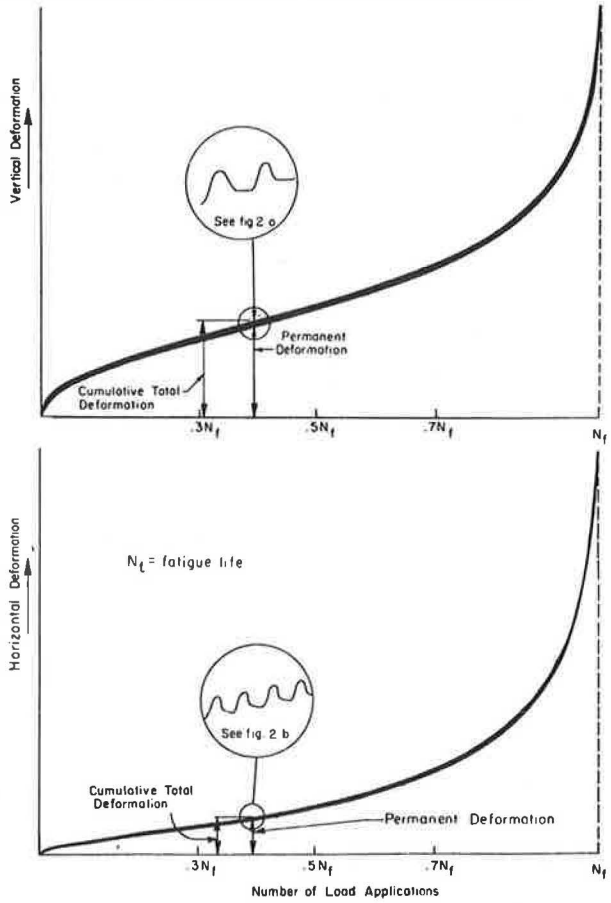

Instantaneous resilient deformations, or recoverable deformations V_{RI} and H_{RI} (Figure 2), and the repeated load were used to calculate the resilient elastic properties under repeated loading.

Because of time restrictions, only a limited number of fatigue tests could be conducted. In some cases the stress level was raised in order to complete the testing program within a reasonable time, to establish the relation between tensile stress and fatigue life, and to determine whether this relation was essentially linear, as shown by previous work. Relatively high stress levels resulted in very low fatigue lives.

Fatigue Failure

Failure was considered to occur when the specimen fractured completely or, in terms of permanent horizontal (tensile) deformation, when deformation increased without additional load applications (Figure 3). Fatigue life (N_f), therefore, is the number of cycles corresponding to this large increase in deformation.

Resilient Elastic Characteristics

Permanent and total deformations increase substantially during the first few load cycles, and then the rate becomes essentially constant until failure (Figure 3). After analyzing a large number of permanent deformation relations, I concluded that the essentially linear portion of the curve occurred between about 15 and 85 percent of fatigue life. Because this range represents a significant portion of the material's design life, estimates of instantaneous resilient modulus and Poisson's ratios were calculated at 30, 50, and 70 percent of the fatigue life. These values were then averaged to obtain a representative value for each specimen.

Variation

One of the objectives of this study was to estimate variations in fatigue life and elastic properties of black-base and asphalt materials from in-service pavement. The coefficient of variation, which is the sample standard deviation divided by the sample mean, was therefore used because it related variation to mean.

Correlations

Possible correlations between the repeated load properties and the static or mixture properties were investigated with a view to developing techniques for estimating fatigue life and elastic properties under repeated loads without having to conduct costly and time-consuming repeated load tests.

ANALYSIS AND EVALUATION

Summaries of the test results for the seven projects are shown in Tables 2 and 3.

Fatigue Life

The black-base specimens for each project were subjected to a minimum of three stress levels to define the stress versus fatigue life relation and to measure the inherent variation in expected fatigue life.

Fatigue Life and Stress Relations

The mean fatigue life and coefficient of variation obtained for the specimens from each project are given in Table 2. The relations between the logarithm of tensile stress and the logarithm of fatigue life were essentially linear, but the slopes and relative positions varied, which indicated that the relations were material or project dependent. The linear relation can be expressed in the form

$$N_f = K_2(1/\sigma_T)^{n2} = K_2'(1/\Delta\sigma)^{n2} \quad (1)$$

where

N_f = fatigue life in cycles to failure;
σ_T = repeated tensile stress in kilopascals;
$\Delta\sigma$ = stress difference, approximately $4\sigma_T$, in kilopascals;
n_2 = slope of the logarithmic relation between fatigue life and the tensile stress or stress difference;
K_2 = antilog of the intercept of the logarithmic relation between fatigue life and tensile stress; and
K_2' = antilog of the intercept of the logarithmic relation between fatigue life and stress difference.

As shown in Table 2, except for the four projects 5, 8B, 17B(1), and 17B(2), the slopes were fairly consistent. Values ranged from 1.50 to 5.08, and most slopes ranged from 3.18 to 5.08. Values for projects 5, 8B, 17B(1), and 17B(2) were smaller and varied from 1.58 to 2.66.

Monismith and others (2) reported values of K_2 and n_2 from previous work on field cores. Values of n_2 ranged from 1.85 to 6.0, and it was suggested that n_2 was a function of stiffness of the mixture.

Values obtained in this study were in the range previously reported. A review of Table 1 shows that three of the four projects with the smaller values of n_2 involved mixtures containing AC-10 rather than AC-20. In addition, project 8B mixtures, which contained an AC-20, used a different basic aggregate type.

Previously reported values of K_2 (2) were 2.85×10^9 and 4.41×10^{23} kPa (8.00×10^7 and 4.10×10^{18} lbf/in^2). Values in this study were smaller, ranging from 5.90×10^7 to 1.30×10^{17} kPa (2.79×10^5 to 7.13×10^{12} lbf/in^2). Thus, the fatigue lives for the materials tested were generally shorter than those previously reported.

Porter and Kennedy (3) compared the fatigue relations obtained by various investigators using different test methods. This comparison indicated that the fatigue life obtained with the repeated load indirect tensile test was significantly shorter than that obtained with other test methods. A large portion of the difference was attributed to the fact that the indirect tensile test involves a biaxial state of stress. It was suggested that stress be expressed in terms of a stress difference, i.e., the maximum principal stress minus the minimum principal stress, which is approximately $4\sigma_T$ in the failure zone.

The relations between the logarithm of fatigue life and the logarithm of stress difference are shown in Figure 4. Values of n_2 did not change, because the relations merely shifted along the x axis. Values of the K coefficient (K_2'), however, were significantly larger than K_2 and ranged from 5.26×10^7 to 1.49×10^{20} kPa (2.49×10^6 to 8.18×10^{15} lbf/in^2), with the majority of the values in the range of 10^{10} to 10^{17} (Table 2). These values are consistent with the previously reported values of K_2.

Variations in Fatigue Life

The coefficients of determination (R^2) for the various relations shown in Figure 4 are summarized in Table 2. These values indicate that a great deal of the variation in data could not be explained by linear relations. In addition, the coefficients of variation were not constant but were stress and project dependent. Coefficients ranged from 26 to 84 percent; however, some of this can

Table 2. Fatigue results for in-service black base and asphalt concrete.

Project	Tensile Stress, σ_T[a] (kPa)	No. of Specimens	Fatigue Life, N_f Mean (cycles)	CV (%)	$N_f = K_2(1/\sigma_T)^{n_2} = K_2'(1/\Delta\sigma)^n$ K_2 (kPa)	K_2' (kPa)	n_2	R^2 (%)[b]
2	110	3	16 984	–	1.85×10^{13}	9.14×10^{15}	4.48	85
	165	5	1 842	29				
	221	5	869	52				
	276	5	252	78				
5	110	5	3 179	30	8.02×10^{8}	3.20×10^{10}	2.66	73
	165	5	1 063	49				
	221	5	567	52				
8B	165	5	5 277	60	8.11×10^{8}	2.02×10^{10}	2.32	42
	221	4	4 281	40				
	276	5	2 586	84				
8C	276	4	7 124	38	4.43×10^{14}	2.08×10^{17}	4.44	84
	331	2	3 513	–				
	386	4	1 678	65				
17B(1) first lift	110	5	3 582	26	5.90×10^{7}	5.26×10^{7}	1.58	50
	165	5	1 985	40				
	221	5	1 374	65				
17B(2) second lift	110	5	3 253	49	8.61×10^{7}	1.77×10^{9}	2.18	53
	165	5	1 593	45				
	221	5	748	52				
25-97(1) first lift (asphalt-stabilized base)	221	5	1 393	80	2.57×10^{10}	2.10×10^{12}	3.18	39
	276	2	382	–				
	331	5	313	61				
25-97(2) second lift (asphalt-stabilized base)	221	1	27 795	–	3.83×10^{14}	2.28×10^{17}	4.61	45
	276	5	1 582	75				
	331	2	924	–				
	386	3	1 081	–				
25-97(3) third lift (type A specimen)	276	5	1 015	69	1.61×10^{11}	1.77×10^{13}	3.39	56
	331	2	450	–				
	386	5	309	50				
25-97(S) surface course (type D specimen)	276	5	1 271	41	1.30×10^{17}	1.49×10^{20}	5.08	49
	331	2	460	–				
	386	5	297	74				
25-100(1, 2) first two lifts (asphalt-stabilized base)	110	4	12 223	66	4.14×10^{12}	1.42×10^{15}	4.21	89
	165	2	2 346	–				
	221	4	655	59				
	331	2	108	–				
25-100(3) third lift (type A specimen)	276	4	799	49	1.74×10^{14}	1.14×10^{17}	4.68	50
	331	2	296	–				
	386	4	180	64				
25-100(S) surface course (type D specimen)	110	1	38 157	–	9.30×10^{12}	2.90×10^{15}	4.14	89
	276	3	644	–				
	331	2	512	–				
	386	4	195	38				

Note: 1 kPa = 0.145 lbf/in^2.

[a] $\Delta\sigma = 4\sigma_T$.

[b] R^2 for regression equation expressed in the form $\log N_f = \log K_2 - n_2 \log \sigma_T = \log K_2' - n_2 \log \Delta\sigma$.

be accounted for by stress, because the coefficients increased with increasing stress or decreasing fatigue life.

A portion of the within-project variation for projects 8B and 8C might be attributed to the larger aggregates used in them. In addition, the cores from project 25-100 (1, 2) were very rough, which would contribute to the total variation by increasing testing error.

There were significant differences in the coefficients of variation for the various projects and stress levels, so no definite recommendation can be made for an exact value for the expected coefficient of variation. It is possible, however, to establish a range of expected values. This study seems to indicate that the coefficients of variation would range from about 30 to 80 percent.

Comparison Between Layers

Comparing the top and bottom layers for projects 17B and 25-97, which had an adequate number of specimens for comparison, indicates that the top layers (2) generally had longer fatigue lives than the lower layers (1). In Figure 4, the stress difference and fatigue life relation for project 25-97(2) is above that for project 25-97(1), but for projects 17B(2) and 17B(1) the reverse is true. However, if the K coefficients for the two projects are compared, the upper lifts exhibit larger values; this indicates that at lower stress values the fatigue lives would be longer for both projects. However, the slope value (n_2) is larger for the upper lifts, indicating that fatigue life shortened more rapidly with increased stress.

Elastic Characteristics

Mean values of the instantaneous resilient modulus of elasticity and Poisson's ratio and the coefficients of variation for each project and stress level are summarized in Table 3. The static values of tensile strength, modulus of elasticity, and Poisson's ratio obtained for the same projects are contained in Navarro and Kennedy (4).

Instantaneous Resilient Modulus of Elasticity

The mean instantaneous resilient moduli were consistent for the various projects and ranged from 152 to 424 MPa (221 000 to 615 000 lbf/in^2). More important, however, are the consistency within each project and the fact that

Table 3. Elastic properties for repeated load indirect tensile tests.

Project	Tensile Stress (kPa)	No. of Specimens	Instantaneous Resilient Modulus of Elasticity		Instantaneous Resilient Poisson's Ratio	
			Mean (MPa)	CV (%)	Mean	CV (%)
2	110	3	1960	—	0.31	—
	165	5	1830	7	0.27	31
	221	5	1920	9	0.44	46
	276	5	2060	4	0.58	12
5	110	5	1550	8	0.11	47
	165	5	1580	4	0.13	39
	221	5	1770	9	0.18	28
8B	165	5	2650	14	0.12	53
	221	4	2810	12	0.06	10
	276	5	3300	28	0.18	54
8C	276	4	3540	12	0.11	23
	331	2	3640	—	0.13	—
	386	4 (3[a])	3140	9	0.16	—
17B(2) top lift	110	5	3030	25	0.09	49
	165	4	3760	5	0.13	37
	221	5 (4[a])	3100	22	0.22	76
17B(1) bottom lift	110	5	3560	17	0.11	18
	165	4	4240	14	0.13	50
	221	5	3340	17	0.11	18
25-97(1) first lift (asphalt-stabilized base)	221	5	1730	17	0.32	33
	276	2	1850	—	0.46	—
	331	5	1720	4	0.39	38
25-97(2) second lift (asphalt-stabilized base)	276	5	1990	21	0.28	37
	331	2	2430	—	0.31	—
	386	3	2110	10	0.31	27
25-97(3) third lift (type A specimen)	276	5 (2[a])	2650	9	0.16	—
	331	2	3430	—	0.22	—
	386	5	2790	9	0.23	33
25-97(S) surface course (type D specimen)	276	5	2780	8	0.18	44
	331	2	2670	—	0.33	—
	386	4 (3[a])	2990	16	0.41	57
25-100(1, 2) first two lifts (asphalt-stabilized base)	110	3	1520	—	—	—
	165	2	1780	—	0.24	—
	221	2	2080	—	—	—
	331	1	2140	—	—	—
25-100(3) third lift (type A specimen)	276	3	2370	—	0.13	—
	331	2	2470	—	0.15	—
	386	3 (2[a])	2370	—	0.14	—
25-100(S) surface course (type D specimen)	276	3	2120	—	0.16	—
	331	2	2370	—	0.15	—
	386	3	2270	—	0.29	—

Note: 1 kPa = 0.145 lbf/in^2 and 1 MPa = 145 lbf/in^2.

[a] Number of specimens analyzed to determine the instantaneous resilient Poisson's ratio.

the modulus value was not overly sensitive to the magnitude of the applied stress, for the range of stresses used in testing. The coefficients of variation for any given project and stress level were low, ranging from 4 to 28 percent, as a result of this consistency.

In contrast, mean static moduli for similar material tested with the static indirect tensile test (1, 5) had much lower values of 266 to 631 MPa (38 600 × 10^3 to 91 500 lbf/in^2) and much higher (24 to 59 percent) coefficients of variation. Mean values in this study ranged from 381 to 1165 MPa (55 200 to 169 000 lbf/in^2), which is consistent with the previously reported values; the coefficient of variation ranged from 14 to 27 percent, which is smaller than previously reported static coefficients but somewhat larger than the coefficients of variation for the moduli resulting from repeated loads. Although it was not completely substantiated by these results, a large portion of the variation associated with static testing can probably be attributed to testing errors, caused by surface irregularities, that would not have much effect on repeated load tests.

A comparison of the mean static moduli and the mean resilient moduli is shown in Figure 5. This figure shows the dynamic moduli to be significantly larger than the static moduli. The ratio of the resilient and static moduli ranged from 10.5 to 2.3, the higher values being associated with the materials with low static moduli.

Instantaneous Resilient Poisson's Ratio

Except for projects 2 and 25-97, resilient Poisson's ratio values were fairly consistent at 0.06 to 0.29, the majority ranging from about 0.10 to 0.22 (Table 3). Values for projects 2 and 25-97 were much higher, from 0.16 to an indicated value of 0.58, with the majority from 0.22 to 0.46.

These values tend to be lower than those for similar materials, which were tested previously with the static indirect tensile test and ranged from 0.16 to 0.34 (1, 5). A comparison of the static and resilient Poisson's ratios obtained from this study indicates that these ratios are of essentially the same magnitude. In most projects, the mean values tended to increase with increasing stress.

Coefficients of variation for Poisson's ratio were much higher—from 10 to 76 percent—than those for resilient modulus of elasticity; the majority ranged between 18 and 57 percent. Nevertheless, these coefficients are lower than the static Poisson's ratios for similar materials, for which coefficients ranged from

39 to 67 percent (1, 5). Coefficients of variation for the static Poisson's ratios from this study ranged from 25 to 41 percent.

Correlations With Fatigue Life

Possible correlations between fatigue life and static properties and between fatigue life and repeated load properties were explored, because repeated load tests are time consuming and costly to conduct. If correlations do exist, it is possible to estimate fatigue properties with either the much simpler static test or the short-term repeated load test. Such correlations could also lead to a better understanding of the fatigue behavior of pavement materials.

Stress-Strength Ratio

Previous work reported by Moore and Kennedy (6, 7) found a relatively good linear correlation between the

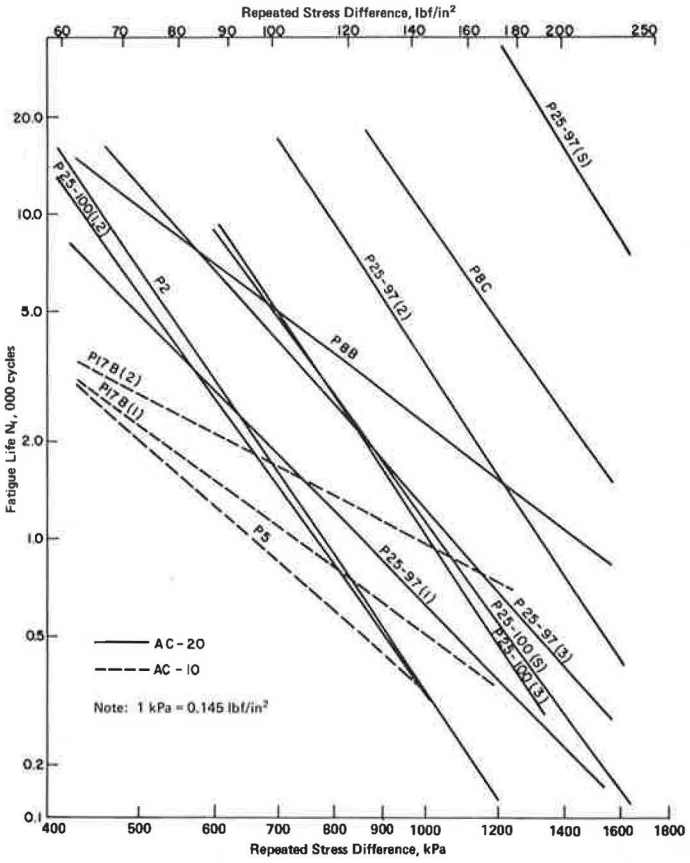

Figure 4. Relations between the logarithms of stress difference and fatigue life.

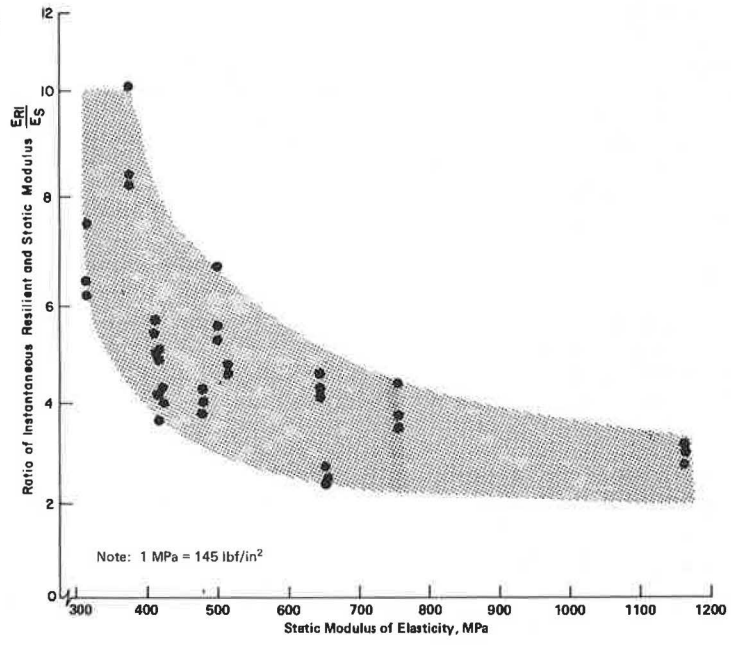

Figure 5. Relation between static modulus and the ratio of static and instantaneous resilient moduli.

Figure 6. Relations between the logarithms of fatigue life and tensile strain.

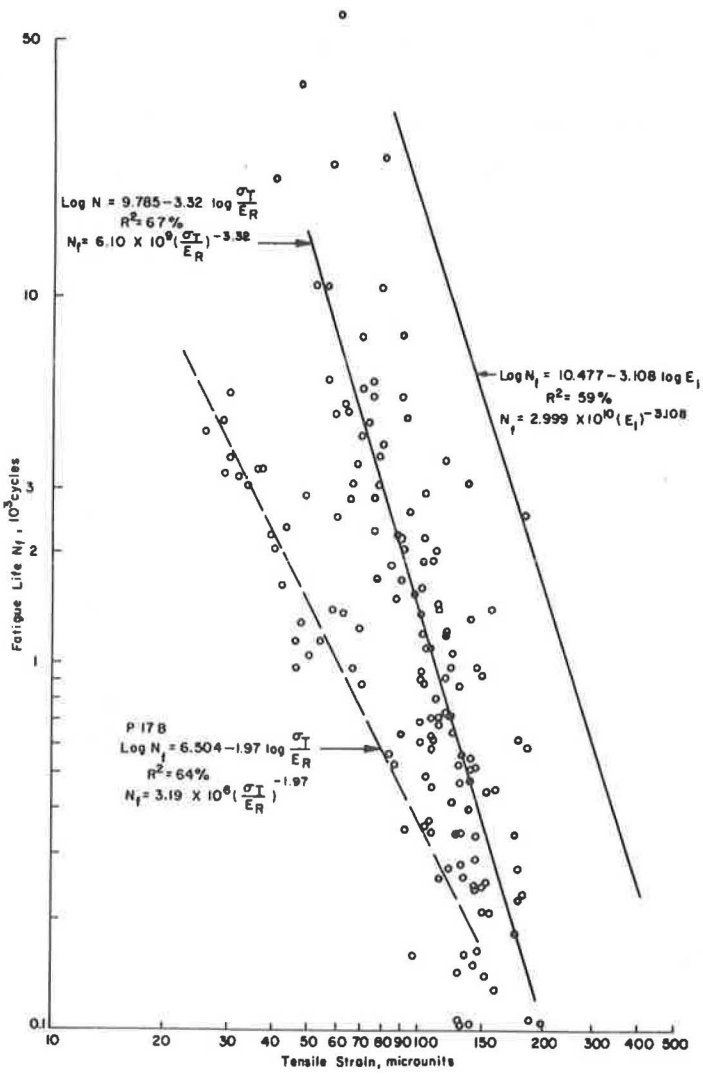

logarithm of the ratio of applied tensile stress to static tensile strength and the logarithm of fatigue life. Such a relation allows fatigue life to be estimated from static test results.

Navarro and Kennedy (4) described the relation between the logarithm of the estimated stress-strength ratio, defined as the ratio of the repeated tensile stress to the mean static tensile strengths, and the logarithm of fatigue life. A coefficient of determination (R^2) of 51 percent indicates that, although a correlation does exist, the reliability of a predicted fatigue life would be questionable and subject to large errors.

Stiffness

Previous work has indicated that stiffness is an important characteristic related to fatigue life. Deacon and Monismith (8) stated that any factor affecting stiffness also affects fatigue behavior. Deacon (9) reported that the effect of stiffness is a function of the mode of loading: under controlled stress loading, a material with a high stiffness will perform well as long as the mixture is not brittle and is well proportioned, but the reverse is true under controlled strain loading.

Epps and Monismith (10) presented data that indicated that stiffness alters the slope of the logarithmic relations between fatigue life and bending stress and showed that a stiff mix had a longer fatigue life. There was an indication that this was true in my study; however, for the limited number of projects and conditions involved, there was no definite correlation, although materials with higher static moduli of elasticity tended to have longer fatigue lives.

Tensile Strain

Previous investigators have shown that fatigue life is related to strain (4, 6, 7, 11, 12). Figure 6, derived from Moore and Kennedy (6, 7), illustrates this relation. Tensile strains were estimated by dividing the repeated tensile stress (σ_T) by the resilient modulus of elasticity (E_R). Included for comparison is the relation previously established by Moore and Kennedy (6, 7).

As shown, there was a definite trend when the data for project 17B were excluded. The relation for all of the other projects exhibited a coefficient of determination (R^2) of 67 percent, which indicates that a great deal of variation could be accounted for by the relation but that substantial estimation errors could be expected if the relation were used to predict fatigue life. The relation, excluding project 17B, was essentially parallel to that previously established by Moore and Kennedy, but the fatigue lives for a given strain were shorter, possibly because of the difference between field cores and laboratory-prepared specimens.

CONCLUSIONS

Fatigue Life

Fatigue failures occurred at indirect tensile stresses ranging from 110 to 386 kPa (16 to 56 lbf/in^2), which was 15 to 65 percent of the indirect tensile strength.

The relation between the logarithm of tensile stress and the logarithm of fatigue life was essentially linear, and that between stress and fatigue life could be expressed as in Equation 1.

Values of n ranged from 1.58 to 5.08 and are approximately equal to those previously reported. In addition, it appeared that n was related to the viscosity of the asphalt, because mixtures containing stiffer asphalts exhibited lower n values.

Values of K ranged from 5.90×10^7 to 1.30×10^{17} when stress is expressed in kilopascals (2.79×10^5 to 7.13×10^{12} when stress is expressed in pound force per square inch). These values are significantly smaller than those previously reported, which is indicative of shorter fatigue lives.

Relating the logarithm of fatigue life to the logarithm of stress difference (i.e., the maximum principal stress minus the minimum principal stress) did not change the values of n, but the values of K′ were larger than the values of K. Values of K′ ranged from 5.26×10^7 to 1.49×10^{20} when stress is expressed in kilopascals (2.49×10^6 to 8.18×10^{15} when stress is expressed in pound force per square inch); the majority of the values ranged from 10^{10} to 10^{17}. These are consistent with previously reported values.

The coefficient of variation generally ranged from 30 to 80 percent, magnitude being stress and project dependent. Variation tended to increase with increasing stress or decreasing fatigue.

There was an indication that the upper layers had longer fatigue lives than the lower layers. However, because only two projects could be evaluated, additional study is required.

Elastic Properties Under Repeated Loads

The mean resilient moduli of elasticity were fairly consistent for the various projects and ranged from 1520 to 4240 MPa (221 000 to 615 000 lbf/in^2).

The resilient moduli of elasticity were significantly larger than the static moduli of elasticity. The ratio of the resilient and the static moduli ranged from 10.5 to 2.3, the higher values being associated with the materials with low static moduli.

The coefficients of variation for the resilient moduli of elasticity were low, from 4 to 28 percent.

The majority of mean resilient Poisson's ratios ranged from 0.10 to 0.22; however, for two projects the values were much higher, from 0.22 to 0.46. In general, Poisson's ratios tended to increase with increased stress.

Coefficients of variation for resilient Poisson's ratio were higher than for resilient modulus of elasticity; the majority of the values lay between 18 and 57 percent.

Correlations With Fatigue Life

A correlation between fatigue life and the ratio of the repeated tensile stress to the static tensile strength was found to exist. However, large errors could be expected if this correlation were used to estimate fatigue life.

No correlation was found to exist between fatigue life and stiffness, except that higher moduli tended to have longer fatigue lives.

A correlation between the logarithm of fatigue life and the logarithm of tensile strain (repeated tensile stress divided by the resilient modulus of elasticity) was found to exist. It was essentially parallel to a similar relation previously reported. This relation, however, should not be used to estimate fatigue life because of the relatively large errors that could be expected.

Recommendation

The information obtained from this study of the fatigue and repeated load characteristics of asphalt-treated mixtures can and should be used in the development and application of stochastic pavement design procedures based on elastic theory. This paper provides estimates of the engineering properties and variation characteristics of in-service asphalt mixtures, rather than those of laboratory-prepared mixtures, that can be used in design.

ACKNOWLEDGMENTS

This investigation was conducted at the Center for Highway Research at the University of Texas at Austin. I wish to thank the sponsors, the Texas State Department of Highways and Public Transportation and the U.S. Department of Transportation, Federal Highway Administration. The contents of this report reflect my views, and I alone am responsible for the facts and accuracy of the data presented. The contents do not necessarily reflect the official views or policies of the Federal Highway Administration. This report does not constitute a standard, specification, or regulation.

REFERENCES

1. B. P. Marshall and T. W. Kennedy. Tensile and Elastic Characteristics of Pavement Materials. Center for Highway Research, Univ. of Texas at Austin, Research Rept. 183-1, Jan. 1974.
2. C. L. Monismith, J. A. Epps, D. A. Kasianchuk, and D. B. McLean. Asphalt Mixture Behavior in Repeated Flexure. Institute of Transportation and Traffic Engineering, Univ. of California, Rept. No. TE-70-5, Dec. 1970.
3. B. W. Porter and T. W. Kennedy. Comparison of Fatigue Test Methods for Asphalt Materials. Center for Highway Research, Univ. of Texas at Austin, Research Rept. 183-4, Apr. 1975.
4. D. Navarro and T. W. Kennedy. Fatigue and Repeated Load Elastic Characteristics of Inservice Asphalt-Treated Materials. Center for Highway Research, Univ. of Texas at Austin, Research Rept. 183-2, Jan. 1974.
5. T. W. Kennedy. Tensile and Elastic Characteristics of Black-Base Materials. TRB, Transportation Research Record 510, 1974, pp. 31-40.
6. R. K. Moore and T. W. Kennedy. Tensile Behavior of Subbase Materials Under Repetitive Loading. Center for Highway Research, Univ. of Texas at Austin, Research Rept. 98-12, Oct. 1971.
7. R. K. Moore and T. W. Kennedy. Tensile Behavior of Asphalt-Treated Materials Under Repetitive Loading. Proc., 3rd International Conference on the Structural Design of Asphalt Pavements, Jan. 1972, Vol. I.
8. J. A. Deacon and C. L. Monismith. Laboratory Flexural Fatigue Testing of Asphalt Concrete With Emphasis on Compound Loading Tests. HRB, Highway Research Record 158, 1967, pp. 1-31.
9. J. A. Deacon. Material Characterization—Experimental Behavior. HRB, Special Rept. 126, 1971, pp. 150-179.

10. J. A. Epps and C. L. Monismith. Influence of Mixture Variables on Flexural Fatigue Properties of Asphalt Concrete. Proc., AAPT, Vol. 38, 1969, pp. 423-464.
11. P. S. Pell. Fatigue Characteristics of Bitumen and Bituminous Mixes. Proc., International Conference on the Structural Design of Asphalt Pavements, Ann Arbor, 1967, pp. 577-593.
12. R. N. J. Saal and P. S. Pell. Fatigue of Bituminous Road Mixes. Kollard-Zeitschrift, Darmstadt, Vol. 17, 1960, pp. 61-71.

Publication of this paper sponsored by Committee on Characteristics of Bituminous Paving Mixtures to Meet Structural Requirements.

Test for Predicting Fatigue Life of Bituminous Concrete

G. W. Maupin, Jr., Virginia Highway and Transportation Research Council

An examination of several simple test methods revealed that the indirect tensile test can be used to predict the fatigue life of bituminous concrete. This replaces the traditional, expensive, and time-consuming flexural fatigue test. The tests examined—indirect tensile, double punch, resilient modulus, flexure, resonant frequency, and pulse velocity—were selected from a literature search for use on several mixes obtained from various locations in the United States and containing a variety of asphalt cements and aggregates. The traditional flexural fatigue test was also performed on each mix, and the results were correlated with those from the simple tests. The correlations indicated that indirect tensile strength and stiffness can be used to predict the fatigue behavior of bituminous concrete. The indirect tensile method can be used for designing mixes with adequate fatigue service lives.

Failures in bituminous concrete pavements can usually be classified as (a) rutting or washboarding, a stability problem; (b) progressive cracking, a fatigue problem; or (c) fracture, a strength problem.

Fatigue is certainly one of the most common causes of failure and probably the most difficult to deal with from a design viewpoint. It is possible to establish the fatigue properties of small asphalt concrete specimens by using any of the many test methods available. However, the required equipment is expensive, and a test series takes several weeks. A materials lab, therefore, cannot routinely design mixes against fatigue, so a simple test is needed if fatigue design is to be routinely implementable.

Some of the research efforts in this area are being made by Barksdale (1) and Majidzadeh (2).

PURPOSE

The purpose of this study was to examine the literature for current fatigue tests and promising simple tests and to develop a simple test procedure capable of predicting the fatigue behavior of asphalt concrete. Several of the most promising tests were conducted, and their results were correlated with laboratory fatigue test results on asphalt concrete mixes from various locations in the United States.

SELECTION OF SIMPLE TESTS

Because tensile stresses cause fatigue failures, I selected those simple tests in which tensile failures occur. Other items considered in the selection of the tests were simplicity of sample preparation, utilization of laboratory and pavement samples, sensitivity of test method to mix properties, and capability of predicting fatigue behavior.

Of the seven test methods considered, the five selected for laboratory testing were the indirect tensile, the punch, the resilient modulus, the flexure, and the sonic. The sonic test was selected because equipment was available, no additional specimens had to be made, and there was some previous experience in which sonic measurements were correlated with fatigue (3).

LABORATORY PROCEDURE

Each of five mixes was tested in constant strain fatigue to develop relations between fatigue life and strain and stress. Similar relations were developed for these five mixes and two additional mixes in constant stress. All five simple tests were performed on each of the mixes. Correlations were made between such simple test results as strength, stiffness, and deformation at failure and constants K and n of the fatigue relation.

The simple tests yielding the best correlations with fatigue properties were judged most suitable for use in designing against fatigue failure.

Mixes

All mixes (Table 1) were of the surface type and of a maximum aggregate size less than 19.1 mm (0.75 in). The mix formula, aggregates, and asphalt from Virginia, Pennsylvania, Ohio, Utah, and California provided a variety of stabilities, aggregates, and asphalt cement types. The aggregates included granite, basalt sandstone, limestone, and gravel. The asphalt cements were AC-20, 85-100 penetration, 50-60 penetration, 120-150 penetration, and AR-40. The asphalt contents were 5.5 to 5.8 percent by design; however, the Utah mix contained 6.8 percent because of the reportedly absorptive nature of the aggregate. I anticipated that the various mixes would yield a wide range of stiffnesses and strengths.

Fatigue Tests

Flexural fatigue tests were performed at 22°C (72°F) on

Table 1. Percentages of mix design aggregates passing through sieves.

Item	Pennsylvania 85-100 Penetration (limestone)	Ohio AC-20 (gravel and natural sand)	Utah 85-100 Penetration (basalt-sandstone and limestone)	California AR-40 (granite)	Virginia No. 1 AC-20 (granite and natural sand)	Virginia No. 2 50-60 Penetration (granite and natural sand)	Virginia No. 3 120-150 Penetration (granite and natural sand)
19.10			100.0				
12.50	100.0	100.0	93.0	100.0	100.0	100.0	100.0
9.50	97.0	95.0	85.0	87.0	95.0	95.0	95.0
4.75	63.7	60.0	62.0	64.0	58.0	58.0	58.0
2.36	44.3	46.0	47.5	50.0	41.0	41.0	41.0
1.18	26.6		36.0	37.0			
0.60	18.0			26.0	19.0	19.0	19.0
0.30	12.0	12.5	22.5	19.0	11.0	11.0	11.0
0.15	7.2			11.0			
0.08	4.8	7.0	3.2		5.0	5.0	5.0
Asphalt content, % by weight	5.5	5.5	6.8	5.7	5.8	5.7	5.7
Marshall stability, kg	—	789	771	991	844	1039	964
Voids total mix, %	2.0	2.5	1.9	2.1	2.0	2.3	2.2

Note: 1 mm = 0.039 in and 1 kg = 2.2 lb.

Figure 1. Flexural fatigue test apparatus.

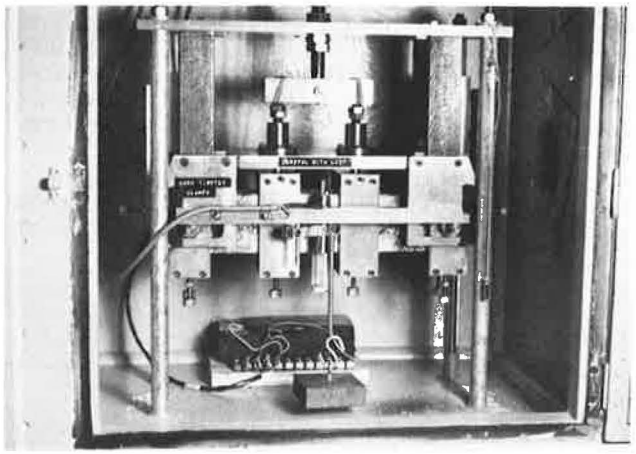

Figure 2. Indirect tensile test apparatus.

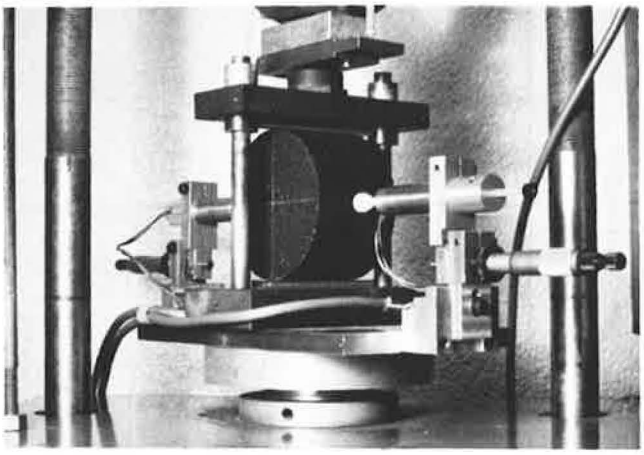

asphalt concrete beams (Figure 1) laboratory fabricated according to ASTM designation D 3202-73 and sawed to 76 by 76 by 381 mm (3 by 3 by 15 in). In the tests, the beams were simply supported and loaded at third points. A 0.1-s haversine load pulse was applied with a closed-loop electrohydraulic load system capable of applying equal repetitions of either load or deflection (strain).

The results of 10 fatigue tests at various stress and strain levels were used to develop the two fatigue relations

$$N = K_1(1/\sigma)^{n1} \quad (1)$$

$$N = K_2(1/\epsilon)^{n2} \quad (2)$$

where

N = number of cycles to failure,
σ = maximum tensile stress at 200 cycles,
ϵ = maximum tensile strain at 200 cycles, and
K_1, K_2, n_1, and n_2 = constants dependent on mix properties.

Failure in the constant stress tests was defined as collapse; failure in the constant strain tests was reached when the initial stiffness was reduced by one-third.

The two relations were obtained by linear regression analyses. Constant stress (load) fatigue tests were performed on seven mixes, but constant strain (deflection) tests were performed on only five mixes because of time and money limitations.

Simple Tests

The indirect tensile test procedure reported by Anagnos and Kennedy (4) was used to test specimens 64 mm (2.5 in) thick and 102 mm (4 in) in diameter. The load was applied at a vertical deformation rate of 51 mm/min (2 in/min) (Figure 2), and the load, horizontal deformation, and vertical deformation were recorded.

The stiffness, strength, and vertical deformation were correlated with the fatigue relation constants K and n.

The punch test reported by Jimenez (5) was used to test specimens 64 mm (2.5 in) thick and 102 mm (4 in) in diameter. The specimen was centered between 25.4-mm (1-in) diameter punches compressed at 51 mm/min (2 in/min) (Figure 3). The stiffness, strength, and vertical deformation were computed and correlated with fatigue properties.

The resilient modulus test was performed on specimens 64 mm (2.5 in) thick and 102 mm (4 in) in diameter by applying a dynamic diametral load and then measuring the perpendicular diametral deformation. A 192-N (43.1-lb) load producing a 20.6-kPa (3-lbf/in^2)

Figure 3. Punch test apparatus.

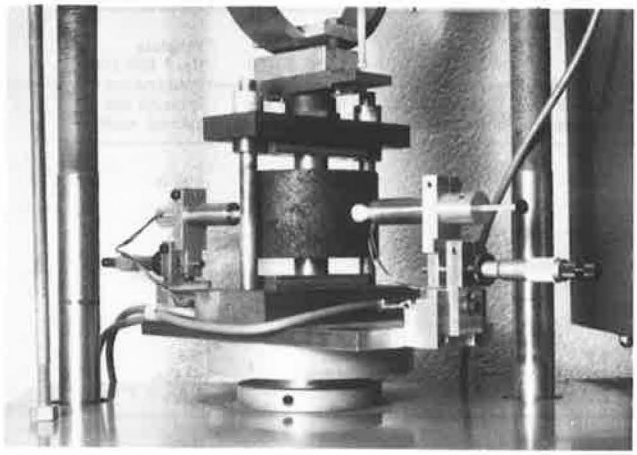

tensile stress was applied for 0.1 s. Stiffness was computed by assuming a Poisson's ratio of 0.3 and then correlating it with the fatigue characteristics.

Flexure tests were performed on 76 by 76 by 190-mm (3 by 3 by 7.5-in) sawed beams. The beams were simply supported on 38-mm (1.5-in) plates and were loaded at the midpoint through a 25-mm (1-in) wide metal plate. The midspan vertical deformation and load were recorded, and elastic theory was used to compute the failure strength and stiffness.

Resonant frequency tests were performed on each fatigue beam prior to fatigue testing by ASTM method C 215-60. Only the transverse frequency measurement was used in computing the dynamic Young's modulus, which was used for correlations. (Young's modulus can be computed from the known velocity at which a sound wave travels through a material.) Pulse velocity measurements were also taken on the fatigue beams, before fatigue testing, to obtain values for use in calculating the dynamic Young's modulus.

RESULTS

Fatigue Tests

The relations developed by linear regression analyses from the fatigue tests are listed in Table 2. As expected, testing in the constant stress mode showed the stiff mixes exhibiting longer fatigue lives than the mixes with low stiffness. The slope of the linear log-log plot of the fatigue life versus stress relation was maximum for the Utah mix and minimum for the Virginia 120-150 penetration asphalt cement (Figure 4). Therefore, the stiffness of the mix may be related to the coefficient n_1 (slope) of the fatigue relation in Equation 1.

No similar observation can be made of the log fatigue life versus log strain plot for the constant strain fatigue tests (Figure 5). Four of the five mixes tested appeared to converge between 500 000 and 1 000 000 cycles, but there is apparently no relation between stiffness and slope of the fatigue relation in Equation 2.

Table 2. Fatigue relations from flexural fatigue tests.

Mix	$N = K_1(1/\sigma)^{n_1}$ (σ, kPa)		$N = K_2(1/\epsilon)^{n_2}$	
	K_1	n_1	K_2	n_2
Constant Stress Fatigue Relations				
Virginia (AC-20)	8.9×10^{21}	5.9	2.8×10^{-8}	3.9
Virginia (50-60 penetration)	2.8×10^{19}	4.8	2.7×10^{-4}	2.6
Virginia (120-150 penetration)	3.0×10^{18}	4.9	8.5×10^{-2}	1.9
Pennsylvania	5.6×10^{22}	6.1	1.0×10^{-6}	3.6
Ohio	1.6×10^{22}	6.2	7.0×10^{-4}	2.5
Utah	5.1×10^{27}	7.5	9.5×10^{-9}	4.1
California	4.0×10^{27}	8.1	6.4×10^{-7}	3.8
Constant Strain Fatigue Relations				
Virginia (AC-20)	4.5×10^{16}	4.0	2.3×10^{-9}	4.4
Pennsylvania	2.6×10^{12}	2.6	3.9×10^{-4}	2.8
Ohio	1.0×10^{12}	2.5	2.3×10^{-2}	2.1
Utah	1.1×10^{21}	5.2	2.4×10^{-5}	3.1
California	8.4×10^{12}	2.9	5.2×10^{-3}	2.4

Note: $N = K_1(0.1451)^{n_1}(1/\sigma)^{n_1}$ when σ is in pound force per square inch.

Simple Tests

Because the stress rates used in the simple tests were not necessarily equal, the failure stresses are not directly comparable. The ranges of the average test results for the seven mixes are summarized in Table 3.

The coefficient of variation was approximately 8 percent for determining strength with the indirect tensile, punch, and flexure tests. The coefficients of variation for stiffness averaged 8 percent for the indirect tensile test, 13 percent for the punch, 8 percent for the flexure, 9 percent for the resilient modulus, 6 percent for the resonant frequency, and 5 percent for the wave velocity test.

The coefficients of variation were approximately equal for all test methods except the punch test, whose coefficient was slightly higher for the stiffness measure-

Figure 4. Constant stress tests.

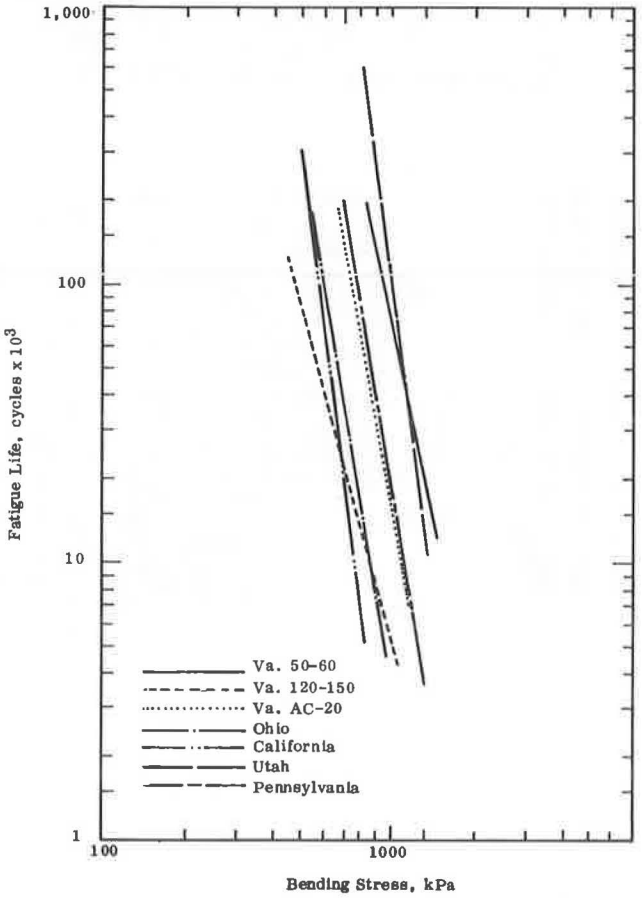

Figure 5. Constant strain tests.

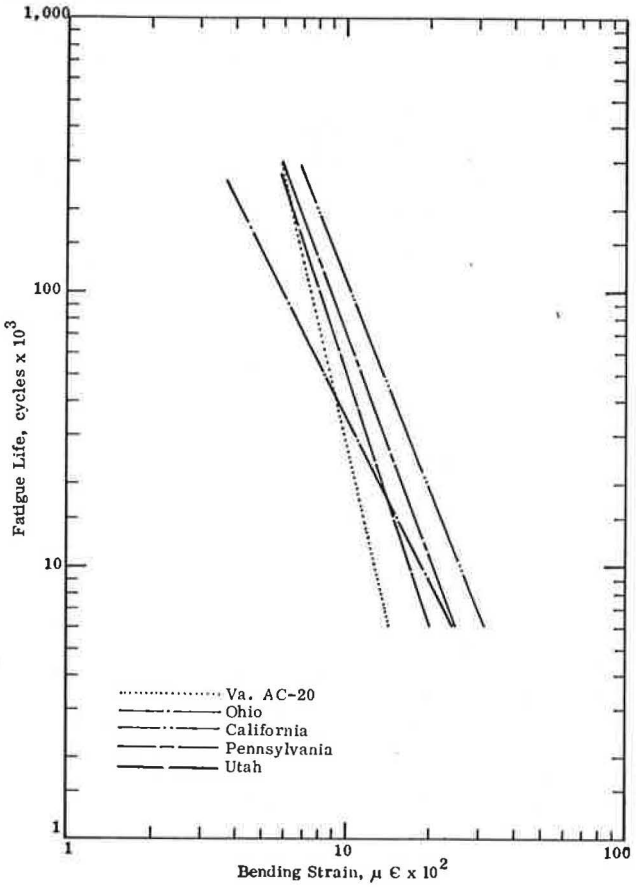

ments. Therefore, test variability was not a major consideration in the evaluation.

Correlation of Simple Test and Fatigue Test Results

Simple linear correlations were performed between simple test results and selected fatigue characteristics. These correlations were performed to determine whether a simple test could be used to predict the fatigue behavior of asphalt concrete.

Constant Stress Tests

The correlation coefficients between simple test results and constant stress test results are listed in Table 4. In order to predict the fatigue relation (Equation 1), K_1 and n_1 must be known. The best correlation coefficients for n_1 were obtained from the indirect tensile stiffness (0.87) and punch stiffness (0.88). The value $\sigma_{n=1}$ is the projected stress on the fatigue curve at N = 1 cycle and allows the prediction of the K_1 value. The fatigue characteristic $\sigma_{n=1}$ yielded a 0.93 correlation coefficient with the indirect tensile stiffness. Therefore, the test results that permit the best prediction of the fatigue relation in Equation 1 are the indirect tensile strength and the stiffness. The following relations that were obtained from the correlations can be used to predict this fatigue relation in pascals.

$$n_1 = 11.6 - 0.000\,396\,E_{IT} \quad (3)$$

$$K_1 = e^{n_1 \ln(12.6\sigma_{IT} - 558)} \quad (4)$$

where E_{IT} is indirect tensile stiffness, and σ_{IT} is indirect tensile strength.

The correlations involving n_2 and log K_2 (Table 4) were inadequate for predicting the fatigue relation in Equation 2 for the constant stress fatigue test.

Constant Strain Tests

The correlation coefficients between simple test results and constant strain test results are listed in Table 5.

One must determine n_2 and K_2 before finding the fatigue relation in Equation 2. The best correlations involving n_2 were the transverse frequency modulus (0.84) and the indirect tensile strength (0.81). The best correlations from which K_2 could be determined were those of the resilient modulus (0.95), the transverse frequency modulus (0.85), and the indirect tensile strength (0.85). For efficiency, I preferred to use the same simple test for both constant stress and constant strain fatigue

Table 3. Simple test average value ranges for seven mixes.

Parameter	Indirect Tensile	Punch	Flexure	Resilient Modulus	Resonant Frequency	Wave Velocity Moduli
Strength, MPa	0.489 to 1.10	0.510 to 0.937	2.31 to 4.97	–	–	–
Failure, stiffness, MPa	75 to 126	101 to 220	33.8 to 57.9	634 to 2210	6340 to 8540	24 800 to 30 900
Failure, vertical deformation, mm	3.78 to 5.33	4.85 to 7.90	3.71 to 4.90	–	–	–

Note: 1 MPa = 145 lbf/in² and 1 mm = 0.039 in.

Table 4. Correlation between constant stress fatigue test and simple tests.

Equation	Fatigue Characteristic	Stiffness[b]						Strength[b]			Vertical Deformation[b]	
		Indirect Tensile	Punch	Flexure	Resilient Modulus	Transverse Frequency	Wave Velocity	Indirect Tensile	Punch	Flexure	Indirect Tensile	Punch
$N = k_1 (1/\sigma)^{n_1}$	n_1	0.87	0.88	0.51	0.52	0.34	0.61	0.70	0.79	0.45	0.08	0.18
		(0.67)	(0.64)	(1.15)	(1.15)	(1.26)	(1.07)	(0.96)	(0.82)	(1.20)	(1.34)	(1.32)
	log k_1	0.79	0.83	0.37	0.35	0.09	0.52	0.53	0.68	0.26	0.18	0.41
		(1.74)	(1.60)	(2.66)	(2.68)	(2.85)	(2.44)	(2.43)	(2.10)	(2.76)	(2.81)	(2.61)
$N = k_2 (1/\epsilon)^{n_2}$	n_2	0.53	0.62	0.28	0.09	0.14	0.45	0.23	0.34	0.05	0.40	0.47
		(0.79)	(0.73)	(0.90)	(0.93)	(0.92)	(0.84)	(0.91)	(0.88)	(0.93)	(0.86)	(0.82)
	log k_2	0.45	0.52	0.16	0.03	0.23	0.31	0.12	0.24	0.08	0.50	0.56
		(2.49)	(2.38)	(2.76)	(2.79)	(2.71)	(2.65)	(2.77)	(2.71)	(2.78)	(2.42)	(2.32)
$\sigma_{n=1}$[a]		0.91	0.81	0.72	0.76	0.77	0.55	0.93	0.81	0.71	0.39	0.10
		(187)	(258)	(308)	(287)	(282)	(371)	(161)	(259)	(315)	(409)	(442)

[a] Refer to definition for Equations 3 and 4. [b] Standard error of estimate listed in parentheses.

Figure 6. Fatigue design of bituminous concrete in the constant stress failure mode.

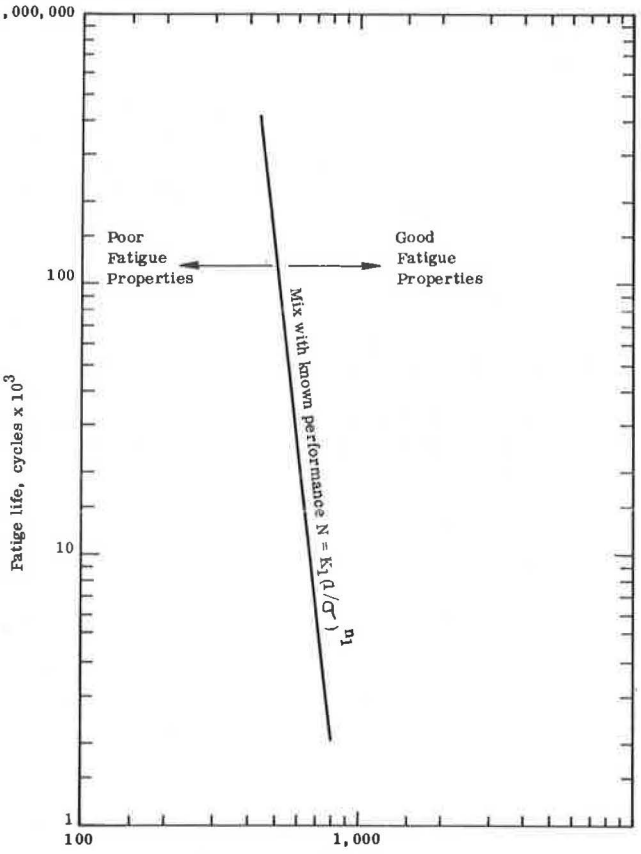

Note: 1 kPa = 0.145 lbf/in².

predictions. Therefore, even though the transverse frequency modulus and resilient modulus are the best predictors of the constant strain-fatigue relation, I selected indirect tensile strength so that the same test could be used.

The relations that can be used to determine the fatigue Equation 2 for constant strain fatigue are

$$n_2 = 0.0374\sigma_{IT} - 0.744 \quad (5)$$

$$\log K_2 = 7.92 - 0.122\sigma_{IT} \quad (6)$$

where σ_{IT} is indirect tensile strength.

The correlations would not allow a reasonable prediction of the fatigue Equation 1 for constant strain fatigue tests.

USE OF THE SIMPLE TEST PROCEDURE

The indirect tensile test procedure is primarily a tool for designing mixes that will have desirable fatigue characteristics. Rather than being used for routine design, the method should probably be used for special situations. An example might be designing a mix for a location having expected high deflections and needing a layer of asphalt concrete approximately 150 mm (6 in) thick. I assumed that the constant strain test is applicable to an asphalt concrete thickness less than 76 mm (3 in) and that the constant stress test is applicable to a thickness greater than 76 mm (3 in). A 150-mm (6-in) layer indicates that the constant stress test analysis would be applicable. Because high deflections are expected, the mix should be designed for high stress magnitudes. The steps in the design procedure are outlined below.

1. Obtain the indirect tensile strength and stiffness of a mix with a known fatigue field performance.
2. From these data, compute the fatigue relation in Equation 1 from Equations 3 and 4.
3. Plot this relation on log-log paper as shown in Figure 6. (It is obvious that mixes located to the right of the relation will have better fatigue properties than those to the left.)
4. Design the potential mix, possibly using a hard asphalt cement.
5. Obtain the indirect tensile strength and stiffness.
6. Compute the fatigue relation in Equation 1 from Equations 3 and 4.
7. Plot this relation on log-log paper.
8. Compare the mix with a known fatigue performance.

If the fatigue properties are not improved, it may be necessary to try other mix designs.

ACKNOWLEDGMENTS

The funding for the research reported here was provided by the U.S. Department of Transportation. Appreciation is expressed to Stewart R. Spelman for his general guidance and cooperation during the study. I also would like to express my appreciation to the following people for providing aggregates and asphalt cements used in the laboratory mixes: E. S. Lindow, Pennsylvania Transportation Institute; Dale E. Peterson and Joseph C. McBride, Utah State Department of Highways; F. M. Williams and R. A. Luce, Ohio Department of Transportation; and Carl L. Monismith, University of California. Appreciation is expressed to J. H. Dillard for encouragement in the project and to C. S. Hughes III for general guidance and advice on the statistical analysis. L. E. Wood, Jr., our laboratory

Table 5. Correlation between constant strain fatigue test and simple tests.

Equation	Fatigue Characteristic	Stiffness[a]						Strength[a]			Vertical Deformation[a]	
		Indirect Tensile	Punch	Flexure	Resilient Modulus	Transverse Frequency	Wave Velocity	Indirect Tensile	Punch	Flexure	Indirect Tensile	Punch
$N = k_1 (1/\sigma)^{n_1}$	n_1	0.15 (1.22)	0.15 (1.22)	0.74 (0.83)	0.44 (1.11)	0.62 (0.97)	0.50 (1.07)	0.53 (1.05)	0.08 (1.23)	0.73 (0.85)	0.64 (0.95)	0.68 (0.91)
	$\log k_1$	0.12 (3.29)	0.22 (3.24)	0.65 (2.51)	0.41 (3.03)	0.67 (2.48)	0.38 (3.07)	0.54 (2.79)	0.10 (3.30)	0.68 (2.45)	0.70 (2.36)	0.72 (2.29)
$N = k_2 (1/\epsilon)^{n_2}$	n_2	0.79 (0.63)	0.28 (0.98)	0.46 (0.90)	0.56 (0.84)	0.84 (0.56)	0.46 (0.90)	0.81 (0.59)	0.47 (0.90)	0.59 (0.83)	0.40 (0.94)	0.18 (1.00)
	$\log k_2$	0.82 (1.82)	0.34 (3.00)	0.64 (2.46)	0.95 (2.69)	0.85 (1.67)	0.51 (2.75)	0.85 (1.69)	0.51 (2.74)	0.64 (2.46)	0.41 (2.91)	0.19 (3.14)

[a]Standard error of estimate listed in parentheses.

supervisor, is acknowledged for scheduling and performing the many tests. And appreciation goes to S. A. Kelley, our computer programmer, for running the analysis program.

The contents of this report reflect my views, and I alone am responsible for the facts and the accuracy of the data presented. The contents do not necessarily reflect the official views or policy of the U.S. Department of Transportation. The opinions, findings, and conclusions expressed in this paper are mine and not necessarily those of the sponsoring agencies.

REFERENCES

1. R. D. Barksdale. Development of Equipment and Techniques for Evaluating Fatigue and Rutting Characteristics of Asphalt Concrete. Research Quarterly Progress Rept., Georgia Technical Research Institute, Project GA DOT 7305, GA Tech. E20-666, July 7, 1975.
2. K. Majidzadeh. Proposal—A Study for Laboratory Implementation of Fatigue Mix Design Procedures. Engineering Experiment Station, Ohio State Univ., May 1974.
3. C. R. Freeme and C. P. Marais. Thin Bituminous Surfaces: Their Fatigue Behavior and Prediction. HRB, Special Rept. 140, 1973, pp. 158-182.
4. J. N. Anagnos and T. W. Kennedy. Practical Method of Conducting the Indirect Tensile Test. Center for Highway Research, Univ. of Texas at Austin, Aug. 1972.
5. R. A. Jimenez. Testing for Debonding of Asphalt From Aggregates. Univ. of Arizona, Research Project Rept., Arizona HPR-1-10(123), Apr. 1973.

Publication of this paper sponsored by Committee on Characteristics of Bituminous Paving Mixtures to Meet Structural Requirements.

Laboratory Measurement of Permeability of Compacted Asphalt Mixtures

Arun Kumar,*Central Road Research Institute, New Delhi, India
W. H. Goetz, School of Civil Engineering, Purdue University, West Lafayette, Indiana

An improved method for measuring the permeability of compacted asphalt mixtures in the laboratory was developed. It eliminates the difficulties encountered with using a rubber membrane for sealing the specimen in a metal cylinder. In the new method, the specimen wall is coated with a one-part silicone rubber sealer that is applied as a paste with a spatula and is permanently flexible and waterproof. After the coating has cured and been checked for leaks, a known pressure difference is created by a vacuum across the specimen. The rate of air flow through the specimen is obtained at various differential pressure values. Flow rate is plotted against pressure difference, and the slope of the straight line portion of the curve is calculated. Permeability is calculated by using this slope value and the specimen height. The technique measures the true permeability, eliminates the possibility of specimen deformation during testing and the problems associated with other methods, permits no asphalt contamination, and is versatile with respect to aggregate gradation and asphalt grade.

The importance of measuring permeability, the small openings in a medium that permit liquids or gasses to pass through it, has long been recognized in the field of asphalt concrete. In 1955 McLaughlin and Goetz (1) hypothesized that using permeability gives a better measure of durability than using void content alone. Permeability, in their opinion, can be used to measure the capacity of a porous medium to transmit fluid, whereas the normal measure using voids in a bituminous mixture does not directly measure the forces producing disintegration.

Hein and Schmidt (2), after conducting a study on air permeability of asphalt concrete, suggested that permeability measurements are essential to routine mix design studies. Their results indicated that the void content of mixtures is not necessarily proportional to permeability when the variation is caused by gradation.

An investigation to evaluate the effects of air permeability and air void content on the durability of asphalt concrete was conducted by Smith and Gotolski (3). One of their conclusions was that air permeability is a good indicator of the extent of accessibility of the air void system.

This literature review indicates a need for a laboratory permeability measuring technique for predicting asphalt concrete behavior from the standpoint of durability.

METHOD

Keyser and Gilbert (4) conducted a study of methods that were then (1973) being used to determine the permeability of bituminous mixtures. They reported that 15 types of permeameters were in use in North America and Europe, of which 9 could be used in the laboratory.

In general, air permeability is measured by creating a known pressure differential across a specimen and then measuring the amount of air flow over a known period of time. The test requires that the specimen be encased so that air flow is limited to passage through it. This has been accomplished by sealing the specimen in a metal cylinder with asphalt or other sealing material. This method, however, is destructive to the specimen; it is also difficult to be certain that a complete seal has been obtained.

Goode and Lufsey (5) used paraffin to prevent leakage of air between the sides of the specimen and the membrane. Before extracting the asphalt, they discarded the outer 0.64 cm (0.25 in) of the specimen with the intention of eliminating paraffin contamination of the extracted asphalt. Even then, they found enough contamination to invalidate their results.

Another procedure is to place the specimen in a cylindrical rubber membrane fastened to a hollow metal cylinder with hose clamps (Figure 1). The membrane is then inflated enough to prevent air from passing between the walls of the specimen and the membrane during the permeability measurement. Macroscopically the procedure seems to be sound, but, when the surface-membrane contact is observed microscopically (Figure 1B), the following points can be noted.

1. The membrane is in contact with only the high points of the aggregates (for example, points a, b, c, d, and e in Figure 1). Thus, air passing between the specimen surface and the membrane would give a permeability value higher than it really is.
2. The gradation of the mix plays an important role. For coarse mixes, specimen-membrane contact will be reduced, which may also result in a deviation from the true permeability value.
3. Inflation pressure in the membrane is important. If the pressure is low, there will be less specimen-membrane contact. If the pressure is too high, the specimen may deform, especially if it is of low density or the binder is of low viscosity.
4. The thickness of the membrane is important. A thick membrane will also result in less specimen-membrane contact. If the membrane is too thin, it will bulge near the hose clamps and increase the probability of bursting.

Figure 1. Permeability measurement of compacted asphalt mixtures using rubber membrane.

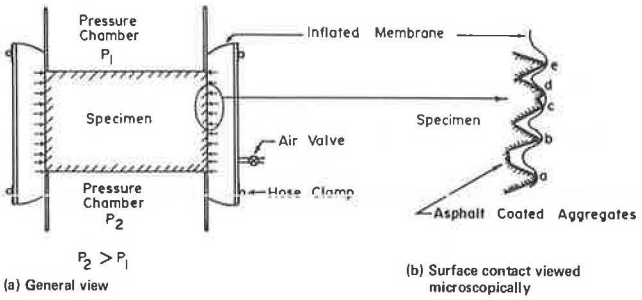

Figure 2. Component parts of the mold assembly: (A) base plate, (B) specimen supporter, (C) wire gauze, (D) lower collar, (E) upper collar with "o" ring, and (F) cover plate.

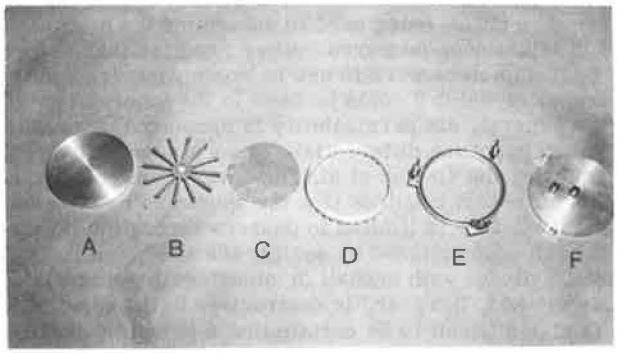

The above points clearly indicate that it is difficult for the experimenter to visualize the extent of the specimen-membrane contact area. As described earlier, the amount of air flow through the specimen is measured at a certain pressure differential across it, which in turn is used to calculate the permeability of the compacted bituminous mixture. Theoretically, the true permeability value of this compacted mixture should be obtained from the total amount of air flowing through each channel in the specimen. In the above procedure, total air flow is measured as the sum of air flowing through each channel plus the amount flowing between the specimen wall and the membrane. Therefore, one will get a permeability value higher than the true value if air passes between the specimen wall and the membrane.

In general, the greater the specimen surface-membrane contact area, the closer the results will be to the true permeability value. Because the extent of the contact area relies on so many factors, especially when coarse mixes are used, it may be rather difficult to obtain the true value of permeability.

TECHNIQUE AND MEASUREMENT PROCEDURE

The present method eliminates the above problems. The idea is to replace the membrane with a rubber coating enveloping the specimen. This procedure for measuring the permeability of asphalt concrete is outlined as follows.

Apparatus

Equipment includes a mold assembly for the 10.16-cm (4-in) diameter specimen (Figures 2, 3, and 4) (suitable modifications should be made for specimens of other sizes), a vacuum pump, flowmeters (range for air, 1 to 77 000 ml/min), a manometer, a pressure line, silicone rubber sealer (6), and a thermometer.

Specimen Preparation

Limestone aggregate and 200-250 penetration asphalt were used in this study. The aggregates, brought from the quarry, were dried and sieved, then washed and dried again. Each specimen was batched by component factions in accordance with the cumulative batch weight formula.

Each individual batch of aggregates was thoroughly mixed and heated to 149 ± 3°C (300 ± 5°F), and the asphalt was heated separately to 135 ± 3°C (275 ± 5°F). The two were mixed in an electric mixer (Hobart model N-50) for 2 min. The batch was then ready for compaction. The gyratory testing machine was used as a compaction device because it provides a good simulation of field compaction (7).

Procedure

1. The specimen supporter is set on the base plate. If the mix is very coarse and has low density, a fine wire mesh may be placed on the specimen supporter to eliminate the chance of being unsupported between the ribs (Figure 2). The lower collar is placed on the base plate. The lower assembly is now ready to receive the specimen for coating (Figure 5).
2. The specimen is placed on the supporter and coated with the silicone rubber sealer all around, leaving only about 2.5 cm (1 in) from the top of the specimen (Figure 6). One should make sure that enough sealer is

applied at the top of the lower collar so that it adheres to the specimen.

3. After the sealer has partially cured (approximately 8 h), the specimen (the lower collar will be fixed to it) is lifted, the upper collar is placed upside down on the base plate, and the specimen is reversed and seated on the supporter. The whole assembly should be elevated so that the upper collar sits properly on the base plate. The rest of the specimen is coated with the same sealer, and adheres to the upper collar (Figure 7). The assembly is then left overnight for the sealer to cure.

4. The next day, the specimen is turned upside down and placed on the supporter. The cover plate is seated on the upper collar and the wing nuts tightened (Figure 8).

5. In checking for leaks, one of the two openings in the cover plate is closed, and pressure is applied gradually through the other. Then the entire assembly is immersed in water and pressure slightly higher than the maximum anticipated suction pressure to be applied during the permeability measurement is applied (Figure 9). Air will start bubbling through the semicircular holes in the lower collar (Figure 10). The sides of the specimen should be checked for any air leaks. If any leak is observed, it should be repaired and rechecked.

6. The height of the specimen (H) is measured (Figure 11).

7. The specimen is now ready for testing. One opening of the coverplate is connected to the flowmeter, through which air is to be drawn by a vacuum pump. The other opening is connected to the manometer to record the pressure differential created across the specimen (Figure 12).

8. The rate of air flow (R) in millileters per minute through the specimen is shown by the flowmeter at various pressure differential values (ΔP), by using a control valve in the vacuum line.

9. The test temperature is recorded.

10. The rate of airflow (Y axis) versus pressure difference (X axis) is plotted, and the slope (S) of the straight line portion of the curve using a linear regression equation is obtained (8). By using this slope value and specimen height, the permeability can easily be calculated.

Figure 3. Exploded view of mold assembly.

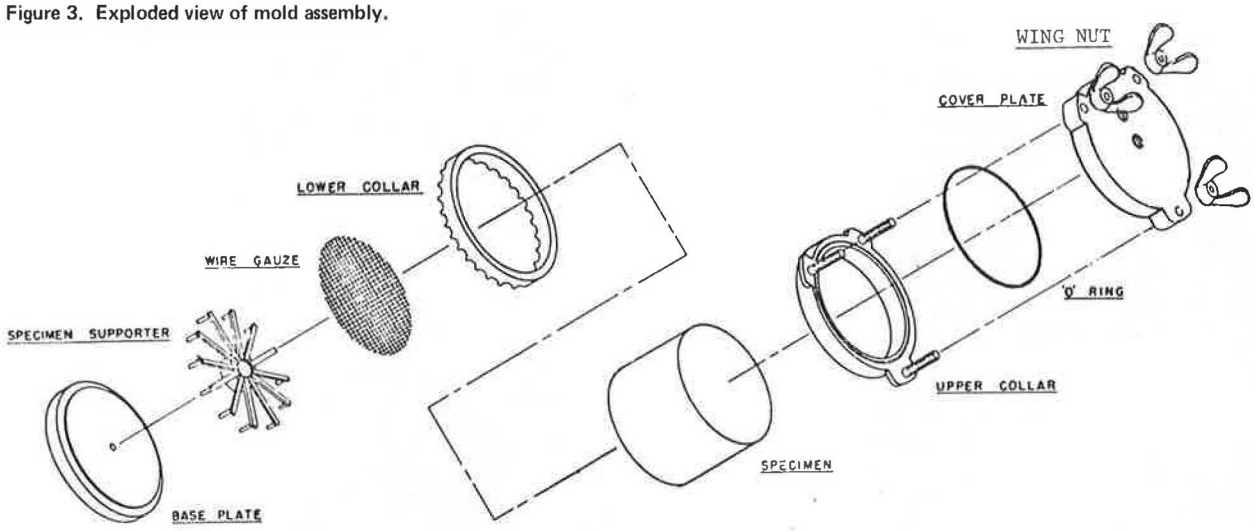

Figure 4. Detailed view of mold assembly.

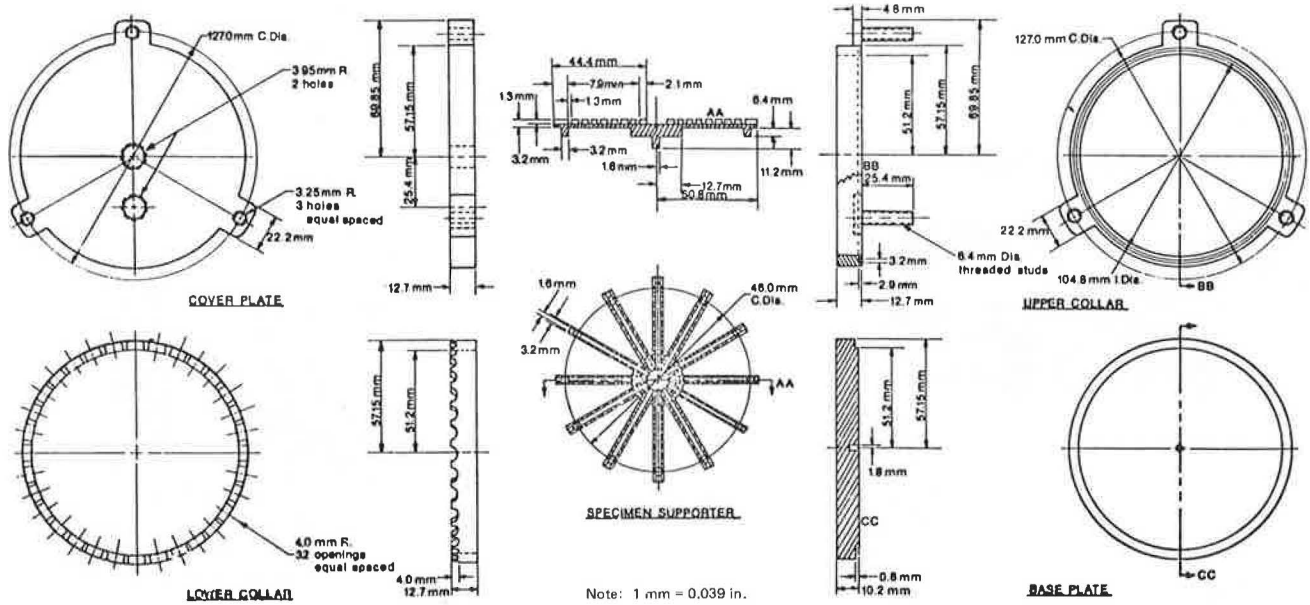

Figure 5. Lower assembly ready to receive specimen for coating.

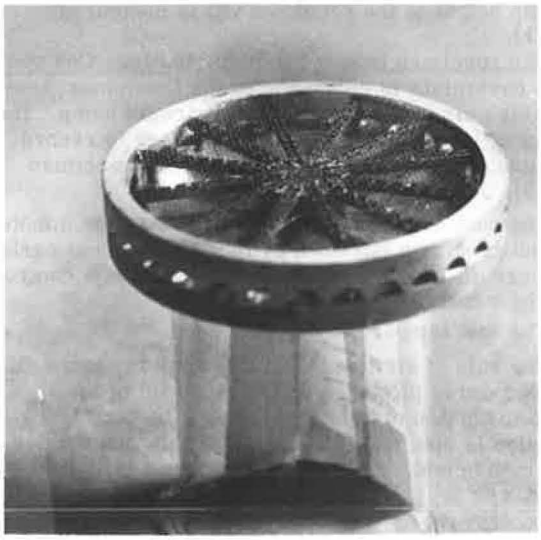

Figure 6. Specimen coated to within 2.5 cm (1 in) of top.

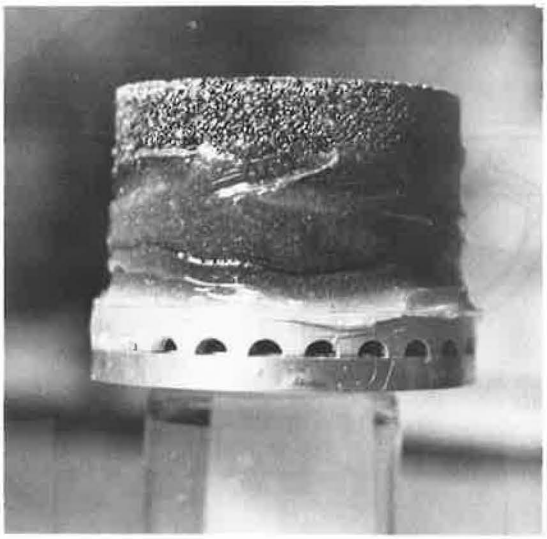

Figure 7. Completely coated specimen.

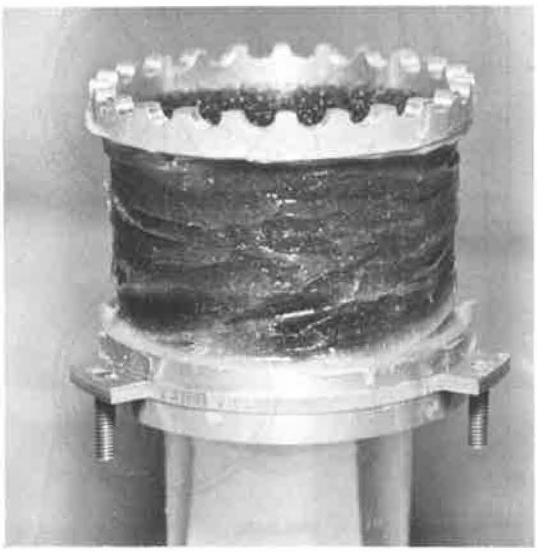

Figure 8. Assembly ready for leak check.

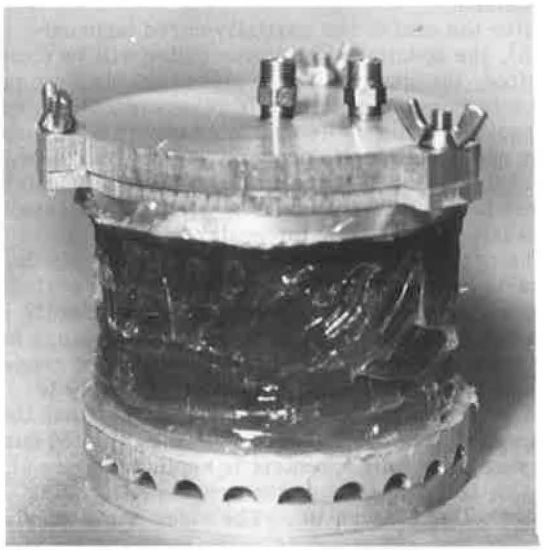

Figure 9. Air leak check set-up.

Figure 10. Air bubbling through openings in lower collar.

Figure 11. Measuring height of specimen.

Figure 12. Measuring permeability of specimen.

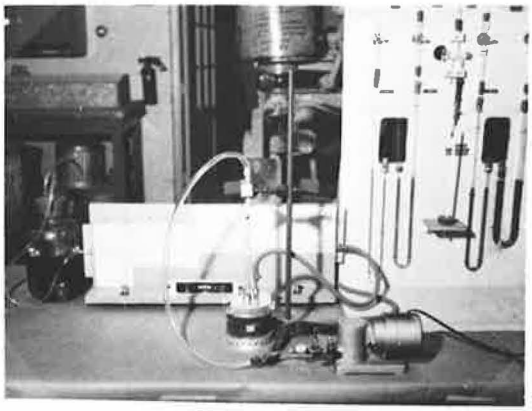

Calculations

The data for four combinations of varying asphalt content, aggregate gradation (Table 1), and compactive effort (8) are presented here in order to demonstrate the technique and its versatility. Values for the various variables involved in mix preparation, compaction, and the properties of the compacted mixes are given in Table 2. Table 3 presents values for rate of flow versus pressure difference across the specimen for various mixtures. These values are plotted in Figures 13, 14, 15, and 16.

The slopes of the straight line portions of the curves were obtained by linear regression (8) and are given in Table 3. The slope and specimen height values were then substituted into the following permeability formula.

$$K = 3.812 \times 10^{-11} \times S \times H \quad (1)$$

Table 1. Gradation of the mixes.

	Percentage Passing			
	Single Size Mix		Graded Mix	
U.S. Sieve Size	A Coarse	B Fine	C[a] Coarse Side	D[a] Mid Point
12.5 mm			100	100
9.5 mm			80	88.5
4.75 mm	100		40	50.0
2.36 mm	0		30	39.0
1.18 mm			18	26.5
600 μm			9	16.5
300 μm		100	3	8.0
150 μm		0	0	0.0

Note: 1 mm = 0.039 in and 1 μm = 0.0039 in.
[a] Type B no. 11 (9).

Table 2. Preparation and properties of single size and graded mixes.

Item	A	B	C	D
Preparation				
Aggregate type	Limestone	Limestone	Limestone	Limestone
Asphalt grade, penetration	200 to 250	200 to 250	200 to 250	200 to 250
Percent asphalt by weight of aggregate	2	8	5.5	5.5
Gyratory settings				
Angle of gyration	1°	1°	1°	1°
Ram pressure, kPa	689.4	689.4	1378.8	689.4
Type of roller	Fixed	Fixed	Fixed	Fixed
No. of gyratory revolutions	12	25	32	19
Properties				
Specimen height, cm	6.31	6.01	6.32	5.85
Unit weight, kg/m^3	1675	1658	2117	2208
Percent air voids (total calculated)	33	30	7.6	11.1
Permeability, cm/s	2.94×10^{-5}	2.50×10^{-7}	5.52×10^{-9}	1.03×10^{-7}

Note: 1 kPa = 0.145 lbf/in^2; 1 cm = 0.39 in; 1 kg/m^3 = 0.062 lb/ft^3.

Table 3. Rate of air flow versus pressure difference across the specimen for single size and graded mixes.

A			B			C			D		
Pressure Difference (cm of water)	Slope[a]	Rate of Air Flow (ml/min)	Pressure Difference (cm of water)	Slope[a]	Rate of Air Flow (ml/min)	Pressure Difference (cm of water)	Slope[a]	Rate of Air Flow (ml/min)	Pressure Difference (cm of water)	Slope[a]	Rate of Air Flow (ml/min)
0.010	308 482	895	1.27	2747	1200	3.81	58	32	2.54	1147	1810
0.020		2025	1.91		1950	5.08		60	3.81		2435
0.031		3230	2.54		2620	6.35		88	5.08		2935
0.041		4740	3.18		3500	7.62		120	6.35		3500
0.051		5790	3.81		3900	8.89		147	7.62		4140
0.061		7040	4.45		4700	10.16		178	8.89		4690
0.071		8215	5.08		5350				10.16		5105
									11.43		5450
									12.70		5590

Note: 1 cm = 0.394 in and 1 ml = 0.035 oz.
[a] Slope of the straight line portion of the curve in milliliters per minute per 25.4 mm.

Figure 13. Rate of air flow versus pressure difference across specimen A.

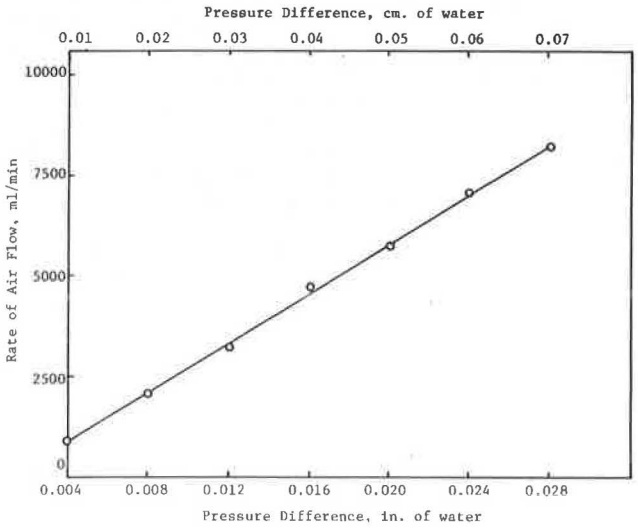

Figure 14. Rate of air flow versus pressure difference across specimen B.

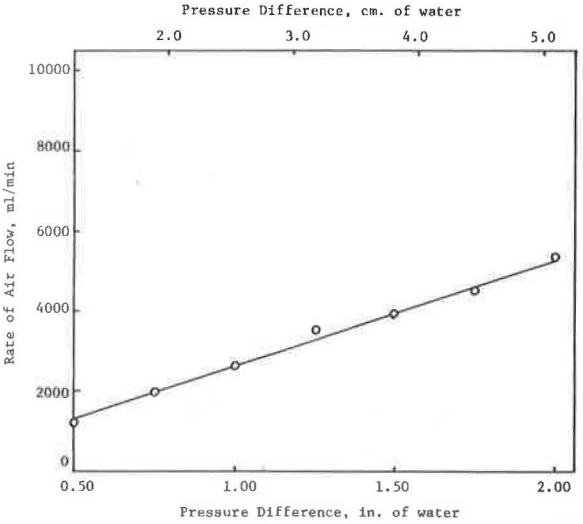

where

K = permeability in centimeters per second,
S = slope of the straight line portion of the curve in millileters per minute per 25.4 mm, and
H = height of specimen, in centimeters.

The above formula is for a testing temperature of 20°C (68°F) and was modified from the conventional formula of permeability, given by Hein and Schmidt (2),

$$K = \mu \bar{Q} L / A(p_1 - p_2) \qquad (2)$$

where

μ = viscosity of air in poises,
$\bar{Q}$ = rate of air flow, in cubic centimeters per second,
L = height of specimen in centimeters,

Figure 15. Rate of air flow versus pressure difference across specimen C.

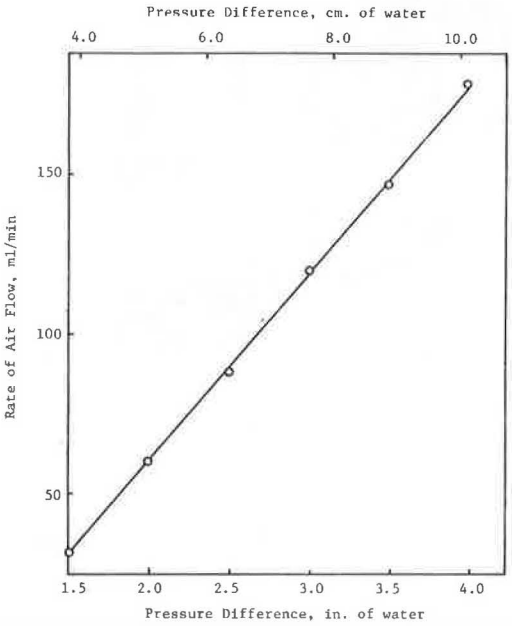

Figure 16. Rate of air flow versus pressure difference across specimen D.

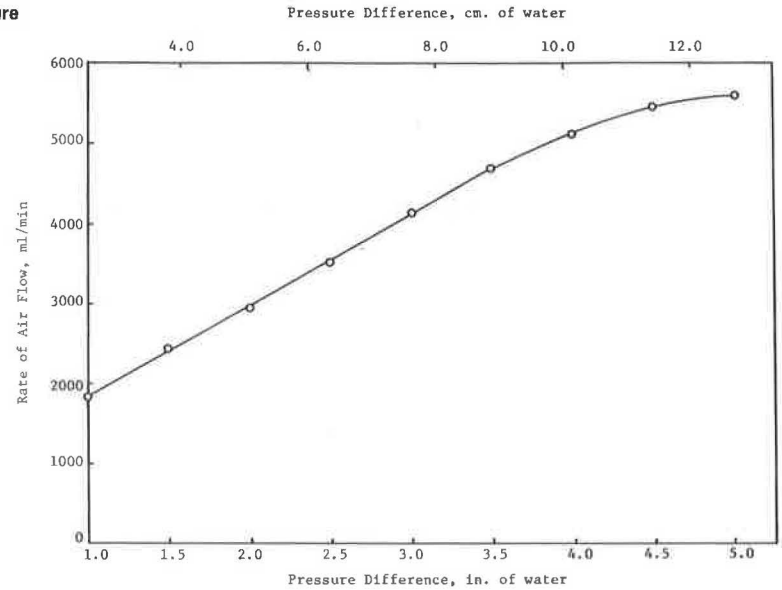

A = cross-sectional area of specimen in square centimeters, and
$p_1 - p_2$ = pressure differential, dynes per square centimeter.

For specimens 10.16 cm (4 in) in diameter, a test temperature of 20°C (68°F), and a value for μ at 20°C (68°F) of 1.813×10^{-4} Pa·s (9), the above formula reduces to:

$$K = (3.812 \times 10^{-11} \times R \times H)/\Delta P \quad (3)$$

where

R = rate of airflow in milliliters per minute,
H = height of specimen in centimeters, and
ΔP = pressure differential in centimeters of water.

By using the slope of the straight line portion of the curve obtained from the plot of rate of airflow (R) (Y axis) versus pressure difference (ΔP) (X axis), this reduces to Equation 1.

For temperatures other than 20°C (68°F), the formula should be suitably modified as

$$K = 3.812 \times 10^{-11} \times S \times H \times (\mu \text{ @ test temperature}/1.813) \quad (4)$$

CONCLUSIONS

The major objective of this work was to develop a technique to measure the true permeability value of compacted asphalt mixtures. It eliminates such variables as selection of membrane thickness and selection of inflation pressure. Also, it avoids the possibility of specimen deformation.

The method has broad applicability; for example, the permeability value can be obtained for both very coarse and very fine single size mixtures (Figure 17) and for mixtures made with low viscosity asphalts, since coating arrests deformation.

Because the slope value of the plot between rate of air flow versus pressure difference across the specimen is used for permeability calculations, the need for adjusting the zero error is eliminated. The method also eliminates the possibility of using incorrect data in the turbulence range (11), because only the slope of the straight line portion of the curve is used in the calculations. It also eliminates asphalt contamination, because no silicone sticks to the specimen when the layer is peeled away (Figure 18).

The assembly prepared in this way for permeability measurement can be very effectively used for laboratory simulation of the weathering of asphalt due to air movements in the pavement.

Figure 17. Single size coarse and fine compacted mixtures.

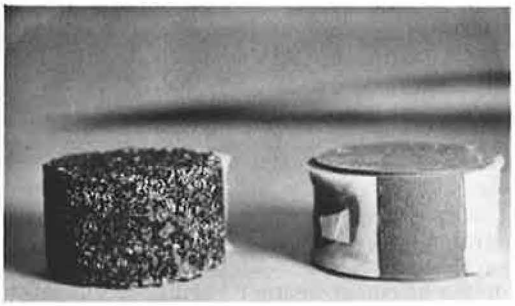

Figure 18. Easily removed coating shows no asphalt contamination.

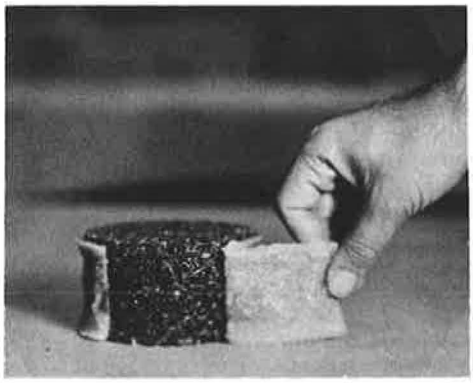

REFERENCES

1. J. F. McLaughlin and W. H. Goetz. Permeability, Void Content, and Durability of Bituminous Concrete. Proc., HRB, Vol. 34, 1955, pp. 274-286.
2. T. C. Hein and R. J. Schmidt. Air Permeability of Asphalt Concrete. ASTM, Special Technical Publication No. 309, 1961.
3. R. W. Smith and W. H. Gotolski. A Study of Physical Factors Affecting the Durability of Asphaltic Pavements: Void Parameters Affecting Asphalt Concrete Durability. Pennsylvania State Univ. Special Rept. No. 3, 1969.
4. P. Gilbert and J. H. Keyser. A Study of Currently Used Methods for Determining the Permeability of Bituminous Mixtures. Journal of Testing and Materials, Philadelphia, Vol. 1, No. 6, 1973.
5. J. F. Goode and L. A. Lufsey. Voids, Permeability, Film Thickness Versus Asphalt Hardening. Proc., AAPT, Minneapolis, Vol. 34, 1965.
6. Information About Dow Corning Silicone Rubber Sealer. Dow Corning Corp., Midland, MI, Bull. 41-113C, Aug. 1974.
7. A. Kumar and W. H. Goetz. The Gyratory Testing Machine as a Design Tool and as an Instrument for Bituminous Mixture Evaluation. Proc., AAPT, Minneapolis, Vol. 43, 1974.
8. V. L. Anderson and R. L. McLean. Design of Experiments, A Realistic Approach. Marcel Debber, New York, 1974.
9. American Institute of Physics Handbook. McGraw-Hill, New York, 1957.
10. Indiana State Highway, Standard Specifications. Indiana State Highway Commission, Indianapolis, 1974.
11. M. Muskat and R. D. Wyckoff. The Flow of Homogeneous Fluids Through Porous Media. J. W. Edwards, Ann Arbor, 1946.

Publication of this paper sponsored by Committee on Characteristics of Bituminous Paving Mixtures to Meet Structural Requirements.

**Mr. Kumar was with Purdue University at the time this research was done.*

Abridgment

Effects of Hydrated Lime on Asphalt and Aggregate Mixtures

Bob H. Welch, Transportation Research Board
Max L. Wiley, Utah Department of Transportation

This paper presents the essential results of a more extensive investigation into the effects of adding hydrated lime to asphalt and aggregate mixes.

High durability is a desirable asset of bituminous materials in highway pavement design and construction. Some characteristics of asphalt aggregates or the mixes that affect the service life of a highway pavement include adhesion between the asphalt-aggregate interface when dry and wet, hardening rate of the asphalt cement, and interaction between different bituminous cements and aggregates.

Additions of hydrated lime to bituminous mixtures have been observed to increase the mix immersion compression for some aggregate sources and to reduce the hardening rate of in-place asphalt cement. The degree to which hydrated lime influences these characteristics varies according to type of asphalt, aggregate, and lime and to amount of lime.

Laboratory samples, designed and prepared with mixes of hydrated lime, aggregate, and asphalt, were used to monitor interactions among the various bituminous mixtures over time. The sample combinations were made in compliance with a design comprising three asphalts (AC-10, AC-15, and AC-20), two aggregates (judged as good and poor performers by field experience), two sources of lime (Utah and South Dakota), and three concentrations of lime (0.0, 0.5, and 1.0 percent). For each combination, 21 samples were prepared that allowed three test replications of each category of bituminous mixture to span seven age-testing periods (24 h, 10 d, 3 months, 6 months, 12 months, 18 months, and 2 years). Test samples were aged by exposure to the weather in Salt Lake City.

Tests used to monitor the bituminous mixtures or their recovered asphalt fractions for each time period include penetration at 77°F (25°C); asphalt content, absolute viscosity at 140°F (60°C); kinematic viscosity at 275°F (135°C); flow, ductility at 39° F (4°C); cannon cone viscosity at 275°F (135°C); immersion compression (wet); specific gravity; asphaltene content; nitrogen base content; first acidaffin content; second acidaffin content; and paraffin content.

Throughout the 2-year period, the absolute and kinematic viscosities increased with age. The rate of increase was higher with the higher AC asphalts, although increases for the AC-10 and AC-15 asphalts are approximately equal after 6 months to a year. Correlation coefficients from an analysis of variance indicate which types of asphalt significantly affect kinematic and absolute viscosities with respect to time.

The effect of aggregate type on viscosity, with respect to time, differs after 3 to 9 months. The difference in degree of viscosity for the asphalt mixes with separate aggregates increases with age. Added hydrated lime has a greater retarding effect on increased viscosity for asphalts in mixes with relatively poor rather than good aggregates.

Use of separate lime sources causes negligible differences in absolute viscosity with respect to time. The degree of viscosity retardation varies directly with the amount of lime added (in the 0.0 to 1.0 percent range). Even though the addition of lime influences viscosity, the relative effect is not the same for all three asphalt sources evaluated. During the 2-year evaluation period, lime helped to reduce hardening rates most when it was mixed with the AC-15 asphalt and helped least when mixed with the AC-20 asphalt.

Ductility values decreased rapidly for 3 months and tapered off after 6 months in an exponential curve. However, original asphalt (as delivered) ductility values did not indicate what the ductility values would be over any specific period of time. Use of the more poorly performing aggregate initially yielded generally higher ductility values from extracted asphalts, but the differences deriving from the aggregate's source became indiscernible after 6 months.

Ductility values were approximately 44 percent higher for asphalts with lime added; amount or type of lime added did not affect this percentage. It is possible that the lime site is saturated and that higher concentrations of lime would extend the effect over a longer period. The greatest factor influencing ductility was the age of the specimen, which corresponds to an exponential decay rate curve.

Original cannon cone viscosity measurements for the three grades of asphalt cement were essentially the same. Residue values showed some difference between the AC-20 and both the AC-10 and AC-15 asphalts. All cannon cone viscosities increased over time, but AC-20 increased at the highest rate. Mixes prepared from the better versus the more poorly performing aggregates did not contribute to variance in cannon cone viscosity increases. Also, the type of lime at the concentrations used did not affect cannon cone viscosities.

The immersion compression (IC) values we obtained generally increased with time. Some variations corresponding to the seasonal weather variations during the year were noted: warmer seasons at the time of testing tended to raise IC. Each warm-cold seasonal cycle resulted in a net increased IC. All the bituminous mixture variables we evaluated influenced IC. The higher graded asphalts showed similar effect on IC, although the rates of IC change between test periods were not significantly different for the three asphalts used.

Large differences (1469 kPa or 213 lbf/in^2) were noted in IC for the two aggregates after 10 d of aging. This value does not hold constant but varies between zero and 1296 kPa (188 lbf/in^2) over the 2-year test period. Higher IC values were noted with mixes prepared from the better performing aggregate. For all six test periods evaluated for IC, the force is greater for higher concentrations of lime. From the 3-month period onward, the magnitude of 0.5 or 1.0 percent lime test results are only 15 percent higher than those for the 0.0 percent lime. For samples evaluated after 2 years, however, the no-lime IC values reached 262 percent above the 1207 kPa (175 lbf/in^2) minimum required for acceptance of bituminous surface courses in Utah.

IC values obtained from the wet, 120°F (48.8°C) test procedure were least variable. Higher curing tempera-

tures resulted in lower test accuracy for specific bituminous mixtures. Test samples cured in dry rather than wet conditions also showed more variability in the test results, possibly because of variations in the samples' water absorption rate.

The influence of aggregate type and concentrations of lime on IC has a much greater effect than the type of asphalt or type of lime used.

In order to further evaluate the effect of aggregate type on IC, 972 bituminous mixtures were prepared from seven aggregate sources, three types of asphalt, and 0.0 and 1.0 percent lime. Results from the IC test indicated that the silicon dioxide (SiO_2) content, calcium oxide (CaO) content, aluminum oxide (Al_2O_3) content, and calcium carbonate ($CaCO_3$) content of the aggregates did not yield a distinguishable pattern in terms of their influence on IC. The ferrous oxide content (Fe_2O_3) in the aggregate with the addition of 1.0 percent lime had a stabilizing influence on the erratic IC values compared with the no-lime mixtures. There was a tendency for higher ferrous oxide concentrations to raise IC values with the addition of 1.0 percent lime, but there were no correlations with no lime.

We checked to see if the natural calcium oxide content of the aggregate would significantly change IC values when combined with ferrous oxide, and their sum ($Fe_2O_3 + CaO$) and ratio (Fe_2O_3/CaO) were compared with IC values. We observed, from an analysis of variance, that the IC values correlated much better with the percentage of asphalt in the bituminous mixtures than with anything else. Without exception, as the optimum percentage of asphalt for a given asphalt-aggregate combination increased, the corresponding IC value decreased. From the data available, it would appear that the optimum asphalt content at an aggregate source had much more influence on mix stability than did the chemical characteristics of either the asphalt or the aggregate.

The addition of hydrated lime to asphalt concrete mixes affected different combinations of asphalt and aggregate differently. For the six possible combinations of relatively well versus poorly performing aggregates and viscosity graded asphalts (AC-10, AC-15, and AC-20), no significantly adverse consequences were seen, and in some instances hydrated lime produced beneficial effects.

Two potential benefits occurred with hydrated lime supplements: an increase of mix stability and a decrease in flow evaluated by the IC test, and decreased hardening rates of the asphalt binder as determined by the absolute, the kinematic, and the cannon cone viscosities. Potential benefits as an antistripping agent were not determined.

Bituminous mixtures made from separate aggregate or asphalt sources were enhanced in varying degrees by the use of hydrated lime. For the materials tested in this investigation, the AC-10 and AC-15 asphalt sources were best suited for bituminous mixtures with hydrated lime, because the effect retarded the hardening rate and increased mix stability. Bituminous mixtures prepared with the AC-20 asphalt indicated that the use of hydrated lime did not reduce the binder hardening over time or result in significant increases of IC.

Originally, it was thought that asphalt cements softened more with a siliceous aggregate, but the results of this study indicated that the more calcareous aggregate yielded slower hardening rates after the bituminous mixtures had aged 6 months. Lime supplements in either of these two aggregate types tended to increase IC values and to decrease hardening of the asphalt binder. The degree of influence on binder hardness appeared more dependent on asphalt type than on aggregate type.

From the types of lime evaluated, the only conclusion we drew was that lime source contributes little if at all to corresponding changes in asphalt binder or mix properties.

Data based on pavement performance that could support or reliably suggest new minimum standards for IC values differing from the 1034 kPa (150 lbf/in^2) present (average of three tests) for bituminous base courses or 1207 kPa (175 lbf/in^2) for bituminous surface courses are not available. Assuming that our present criteria are adequate, a minimum IC value of 2103 kPa (305 lbf/in^2) on surface courses and 1931 kPa (280 lbf/in^2) on base courses would be required for an average of three tests ($\alpha = 0.10$) to compensate for the variability of the testing procedure.

In most cases, the addition of 0.5 percent lime will yield results comparable to those for 1.0 percent lime.

Publication of this paper sponsored by Committee on Characteristics of Bituminous Paving Mixtures to Meet Structural Requirements.

Vibratory Compaction of Asphalt Concrete

Robert J. Nittinger, Engineering Research and Development Bureau, New York State Department of Transportation

Over the last few years, the New York State Department of Transportation has been investigating the feasibility of using vibratory compaction on asphalt concrete. A total of 10 different roller models were used on three overlay contracts and seven new construction projects. The rollers represented a wide range of dimensional and operating characteristics, which initially led to greatly varying results. Discovery of two important operating parameters resulted in development of performance criteria applicable to any roller. These parameters—the spacing of drum impacts and their magnitudes—can be controlled by adjusting forward speed, drum frequency, and drum amplitude. Impact magnitude, termed unit total applied force, was correlated with layer thickness to produce the ranges necessary for each lift. As expected, the force necessary for adequate compaction increased with lift thickness, but on lifts thinner than 76 mm (3 in) the maximum force applied was found to be equally critical. When the force was too great, roller rebound occurred, which reduced densities. Vibratory rollers also compacted single-lift wearing courses and base courses—6.3 to 20.3 cm (2.5 to 8 in) thick respectively—more efficiently than conventional rolling. When operated properly, vibratory rollers were found to be effective in compacting asphalt concrete. Operating criteria were developed to determine the ability of any roller to compact a given lift thickness.

For many years, the concept of vibrating during compaction to seat individual particles better and to produce a denser layer has been employed in working with granular materials. During the 1960s, engineers in several European countries—notably Germany and Sweden—began applying these principles to asphalt paving. Eventually, manufacturers in the United States began experimenting with vibratory rollers on asphalt, and their inquiries addressed to the New York State Department of Transportation were received with interest.

A study was initiated to evaluate use of these rollers on asphalt courses. Ultimately 10 different rollers were tested on 10 construction projects. Both standard lift thicknesses and experimental "thick-lift" sections were compacted under a variety of conditions. The standard comparison was made with results obtained from the conventional rolling trains—a steel-wheel breakdown roller, a pneumatic roller, and a steel-wheel finish roller. These comparisons were used to determine whether vibratory rollers could achieve at least comparable densities with less equipment and lower labor costs.

Initially, the study was designed to determine the feasibility of using the vibratory concept on asphalt, but the rollers represented so wide a range of design and operating characteristics, that we achieved a more thorough analysis of these attributes than anticipated. The result was a comprehensive evaluation of roller variables in terms of the finished pavement.

INVESTIGATION

Test Program

The 10 projects comprise 3 resurfacings and 7 new construction projects. Figure 1 shows job locations and roller models used, and Table 1 lists the various courses compacted by vibratory rollers at each site. Both standard and experimental lift thicknesses were constructed on most jobs. The standard thicknesses were either 7.6 or 10.2 cm (3 or 4 in) for base course, 3.8 cm (1.5 in) for binder, and 2.5 cm (1 in) for top.

Measurements

Test sections 457 m (1500 ft) long and one lane 3.7 m (12 ft) wide were established, and all measurements were made in those areas. Several roller operating characteristics were checked or verified before each test. Frequencies were measured with a vibrating reed tachometer, and roller speeds were monitored by timing them over premeasured distances. Generally, because there were no methods for measuring drum amplitudes or static weights, the manufacturers' figures were used. Operators in the conventional train

Figure 1. Numbered job locations.

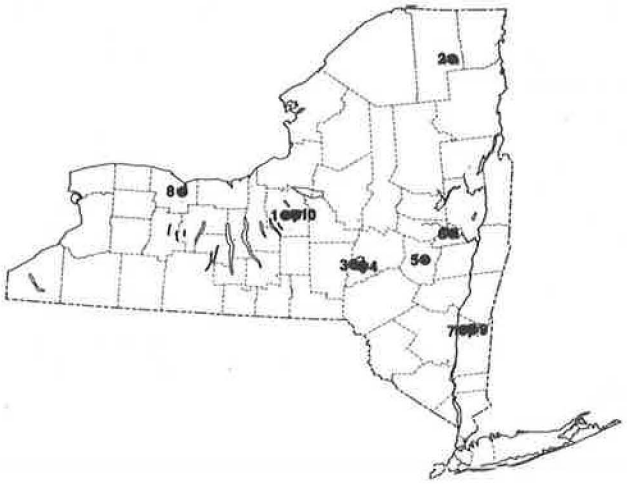

Table 1. Types of courses and rollers at job locations.

Job	Location	Rollers[a]	Base Course	Wearing Course
1	I-690 Syracuse	A, E	Two 10.2-cm lifts One 20.3-cm lift	3.8-cm binder 2.5-cm top
2	NY-30 Tupper Lake	D, F	Two 7.6-cm lifts One 15.2-cm lift	3.8-cm binder 2.5-cm top
3	County Rt-47 Oneonta	H	Two 7.6-cm lifts One 15.2-cm lift	3.8-cm binder
4	NY-205 Oneonta	A, B, G	—	3.8-cm binder
5	NY-20 Carlisle	F	Resurfacing (no base needed)	2.5-cm top 6.4-cm top
6	NY-147 Glenville	E	Resurfacing (no base needed)	2.5-cm top 6.4-cm top
7	I-684 Golden's Bridge	B, C	Two 10.2-cm lifts One 20.3-cm lift	3.8-cm binder 10.2-cm top 2.5-cm top
8	NY-19 Rochester	I	Resurfacing (no base needed)	2.5-cm top
9	I-684 Golden's Bridge	C	—	6.4-cm top
10	I-690 Syracuse	J	—	6.4-cm top

Note: 1 cm = 0.39 in.

[a] Manufacturers' roller names are A = Vibro-Plus CA 25A, B = Vibro-Plus CC 42A, C = Vibro-Plus CC 50A, D = Galion VOS-84, E = Bros SPV-735VA, F = Raygo 404B, G = Buffalo Bomag BW 210-A, H = Hyster C615-A, I = Tampo RS-166A, and J = Ingersoll-Rand SPA-54.

used normal techniques while rolling; operators of vibratory rollers attempting to achieve proper density relied (primarily on earlier jobs) on the advice of manufacturers' representatives who recommended that they vary the rolling patterns, speeds, or frequencies. However, this type of consultation became less important as operators gradually identified the proper parameters.

OPERATING PARAMETERS

Vibratory rollers compacted the various asphalt courses to at least the same densities as the conventional rolling train and, in the latter portions of the study, to slightly greater densities. Table 2 gives results from jobs 1 and 7. Densities from vibratory rollers on job 1 are slightly lower than, but statistically equal to those on job 7, where, however, they are slightly higher on the base course and significantly higher on the binder and top. This improvement in vibratory densities resulted from identifying and quantifying the following two basic relations among several roller variables:

1. Proper matching of the roller's forward speed and the vibrating drum's frequency, a combination that determines the spacing of impacts along the pavement, and
2. Several static and dynamic characteristics of each roller that produce the force applied to the pavement.

Both relations became apparent about a third of the way through the sequence of jobs and were verified and refined on the remainder.

Impacts Per Meter

The need to carefully match the roller's forward speed with drum frequency became obvious in two ways.

The first was physical. When the intervals between impacts were too long, ripples were left in the pavement surface. Although this is not critical on base course layers, it becomes intolerable on binder and top courses. One remedy was following the vibratory roller with a steel-wheel static roller that ironed out the ripples if applied before much additional cooling occurred.

Second, problems began to appear when data were being compiled and summarized. Base course data from jobs 1 and 2 were as follows (1 kg/m^3 = 0.062 lb/ft^3).

Job	Roller	Density (kg/m^3) Vibratory Rolling	Static Rolling
1	E_1	1888	1878
	E_2	1811	
2	D_1	1821	1811
	D_2	1829	
	D_3	1747	
	F	1809	

Each density figure is an average of about 60 nuclear density readings. On each job, one vibratory rolled section's density (E_2, D_3) is well below that of the conventionally rolled, while others are similar. Reexamination of the data showed that, for sections with higher densities, the combination of roller speed and frequency resulted in the drum's hitting the pavement at 20.3 and 25.3 impacts/m (6.2 and 7.7 impacts/ft). Conversely, on low-density sections, these figures were 12.1 and 16.0 impacts/m (3.7 and 4.8 impacts/ft).

To check the premise that this impact spacing was the cause of the lower densities, we varied roller speed on the 3.8-cm (1.5-in) binder course of one job and maintained a frequency of 1700 vibrations/min (vpm). The results for one roller pass at each speed were as follows (1 km/h = 0.62 mph; 1 m = 3.28 ft; 1 kg/m^3 = 0.062 lb/ft^3).

Speed (km/h)	Impacts per Meter	Nuclear Density (kg/m^3)
3.2	31.5	2023
3.9	26.2	2005
4.5	22.6	1995
6.4	15.7	1958

On another job, where a dual-drum roller was being tested, two speeds—4.0 and 9.7 km/h (2.5 and 6.0 mph)—were checked on a 2.5-cm (1-in) top course. At a 2300-vpm frequency, this produced 34.1 and 14.1 impacts/m (10.4 and 4.3 impacts/ft), which resulted in respective nuclear densities of 2323 and 2238 kg/m^3 (144.8 and 139.5 lb/ft^3).

Finally, another change was tried. Frequency was increased with speed. The net result was a drop in the number of impacts per meter from 27.9 to 22.3 (8.5 to 6.8 impacts/ft) and a slight drop in density from 1833 to 1813 kg/m^3 (114.3 to 113.0 lb/ft^3) compared with the density of 1837 kg/m^3 (114.5 lb/ft^3) under conventional rolling.

Because much of this is obvious (fewer impacts mean lower density) the natural response might be to increase the number of roller passes. Unfortunately, this defeats the roller operator's primary reason for increasing speed: keeping up with the paver. The result was the decision that speed and frequency should be matched to produce at least 21.3 impacts/m (6.5 impacts/ft).

Unit Total Applied Force

Although the primary aim of this study was to determine the feasibility of using vibratory compaction on asphalt, the number of roller models provided by the manufacturers presented an excellent opportunity to determine which roller characteristics best achieve sufficient densities. Conversely, this presented additional problems by bringing together rollers with a wide range of static and dynamic properties (1 cm = 0.39 in; 1 mm = 0.039 in; and 1 kg = 2.2 lb).

Property	Maximum	Minimum
Drum width, cm	216	168
Low frequency, vpm	2200	900
High frequency, vpm	2500	1700
Amplitude, double, mm	2.7	0.8
Net roller weight, kg	13 733	7059
Drum weight, kg	7131	3790

Table 2. Nuclear densities on jobs 1 and 7.

Course	Rolling	Job 1 Density (kg/m^3) No.	Mean	SD	Job 7 Density (kg/m^3) No.	Mean	SD
Base, first lift	Conventional	58	1873.6	139.2			
	Vibratory	119	1896.0	80.0			
Base, second lift	Conventional	61	1896.0	115.2	51	1966.4	137.6
	Vibratory	191	1883.2	83.2	51	2003.2	134.4
Binder	Conventional	61	2004.8	88.0	51	1926.6	89.6
	Vibratory	60	1980.8	52.8	51	2054.4	88.0
Top	Conventional	62	2046.4	59.2	87	2214.4	54.4
	Vibratory	156	2033.6	126.4	121	2278.4	44.8

Note: 1 kg/m^3 = 0.062 lb/ft^3.

These ranges, plus the fact that not all these data were initially available, made comparisons difficult. Because this and not the certification of individual rollers was the concept being investigated, it was important that a common measure be developed for a roller's ability to compact asphalt. This was further emphasized by the range and variation in densities at initial test sites. Ultimately, the actual force with which each roller impacted the asphalt was calculated, and we found a factor that standardized the compactive ability of otherwise widely different rollers

This factor was named "unit total applied force" (UTAF) by the Construction Industry Manufacturers Association (1) and is expressed in kilograms per linear centimeter. These linear measurements refer to the width of the roller drum. The UTAF factor can be calculated by using

$$UTAF = (F + S)/L \quad (1)$$

where

- $F = (A/2)(w)\,[4\pi^2/g(60^2)]\,(f^2)$,
- S = static drum reaction (including weight of drum, yoke, and all other equipment attached to drum) in kilograms;
- L = drum width in centimeters;
- A = peak-to-peak amplitude in centimeters;
- W = drum weight (only drum and internal parts) in kilograms;
- f = frequency in vibrations per minute; and
- g = acceleration of gravity [979 cm/sec^2 (385.6 in/sec^2)].

This was the key to understanding why sufficient densities were not achieved on some test sections. Figure 2 shows results of a regression analysis comparing UTAFs with lift thickness where satisfactory densities were achieved. Included in the figure, but not in the regression analysis, are results from test sections where less than satisfactory densities were achieved. As might be expected, the UTAF across the drum that was required increased with thickness, from about 53.6 kg/cm (300 lb/in) for 2.5-cm (1-in) top course to about 98.3 kg/cm (550 lb/in) for the experimental 20.3-cm (8-in) base course.

However, Figure 2 also shows that most of the unsatisfactory results occurred on the 2.5- and 3.8-cm (1.0- and 1.5-in) lifts, where UTAF was high in all but one case. This was probably caused by roller rebound, which is the impact force reflected off the underlying layer. If the layer being compacted is too thin to absorb the force in its total travel down to the underlying course and back up, the shock waves reach the surface and counteract the roller and make it bounce irregularly. Thus, impact UTAF, particularly on thin lifts, must be carefully controlled to achieve compaction but to avoid the rebound phenomenon.

The UTAF concept ties in directly with impacts per meter and illustrates why there is a limit on roller speed. Because frequency is a factor in determining UTAF, it cannot be increased indiscriminately, particularly on the thinner courses. Although each roller's exact limits might differ from those of other rollers, it was found that, at speeds above 4.0 to 4.8 km/h (2.5 to 3.0 mph), achieving satisfactory densities presented problems.

The amplitude, frequency, and ballast must be coordinated to produce the proper UTAF. In turn, the roller's forward speed must be linked to its frequency to ensure sufficient compaction and to avoid a rippled surface. In the course of investigating the various rollers, the optimum settings for each lift thickness were determined for all rollers. These were used on the last few jobs with encouraging results.

Figure 2. Effects of various UTAFs on lifts of various thicknesses.

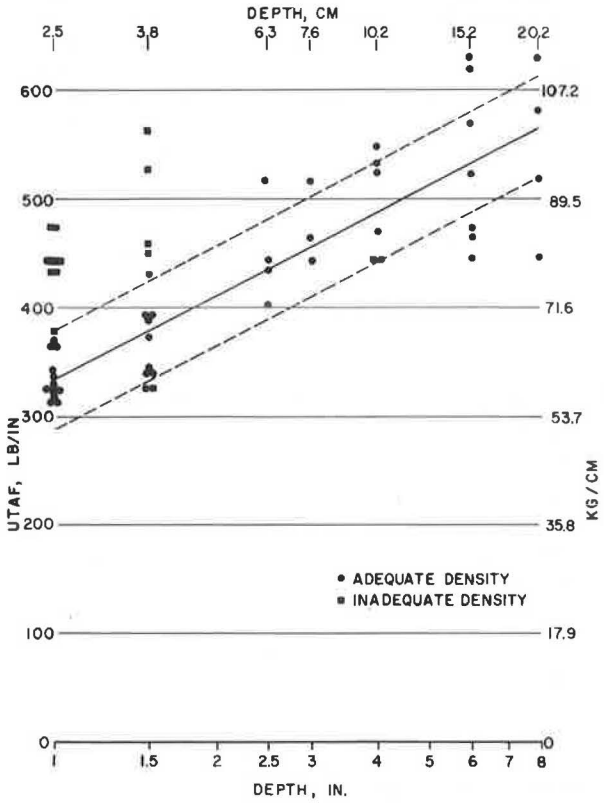

It should be noted that both the compacting techniques and the material lay-down temperatures were similar on the test sections compacted by vibratory rollers. On every test section the vibratory roller was kept close behind the paver, at no time exceeding a distance greater than 76.2 m (250 ft) from it. The average and most common distance between paver and roller was approximately 45.7 m (150 ft).

After selecting the most roller passes required on any given test section—on the thinnest course of pavement [2.5 cm (1 in)], under the coldest ambient air temperature, with the lowest lay-down mat temperature, and at the greatest distance possible between the paver and roller [76.2 m (250 ft)]—the longest time required for complete rolling and compacting the material at any given spot to a desired density was 7.5 min. The maximum time for effective compaction of a freshly placed mat, under the worst conditions this investigation encountered, was 10 min. This calculation (Table 3) is based on an Illinois study (2).

DENSITY OF INDIVIDUAL COURSES OF STANDARD LIFT THICKNESSES

Results for each pavement course are given in Table 4, which includes job and test numbers, vibratory roller identification, speed, impacts per meter, and nuclear densities. Results for conventional static rolling are also listed. Even though several vibratory tests were made on most jobs, only one control section was measured. However, considering the number of readings taken, these results were representative. Density values were obtained with a nuclear device, so they do not represent absolute values. The primary evaluation was a comparison of rolling methods, and, as all read-

Table 3. Vibratory compaction time for a 2.5-cm wearing course.

Job	Test	Roller	Mat Temperature (° C)	Ambient Air Temperature (° C)	Time to Complete Compaction (min)	Maximum Time Allowed for Effective Compaction[a] (min)
1	13	A	137.8	25.6	6.5	15
	14	E_1	140.5	27.2	6.5	15
	15	E_2	140.5	27.2	6.5	15
2	34	D	140.5	23.9	6.5	13
	35	F_1	140.5	23.9	6.5	13
5	47	F_2	143.3	15.6	6.5	11
7	65	B_1	143.3	17.8	6.0	10
	66	B_2	143.3	17.8	7.5	10
	67	C	143.3	17.8	3.5	10
8	70	I_1	137.8	16.7	7.5	10
	71	I_2	148.9	16.7	7.5	12

Note: 1°C = (1°F - 32)/1.8 and 1 cm = 0.39 in.

[a] Maximum time for effective compaction of a freshly placed mat, derived from a University of Illinois study (2).

ings were made with the nuclear gauge, these comparisons are valid.

Base Course

Table 4 summarizes all test sections established on the 7.6- and 10.2-cm (3- and 4-in) base course lifts. On jobs 1 and 7, the design called for a 20.3-cm (8-in) base course constructed in two 10.2-cm (4-in) lifts, while jobs 2 and 3 had 15.2-cm (6-in) bases placed in two 7.6-cm (3-in) lifts. Densities the vibratory rollers achieved were generally the same as those the conventional roller train produced. That is, there was no statistical difference at the 95 percent confidence level. In the few cases where they did differ, vibratory rolling appeared to be insufficient.

The two cases on the first lift have already been discussed in connection with impacts per meter. A similar situation existed on the second lift, where roller H was operated at 8 km/h (5 mph) and gave only 13.4 impacts/m (4.1 impacts/ft) and densities on two sections significantly lower than on the control section. A third section was established on job 3, where a static steel-wheel roller followed the vibratory roller. This increased density but considerably reduced the value of using the vibratory roller.

This illustrates that, while slower operation is more time consuming, it saves time and effort in the long run by eliminating the need for a second roller. Unfortunately, this job was investigated before impacts per meter and UTAF (1 kg/cm = 5.6 lb/in) were found to be the keys to successful vibratory rolling; no tests were run at slower speeds.

Base Course, Both Lifts

Roller	Frequency (vpm)	Amplitude Setting	UTAF (kg/cm)
C	2400	High	113.2
D	1700±25	Normal	93.1
E	1650	High	98.6
F	1700	High	80.3
H	1800	Normal	83.3

Binder Course

Results of vibratory compaction on the 3.8-cm (1.5-in) binder courses were similar to those on base courses:

Table 4. Comparative nuclear densities by paving course.

		Vibratory Rolling							Static Rolling				
						Density (kg/m³)				Density (kg/m³)			
Course	Job	Test No.	Roller	Speed (km/h)	Impacts/m	No.	Mean	SD	Test No.	No.	Mean	SD	Significance (95% confidence level)
Base, first lift	1	4	E	4.8	20.5	61	1883.2	78.4	3	61	1873.6	139.2	No
		5	E	8.0	12.2	60	1806.4	83.2					Yes
	2	20	D	4.8	21.1	60	1816.0	89.6					No
		21	D	4.0	25.4	61	1823.4	104.0	19	61	1807.2	105.6	No
		22	D	6.4	15.8	62	1743.2	120.0					Yes
		23	F	4.8	21.1	59	1804.2	121.6					No
Base, second lift	1	6	E	3.2	31.0	71	1859.4	102.4	1	61	1839.7	155.2	No
		8	E	4.8	20.5	61	1889.6	83.2	7	61	1896.0	115.2	No
		9	E[a]	4.8	20.5	59	1907.4	70.4					No
	2	24	F	4.8	21.1	59	1762.4	140.8					No
		25	F	4.8	21.1	61	1779.7	112.0	16	61	1752.0	107.2	No
		26	D	4.0	25.4	61	1764.8	112.0					No
		27	D	4.8	21.1	66	1722.6	113.6					No
	3	38	H	8.0	13.5	61	1795.5	107.2					Yes
		39	H	8.0	13.5	61	1796.8	100.8	36	61	1853.0	128.0	Yes
		40	H[a]	8.0	13.5	61	1843.8	104.0					No
	7	59	C	4.8	30.0	51	2003.2	134.4	57	51	1966.4	137.6	No
Binder	1	11	A	4.8	28.7	60	1980.8	52.8	10	61	2004.8	88.0	Yes
	2	29	D_1	3.2	28.1	61	1829.3	76.8					No
		30	D_2	4.8	22.4	61	1807.8	120.0	28	61	1831.2	84.8	No
		31	F_1	5.6	22.4	61	1837.3	118.4					No
		32	F_2	5.6	18.2	61	1824.0	102.4					No
	3	42	H	8.0	13.5	61	1938.2	148.8	41	61	2012.2	99.2	Yes
		43	H	8.0	13.5	61	1950.7	132.8					Yes
	4	45	B	4.0	37.6	36	2052.8	83.2	44	36	2041.6	89.6	No
	7	61	C	4.8	28.7	51	2054.4	88.0	60	51	1926.6	89.6	Yes
Top	1	13	A	4.8	28.7	62	2062.2	59.2					No
		14	E_1	4.8	21.1	62	2027.4	73.6	12	62	2046.4	59.2	No
		15	E_2	4.8	21.1	32	1988.0	73.6					Yes
	2	34	D	4.8	22.4	61	2104.2	62.4	33	62	2119.7	56.0	No
		35	F_1	4.8	28.7	61	2078.1	67.2					Yes
	5	47	F_2	4.8	23.1	32	2156.8	41.6	46	32	2158.4	51.2	No
	7	65	B_1	9.6	14.9	43	2231.8	48.0					No
		66	B_2	4.0	36.0	27	2316.2	33.6	64	36	2240.0	51.2	Yes
		67	C	4.8	27.1	51	2299.4	52.8					Yes
	8	70	I_1	4.0	33.0	22	2164.3	33.6	68	40	2076.8	94.4	Yes
		71	I_2	4.0	33.0	33	2091.2	33.6	69	24	2012.8	94.4	Yes

Note: 1 km/h = 0.62 mph; 1 m = 3.28 ft; and 1 kg/m³ = 0.062 lb/ft³.
For specific roller frequencies, amplitude settings, and UTAFs, see the text tables on the base, binder, top courses.

[a] Followed by steel-wheel roller.

they equaled conventional rolling at the 95 percent level, with a few exceptions. In all but one case, where the two methods did not achieve similar densities, compaction by vibratory rolling was lower.

On job 1, where vibratory densities were significantly lower, the UTAF was found to be 68.1 kg/cm (325 lb/in) below the one standard error limit in Figure 2. The other low densities were on job 3, where roller H again was operated at 8 km/h (5 mph) and produced only 13 impacts/m (4.1 impacts/ft). Thus, on these jobs the two important criteria were not met, and adequate densities were not achieved.

Two other important points are evident in Table 4. The first is on job 4, where roller B produced a UTAF of 60.8 kg/cm (340 lb/in) (1 kg/cm = 5.6 lb/in), close to the lower limit, but compacted the asphalt to a slightly higher higher density than conventional rolling.

Binder Course

Roller	Frequency (vpm)	Amplitude Setting	UTAF (kg/cm)
A	2300	Low	58.5
B	2500	Low	61.2
C	2300	Low	69.7
D_1	1500	–	77.8
D_2	1800	–	101.2
F_1	2100	Low	70.2
F_2	1700	High	80.3
H	1800	–	83.3

Apparently, what counteracted this low UTAF was the very high frequency, which resulted in 37.4 impacts/m (11.4 impacts/ft). Also, on job 2, two test sections were each compacted with rollers D and F, with operational changes for each.

All densities were statistically equal to conventional densities, but there were practical differences. Roller D was run initially at 3.2 km/h (2 mph) and a frequency of 1500 vpm, then at 4.8 km/h (3 mph) and 1800 vpm, lowering the impacts per meter from 27.9 to 22.3 (8.5 to 6.8 impacts/ft) and increasing the UTAF from 77.2 to 100.4 kg/cm (432 to 562 lb/in). The net result was a drop in density of 20.8 kg/m^3 (1.3 lb/ft^3), which illustrates too great a UTAF for the thickness of the asphalt being compacted.

A similar situation resulted when the frequency was reduced on roller F from 2100 to 1700 vpm and the amplitude changed from 1.3 to 2.3 mm (0.05 to 0.09 in), while maintaining a forward speed of 5.6 km/h (3.5 mph). The net result was an increase in UTAF from 69.7 to 79.7 kg/cm (390 to 446 lb/in) and a drop in density of 13.3 kg/m^3 (0.83 lb/ft^3). In this instance, the impacts per meter dropped from 22.3 to 18.0 (6.8 to 5.5 impacts/ft), and the UTAF was at the upper limit.

Top Course

The 2.5-cm (1-in) top course required the most care in establishing and maintaining proper roller operating characteristics. However, it also appeared to benefit most from vibratory rolling in terms of density (Table 4). On the first three jobs (1, 2, and 5) the vibratory rolling produced significant density differences (lower) on two test sections. Conversely, on the last two jobs (7 and 8), four of five sections showed significant differences (higher) with vibratory rolling.

These figures again indicate that, once limits were determined for impacts and UTAF, results improved. It should be noted that the UTAF was over 71.5 kg/cm (400 lb/in) (1 kg/cm = 5.6 lb/in) on three test sections and that density was lower than conventional on all three, on two of them significantly.

Top Course

Roller	Frequency (vpm)	Amplitude Setting	UTAF (kg/cm)
A	2300	Low	58.5
B_1	2400	Low	58.6
B_2	2400	Low	58.7
C	2200	Low	66.6
D	1800	–	101.2
E_1	1700	½	65.2
E_2	1700	¾	84.1
F_1	2300	Low	79.7
F_2	1850	Low	59.4
I_1	2200	Medium	60.8
I_2	2200	Medium	60.8

In both latter cases, two sections were compacted with each roller, and changes were made in their operation. On roller E the amplitude setting was changed and on roller F the frequency. In the former, changing the amplitude from 1.1 to 1.6 mm (0.042 to 0.063 in) increased the UTAF from 64.7 to 83.5 kg/cm (362 to 467 lb/in) and decreased the density by 40.1 kg/m^3 (2.5 lb/ft^3). Roller F's frequency was changed from 1850 to 2300 vpm, increasing the impacts per meter from 23.0 to 28.5 (7.0 to 8.7 impacts/ft) and the UTAF from 59 to 79 kg/cm (330 to 443 lb/in), resulting in a 78.6-kg/m^3 (4.9-lb/ft^3) density decrease.

In both cases, the excess force apparently resulted in roller rebound, which demonstrates that, on thin asphalt courses, the maximum force is as important as the minimum. It also demonstrates the danger of increasing frequency in a way that might increase roller speed.

On the last two jobs, only one of five sections, job 7 with roller B_1, was not significantly better than conventional rolling. This was caused by the low number of impacts per meter—14.8 (4.5 impacts/ft)—as the roller was operated at 9.7 km/h (6 mph). The reason it was even close to the conventional figures was that three additional passes were made. When slowed to 4 km/h (2.5 mph), with 35.8 impacts/m (10.9 impacts/ft), density increased to 85.0 kg/m^3 (5.3 lb/ft^3).

DENSITY OF EXPERIMENTAL THICK LIFTS

Thick-Lift Wearing Course

The qualified success of vibratory rollers on the earlier jobs made possible another study, that of constructing the wearing course in one lift instead of separate binder and top lifts. Basically, effort was directed to finding means of prolonging the paving season. There was a secondary advantage however: more efficient operation with fewer passes of the paving train and fewer mix changes at the batch plant.

The anticipated problems of compacting thicker lifts of the New York State top course mix with vibratory rollers did not materialize, but several attempts to use conventional rollers resulted in excessive shoving of material both longitudinally and laterally.

Table 5 summarizes nuclear densities measured on four jobs where the single-lift wearing course was tested. These are given here to show the effectiveness of vibratory rolling and the roller adjustments used (1 kg/cm = 5.6 lb/in).

Thick-Lift Wearing Course

Roller	Frequency (vpm)	Amplitude Setting	UTAF (kg/cm)
C	2400	Low	72.7
E	1600	¾	77.6
F	1700	High	80.3
J	2200	–	85.5

Table 5. Comparative nuclear densities for experimental lift thicknesses.

Course	Job	Vibratory Rolling: Test No.	Roller	Speed (km/h)	Impacts/m	Density (kg/m³): No.	Mean	SD	Static Rolling: Test No.	Density (kg/m³): No.	Mean	SD	Significance (95% confidence level)
Thick-lift wearing	5	48	F	4.0	25.4	36	2233.6	60.8	46	30	2158.4	51.2	Yes
		49	F	4.0	25.4	35	2249.6	40.0					Yes
		51	F	4.0	25.4	33	2276.8	60.8	50	36	2222.4	44.8	Yes
		52	F[a]	4.0	25.4	36	2238.4	41.6					Yes
	6	54	E	4.0	24.1	36	2198.4	73.6					Yes
		53	E[a]	4.0	24.1	36	2259.2	67.2	53	36	2169.6	83.2	Yes
		55	E[a]	4.0	24.1	35	2243.2	65.6					Yes
	9	73	C	4.0	36.0	51	2292.8	43.2	72	51	2196.8	59.2	Yes
		74	C	4.0	36.0	51	2241.6	52.8					Yes
	10	76	J	4.0	33.0	51	2140.8	48.0					No
		77	J	4.0	33.0	51	2224.0	54.4	75	51	2140.8	56.0	Yes
		78	J	4.0	33.0	51	2145.6	65.6					No
Thick-lift base	1	2	E	4.8	21.1	65	1807.8	120.0	1	61	1839.7	155.2	No
	2	17	F	4.8	21.1	61	1767.8	121.6	16	61	1752.0	107.2	No
		18	D	4.8	22.4	64	1742.4	110.4					No
	3	37	H	4.8	22.4	61	1816.2	91.2	36	61	1853.0	128.0	No
	7	58	C	4.0	36.0	51	1955.2	185.6	57	51	1966.4	137.6	No

Note: 1 km/h = 0.62 mph; 1 m = 3.28 ft; and 1 kg/m³ = 0.062 lb/ft³.
For specific roller frequencies, amplitude settings, and UTAFs, see the text tables on the thick-lift wearing and base courses.
[a] Followed by steel-wheel roller.

Other factors are covered in greater detail in a separate report on that study (3). The figures for conventional rolling represent not only a three-roller train, but also a conventional two-lift wearing course. Table 5 shows that densities on all test sections are statistically the same as, or greater than those achieved on conventionally constructed sections.

Thick-Lift Base Course

In 1970, New York experimented with a thick-lift base course, putting down 15.2 cm (6 in) of asphalt in one lift. That test, using a heavy "air-on-the-run" pneumatic roller for breakdown rolling, was successful (4), but two rollers and at least 15 passes were needed to achieve adequate compaction. Once the new study was under way, it was proposed that a vibratory roller could accomplish this more efficiently. Sections on four jobs were constructed in one lift. These were from 457 to 853 m long (1500 to 2800 ft), 20.3 cm (8 in) thick on jobs 1 and 7, and 15.2 cm (6 in) thick on jobs 2 and 3.

Table 5 densities show no significant differences between thick-lift bases compacted conventionally or with vibratory rollers. Four sections received 20 to 23 impacts/m (6 to 7 impacts/ft) and a fifth almost 36 impacts/m (11 impacts/ft); UTAFs ranged from 79.7 to 112.4 kg/cm (446 to 629 lb/in). The two lowest UTAFs were actually below the lower limit but produced adequate densities. This indicates that, above a certain thickness, there is little need to increase the UTAF. Nor should there be concern about exceeding any magnitude of UTAF (1 kg/cm = 5.6 lb/in).

Thick-Lift Base Course

Roller	Frequency (vpm)	Amplitude Setting	UTAF (kg/cm)
C	2400	High	113.2
D	1800	—	101.3
E	1700	Full	102.8
F	1700	High	80.3
H	1800	—	83.3

Twenty-seven cores were taken from the 20.3-cm (8-in) thick-lift base section on job 1 to determine density uniformity down through the layer. They were cut into thirds horizontally, and bulk density was measured. These results and, for comparison, those from the earlier study were as follows (1 kg/m³ = 0.062 lb/ft³).

Portion Tested	Job 1 (kg/m³)	Earlier Study (kg/m³)
Top third	2117.3	2152.6
Middle third	2125.3	2279.3
Bottom third	2110.9	2144.5
Whole core	2115.7	2138.1

The same pattern is evident in both cases: greatest density in the center and least at the bottom. Results from vibratory rollers are more uniform, however, and indicate better seating of aggregates through the entire lift.

OTHER FINDINGS

Roller Passes

Before the impacts per meter and UTAF factors were accurately quantified, attempts to improve inadequate densities consisted primarily of additional roller passes. The results, however, were typical of what occurs with conventional rolling: density increases up to a certain point, then levels off or even decreases with further passes.

Figure 3 shows the results of varying the number of passes on several courses. In each case, an optimum

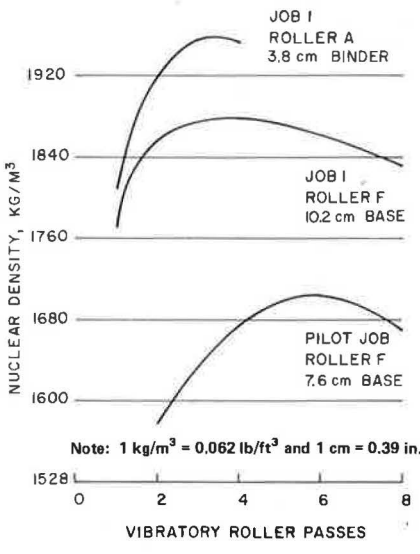

Figure 3. Effects of additional roller passes on asphalt density.

number is apparent and produces maximum density on a given course. Densities on the earlier jobs were sometimes insufficient, because rollers were not necessarily operating properly.

Once impacts per meter and UTAF were identified as the critical operating factors, determining optimum total roller passes for each course was relatively simple. (It should be noted that a roller pass is one passage of a vibrating drum over a given spot on the pavement.) In the later stages of this study, several rollers with two vibrating drums were evaluated. By definition, one dual-drum passage equals two roller passes.

Before regulating impacts per meter and UTAF, up to ten passes were being made on the 7.6- and 10.2-cm (3- and 4-in) base courses. Once these factors were controlled, three to four passes sufficed. Similarly, four passes were generally sufficient for thick-lift base course, although occasionally six were needed. For binder, two passes generally sufficed. The top needed only two, while the 7.6-cm (3-in) wearing course required four.

In some instances, additional static passes rolled out either ridges formed by not overlapping sufficiently or ripples resulting from too few impacts per meter. These problems were more critical on the binder or top courses, and in many instances a 9091- to 10 909-kg (10- to 12-ton) steel-wheel roller followed up on the top course.

Joint Construction

Construction of longitudinal joints differed with each course. For either normal or thick-lift base course, one of two procedures was used: the roller pinched the joint either from the cold lane in the static mode or from the hot lane in the vibratory mode, in both cases with the drive wheel centered on the joint (Figure 4). It could not vibrate while rolling on the cold lane, however, without causing roller rebound.

The same procedure can be used for binder, and the best results were achieved with procedure A in Figure 4. Top course required procedure B. The drum pinching the joint from the hot lane resulted in loss of pavement crown and in a corrugated or undulating surface when used on the top course.

Figure 4. Alternative longitudinal joint compaction procedures.

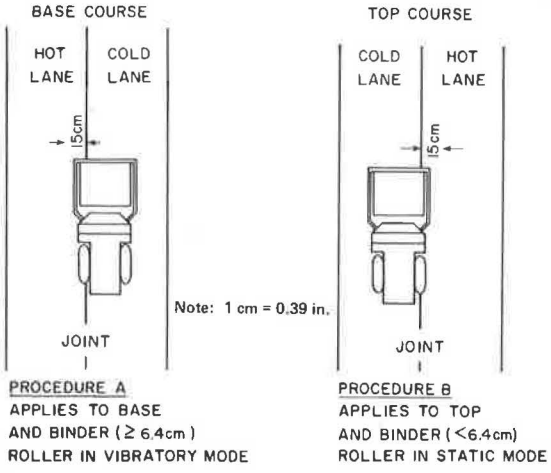

Aggregate Fracture

Aggregate fracture was another concern with vibratory rollers, but visual observations showed it to be no worse than that produced by conventional rolling.

Drive Wheels

Vibratory rollers with both pneumatic and steel drive wheels were included in this study, and both presented problems. Pneumatic wheels tended to pick up asphalt when they were cold. Steel wheels, although they operated well on binder and top courses, had problems obtaining proper traction on the base course—a situation aggravated on grade. Dual-drum rollers, which by definition and necessity use the vibrating steel drum for traction, had no such problems on any course.

Operating Considerations

Several practical precautions in operating vibratory rollers should be discussed. One noted earlier bears repeating: they should not be turned on fresh asphalt. When they must be moved laterally, it should be on material that is fully compacted. Another precaution is never to stop these rollers while the drum is vibrating, or a depression will result. This is particularly important when reversing direction, when the operator is more likely to overlook the fact that the drum is being allowed to vibrate in place, however briefly. Several rollers did have an automatic shutoff for the vibrating mechanism when roller speed dropped below 0.8 km/h (0.5 mph).

After the early jobs were completed, optional vibratory rolling was allowed on several projects. Unfortunately, rippled surfaces and inadequate densities appeared. The cause was generally excessive roller speeds, which must be watched carefully because operators new to vibratory rollers seem to feel they must avoid falling behind the paver. However, a few simple calculations involving the various speeds show that this will not occur.

Drum Width

Most rollers tested had a drum width of 210 cm (84 in). Several were narrower, however, 170 and 180 cm (60 and 72 in), and required a third pass for a 3.6-m (12-ft) lane, to ensure sufficient overlap. If a pavement is being placed full width—two lanes or 7.2 m (24 ft)—the situation changes. While two lanes still require one additional pass, in such paving this means five passes instead of four, rather than three instead of two as on a single lane.

Drum Diameter

All machines with a drum width of 216 cm (84 in) had a drum diameter of about 152 cm (60 in), and the machines with a drum width of 167 cm (66 in) had a diameter of 122 cm (48 in).

SUMMARY AND CONCLUSIONS

Vibratory rollers can compact New York State asphalt mixes to densities at least equal to those achieved by the conventional three-roller train. To accomplish this, they must operate within certain limits of speed, frequency, and amplitude, but, because the range of these factors as well as weights varied considerably among rollers, general guidelines could not be established to govern frequency and amplitude of all rollers. Fortu-

nately, this proved to be an advantage that allowed development of a more specific method of determining what was necessary to compact the various layers of asphalt.

The method involves calculating the force being applied to the asphalt and includes vibration frequency, vibration amplitude, and roller weight. This UTAF concept not only simplified roller evaluation but also provided a method for determining in advance whether a specific roller could compact a given layer.

Thus, the most significant result of this study was developing and relating this dynamic force concept to the degree of compaction achieved. Other specific conclusions in the course of this study included the following.

1. The force each roller applied to the asphalt under any given set of operating conditions (UTAF) is determined by the expression

$$UTAF = \left\{ [A(w)/2]\,[4\pi^2/g(60^2)]\,(f^2) + S \right\}/L \qquad (2)$$

2. The desired UTAF ranges (1 cm = 0.39 in and 1 kg/cm = 5.6 lb/in) for each pavement course were found to be

Course (cm)	UTAF Range (kg/cm)
Base, ≥10.2	78.6 to 107.2
Base, 7.6	72.4 to 88.5
Binder, 3.8	59.0 to 75.0
Top, 2.5	51.8 to 66.1
Top, 6.4	69.8 to 85.9

Up to about 10.2 cm (4 in), the minimum force increased linearly, then appeared to level off. Also, up to about 7.6 cm (3 in), the maximum limit is extremely important, because layers are not thick enough to absorb the additional energy and the roller may rebound.

3. The spacing of vibratory drum impacts is critical to producing both adequate densities and smooth surfaces. Forward speed of the roller must be coordinated with drum frequency to produce at least 19.7 impacts/m (6 impacts/ft).

4. Vibratory rollers can effectively replace the conventional three-roller train and produce equivalent densities with considerably fewer roller passes. On all courses 7.6 cm (3 in) or thicker, four to six vibratory passes were sufficient; three to four were needed on 3.8-cm (1.5-in) binder and two on 2.4-cm (1-in) top course.

5. Occasionally static passes were required to remove ripples or ridges, but judicious operators can virtually eliminate these. Transverse ripples are avoided by proper coordination of forward speed and drum frequency; longitudinal ridges are eliminated by sufficient overlapping of succeeding roller passes.

6. Apart from proper adjustments, the most critical factor in producing a smooth, well-compacted mat is a well-trained operator. There are three important operating considerations: never exceed a speed of 4.8 km/h (3 mph) or one that will produce less than 19.7 impacts/m (6 impacts/ft), never turn on uncompacted asphalt, and never leave the drum vibrating when the roller is stopped.

7. Thick-lift wearing and base courses, both tried experimentally on several jobs, were adequately compacted by vibratory rollers.

8. The amount of aggregate fracture was not increased by vibratory rollers.

9. Rubber drive wheels, although they tend to pick up asphalt when cold, provide better traction on courses more than 3.8 cm (1.5 in) thick, except for dual-drum rollers, which had no traction problems.

10. Longitudinal joints should be rolled either statically with the roller on the cold lane or vibrated with it on the hot lane.

ACKNOWLEDGMENTS

The work reported was conducted under the supervision of John M. Vyce, who provided invaluable assistance in preparation of the manuscript. Appreciation is also extended to Joseph C. Montgomery, who helped organize the data. The investigation originated under administrative supervision of James E. Bryden. Contributions of Engineering Research and Development Bureau staff members Joseph J. Bologna, Eugene F. DiCocco, James A. Monda, Robert W. Rider, Gerald K. Smith, and James H. Tanski are gratefully acknowledged, as is the assistance of personnel of the New York State Department of Transportation's regions 1, 3, 4, 7, 8, and 9 and the vibratory roller manufacturers and their representatives.

This paper was prepared in cooperation with the U.S. Department of Transportation, Federal Highway Administration. Its contents reflect my opinions, findings, and conclusions, and not necessarily those of the New York State Department of Transportation or the Federal Highway Administration. The state of New York, the federal government, and the Transportation Research Board do not endorse products or manufacturers; trade and manufacturers' names appearing here are cited only because they are considered essential to the purposes of this paper.

REFERENCES

1. Nomenclature and Definitions Pertaining to Vibratory Compaction Equipment. Construction Industry Manufacturers Association, Milwaukee, 1972.
2. P. A. Tegeler and B. J. Dempsey. A Method of Predicting Compaction Time for Hot-Mix Bituminous Concrete. Engineering Experiment Station, Univ. of Illinois, Highway Engineering Series No. 43, Rept. U/LU-ENG-72-2008, May 1972.
3. R. J. Nittinger. Thick-Lift Flexible Pavement Wearing Courses. Engineering Research and Development Bureau, New York State Department of Transportation, Rept. 41, Feb. 1977.
4. J. M. Vyce, L. Hartvigas, and J. W. Reilly. Thick-Flexible Paving. Engineering Research and Development Bureau, New York State Department of Transportation, Research Rept. 9, Mar. 1972.

Publication of this paper sponsored by Committee on Flexible Pavement Construction.